UMCS

MARIA CURIE-SKŁODOWSKA UNIVERSITY in LUBLIN

Faculty of Mathematics, Physics and Computer Science

Bartłomiej Kiczek
Register No.: 260923

Structures and traces of dark matter in different physical systems – from condensed matter to black hole physics

A doctoral thesis
prepared in the Department of Theoretical Physics
under supervision of prof. Marek Rogatko

LUBLIN 2023

Bartłomiej Kiczek

Nr albumu: 260923

Struktury i ślady ciemnej materii w różnych układach fizycznych – od materii skondensowanej do fizyki czarnych dziur

Abstract

English

This thesis is concerned with several scenarios of non-gravitational interactions between dark matter (represented by dark photons and axions) and visible matter, which were investigated using a similar theoretical framework. Using the general relativity with different matter contributions we modelled, i. a. , the structures around black holes – both visible and dark – and showed possible implications on their physics generated by interaction terms between two kinds of matter. The thesis consists of two parts, first provides an introductory material to the conducted research. The second one collects the articles, published in peer-reviewed scientific journals, being the substantive scientific contribution of this dissertation.

Polski

Niniejsza praca dotyczy kilku scenariuszy związanych z niegrawitacyjnymi oddziaływaniami pomiędzy ciemną materią (reprezentowaną przez ciemne fotony oraz aksjony), a widzialną materią, które zostały zbadane z wykorzystaniem podobnych technik teoretycznych. Bazując na ogólnej teorii względności z dodatkowymi wkładami materii zamodelowano m. in. struktury wokół czarnych dziur - zarówno widzialne, jak i ciemne - i pokazano ich możliwy wpływ na fizykę, który wynika z oddziaływania pomiędzy dwoma rodzajami materii. Praca składa się z dwóch części: pierwsza stanowi materiał wprowadzający do podjętej tematyki badawczej, w drugiej zebrano artykuły opublikowane w recenzowanych czasopismach naukowych, stanowiące merytoryczny wkład naukowy tej rozprawy.

Acknowledgements

My gratitude is directed twofold. First, I would like to thank my advisor, professor Marek Rogatko for excellent mentoring during my doctoral studies. I truly appreciate our discussions, engagement in scientific projects and enormous dose of freedom. On the other hand, I would like to thank my wife Anna, for gigantic patience and endless support. Her efforts allowed me to work on this thesis and complete it in the best possible way I could.

Contents

Chapter 1

Introduction

Space research constitutes a specific part of science. Except its solid, methodologically rigorous part it also contains a pinch of mystery and poetry. The view of a starlit sky has not been an inspiration only to generations of researches and philosophers, but also to ordinary people. This phenomenon was extensively used in culture, mostly in science-fiction genre, where thousands of authors stimulated their reader's curiosity and need to explore the unknown.

The issue of dark matter (DM) fits perfectly into this theme of galactic secrets. Despite the solid observational foundations it also has an element of mystery. The mystery that has been bothering minds of many scholars for almost one hundred years, yet still remains without definite answers, and even constantly brings more questions.

It seems quite complicated to start a brief historical review from nobody else but Fritz Zwicky [1]. Although the premises for the existence of an additional, invisible matter in galaxies were given by researches such as Jan Oort, the Swiss astronomer is considered the father of dark matter. In 1930s, he collaborated with Edwin Hubble, who provided him the observational data, related to galaxy clusters and their dynamics. Zwicky built a model based on the viral theorem to describe the motion of the galaxies in a cluster. The viral theorem gives the relation between mean kinetic energy and mean potential energy of the system in question.

Zwicky concentrated his efforts on the Coma Cluster data, especially on the velocities of the galaxies that built this cluster. In the next step, he calculated the difference between the slowest and the fastest galaxy. Then he compared observationally measured velocities to these determined by his model. The result was stunning as the difference was to the order of several hundred percent. It lead him to the conclusion that there is a large amount of dark, unobserved matter in the system, which significantly affects the dynamics of the galaxy motion.

Another clue for dark matter existence has been brought by spectroscopic observations of spiral galaxies with 21 cm wavelength. The rotation curve was the key characteristic - the velocity of a galaxy element as a function of its distance from the centre. Although such measurements were carried out since the 1920s, a significant breakthrough in this field

took place in 1970s. The milestone was the device built by Vera Rubin and Kent Ford [2]. The authors studied the neighbouring Andromeda Galaxy. The new spectrograph allowed the collection of the rotation curve far from the centre of the galaxy, much farther than its predecessors.

It turned out that the measured rotation curve behaved as predicted up to a certain point. However the farther from the centre, where it should have decreased, it reached a plateau. Similar behaviour was also observed in other spiral galaxies such as NGC2403, NGC6946 and M101. This observation shows that the spatial distribution of mass does not correspond to that of visible matter. Moreover, the galaxies extend much further beyond the range of glowing visible matter.

In those days, it was a truly shocking discovery that many researches of that time did not believe in. Even though, new evidence was emerging in favour of this hypothesis in the following years. More accurate measurements of rotation curves or gravitational lensing caused by clouds of dark matter are among many examples.

Nowadays, however, few dare to doubt the existence of dark matter. The number of astrophysical and cosmological implications makes the explanation of this mystery one of the burning problems of contemporary physics. However, it is not known how and when the experiment will yield a robust answer. Despite the significantly greater abundance of 27% of the mass-energy in the Universe [3], dark matter remains elusive to the most sublime apparatus.

However it is not so certain that any dark matter particle will be discovered in the Earth-based experiments. Particle colliders seem to lack power to achieve the high enough energy levels. On the other hand, there is a severe problem with the detection itself. As dark matter is defined to surely interact gravitationally, the non-gravitational interactions are predicted to be ultra-weak at best. Different particle probes located on our planet have not brought unquestionable results.

It seems, however, that the traces of dark matter may appear in the distant stellar systems. From the theoretical point of view, it is extremely fascinating to study known physical systems enriched with additional dark sector fields and novel interactions. This may be of particular importance in some astrophysical systems, where a high density of dark matter is expected. The research performed for the sake of this thesis fits in this newly emerging tide in the dark matter community. The lessons learned in the past three decades show that it is imminent to look for indirect methods for testing different dark matter candidates. These scenarios developed on paper and in computer simulations might be confronted with better and better astronomical surveys.

Therefore, the incoming decades will be exceptionally interesting in the study of dark matter. The variety of theoretical models might eventually obtain some feedback from the experiment, thanks to the continuous development of empirical methods. Since the 2010s managed to "catch" a gravitational wave, it is possible that the following years will bring a coveted discovery of an exotic phenomena related to a particular dark matter candidate.

Chapter 2

Theoretical background

The dark matter community used to suffer from some kind of stagnation. Multiple proposed solutions seemed not to meet requirements brought by cosmological surveys and the data from experiments aimed at detecting them remained meaningless. Recently Bertone and Tait in their short Nature paper [4] raised a call to the community, that our research methods should be diversified and new ideas are dramatically needed. The community reacted suitably to the manifest and by browsing scientific journals devoted to astronomy, gravitation and cosmology we can notice the appearance of the new trend. Not only new ideas for ground-based experiments are emerging, but also, which personally are far more interesting to me, ones related to astrophysical observations.

In this chapter I would like to discuss theoretical foundations and sources of inspiration for the research of this thesis. Because the dark matter community is very diverse, containing particle physicists, cosmologists, astronomers and relativists, the points of view are different and ideas versatile. I will briefly review the state-of-the-art, aforementioned new ideas (some of them are rather new-old) and where do I fit between them.

In whole work I use the geometrized unit system, with $c = G = k_B = 1$ and naturally the Einstein summation convention.

2.1   Dark matter in a nutshell

Since classical investigations by Zwicky through the Rubin-Ford breakthrough the contemporary dark matter market has split into three most popular branches, that used to be seemingly mutually exclusive. First branch says that dark matter is made of some new particles, living beyond the Standard Model (SM). This idea emerged from particle physicists studying cosmology, where on particular stages of the Universe evolution different ingredients were needed to match the observational data. Although it is not always the case, particle physics theory creates new beings that occasionally seem to be a nice dark matter candidate.

However, what are the requirements that particle ought to meet to be promoted with a candidate title? Large astronomical and cosmological evidence requires four basic features from such particles. They should be massive, stable for at least several billions of years, non-

relativistic, and very weakly interacting. If one takes all these requirements and compare them to all particles known by particle physics there is only conclusion - dark matter most likely cannot be a part of the Standard Model. Therefore there is large pressure on proposing and testing various scenarios involving hypothetical particles, where some of them solve both existing problems in SM and make a great DM candidate.

WIMPs (Weakly Interacting Massive Particles) used to be one of the most prominent candidates for dark matter. They constitute a thermal relic of the early stages of the evolution of the Universe. At larger energy scales they used to be coupled to the baryonic matter, being in thermal equilibrium with it. As the Universe cooled down the WIMP dark sector decoupled from the other ingredients and created a medium which interacted mostly gravitationally (hopefully not only) with the visible matter. WIMPs' masses are supposed to be heavier than 100keV, moreover they are supposed to have self-annihilation cross section on the order of 10^{-26} cm^3/s.

We owe WIMPs the burst of interest in direct detection of dark matter. The so-called WIMP paradigm fuelled a lot of ideas for stand alone experiments, but also for studying Large Hadron Collider (LHC) reactions for traces of dark matter. Unfortunately, so far all in vain, and it looks like the WIMP paradigm is falling apart. This lack of direct evidence turns the attention of the scientific community to new methods and new candidates for DM particles.

Under these circumstances, more and more different particles are considered in the planing of dark matter experiments. Modern literature contains a plethora of ideas based on various assumptions - from supersymmetry and string theories to fixes in SM and their by-products. Picking one of them makes a first challenge for a researcher starting one's investigations in the area of dark matter.

2.1.1 Axions and axionlike particles

Axions

From the big family of potential candidates I was specifically interested in axions and dark photons. Axions originate from the so-called charge-parity (CP) problem of quantum chromodynamics (QCD). This vital part of SM describes the strong interaction of quarks and their gauge bosons gluons. It is widely known that symmetries play key role in modern physics. They govern they existence of conserved quantities, what we know from Noether theorem, and the interaction among elementary particles. We expect a physical quantum field theory to be invariant under charge-parity-time (CPT) symmetry, that stands for charge, parity and time. In other words CPT symmetry corresponds to Lorentz invariance, which is of the key importance in Minkowski spacetime, where the quantum field theory (QFT) lives.

Naturally, we know that some physical phenomena may break the time invariance. For instance the presence of magnetic field in the system can break time symmetry (T). However, as we stated before, the whole CPT symmetry must stay intact, for the sake of physicality of the theory. Therefore the remaining CP symmetry should break in such way, that compensates the breaking of T symmetry, so the total CPT symmetry is not violated.

In Standard Model, breaking of CP symmetry occurs in weak interactions. This can be (and actually was) seen experimentally in different counts of some process and its CP transformed counterpart. In the realm of strong interactions no CP symmetry breaking was observed. This appeared to be a very surprising fact to the community as the QCD theory expects CP violation to occur. The so-called θ term is the suspect here

$$\frac{g^2\theta}{32\pi^2}G^{\mu\nu}\tilde{G}_{\mu\nu}, \tag{2.1}$$

where $G^{\mu\nu}$ is the gluon field strength tensor and g is a coupling constant and is currently constrained to $g > 6 - 34 \times 10^{-14} GeV^{-1}$. Theta itself is an angle, so it naturally should take some value from 0 to 2π. On the other hand, the presence of this term induces an electric dipole moment of the neutron. This dipole moment is proportional to theta $|d| \sim 3.6 \times 10^{-16}\theta e$ cm. From precise measurements we know that $|d| < 1.8 \times 10^{-26}e$ cm, which means that $\theta < 5 \times 10^{-11}$. This is extremely tiny, and it tends to be called unnatural by several researchers, especially if this parameter is theoretically allowed to be $\theta \in [0, 2\pi]$. This diminishing of θ might be either a coincidence or a sign of new physics.

One of solutions to this fascinating problem was proposed by Roberto Peccei and Helen Quinn in their paper from 1973 [5]. In their idea θ was promoted to a dynamical field instead of being merely a SM constant. In this way a new fundamental field and a particle - axion - was born, with properties that keep θ close to zero, so the electric dipole moment of neutron vanishes.

The emergence of axion is connected with introduction of a new symmetry, called the PQ symmetry from the names of the authors. In the early stage of the Universe PQ symmetry was present in particle interactions. As the universe cooled down a spontaneous symmetry breaking took place, leaving the axion as the Nambu-Goldstone boson of PQ symmetry. In consequence a new fundamental boson, next to Higgs boson, is added to the set of particles of SM. Its mass is estimated to be

$$m_a = 5.70 \pm 0.007\mu eV \left(\frac{10^{12}\text{GeV}}{f_a}\right), \tag{2.2}$$

where f_a is the energy scale of spontaneous breaking of PQ symmetry. However, this value remains unknown so far. It is speculated that it might be grand unification scale or even Planck scale. From current estimations of possible PQ symmetry breaking energy scale the QCD axion mass bounds range from 1×10^{-13} to 2×10^{-11} eV.

Axions are pseudo-scalar particles, therefore there are certain possible interactions allowed for them with other SM sectors. The nonrelativistic Hamiltonian density schematically expresses them

$$\mathcal{H} = \sqrt{\frac{\epsilon_0}{\mu_0}}g_{a\gamma\gamma}a\mathbf{E}\cdot\mathbf{B} + g_{aff}\hbar c\nabla a\cdot\hat{\mathbf{S}} + \sqrt{\epsilon_0(\hbar c)^3}g_{EDM}a\hat{\mathbf{S}}\cdot\mathbf{E}, \tag{2.3}$$

where a is axion field; $g_{a\gamma\gamma}$ is the axion coupling to photons; g_{aff} is coupling to fermionic matter and g_{EDM} is the strength of axion induced neutron electric dipole moment. Vectors

E and **B** are the electric and magnetic fields, $\hat{\mathbf{S}}$ is the spin direction of the particle that an axion interacts with.

However, on the macroscopic level in a gravitational setup we are the most interested in the first term of this Hamiltonian, which enables interactions with electromagnetism. The covariant Lagrangian of the axion is following:

$$\mathcal{L}_{axion} = -\frac{1}{2}\nabla_\mu a \nabla^\mu a - \frac{1}{2}m_a^2 a^2 - \frac{1}{2}g_{a\gamma\gamma}a * F^{\mu\nu}F_{\mu\nu}, \tag{2.4}$$

where $F_{\mu\nu} = 2\nabla_{[\mu}A_{\nu]}$ is electromagnetic field strength tensor and $*$ denotes Hodge dual operator. The first term of the Lagrangian is a dynamical one, second is the mass term, while the third one enables interactions of axions with photons in the magnetic field.

Soon after the appearance of the axion it was found that it might be a very good dark matter candidate. The idea was proposed independently by three groups in their papers published in Physics Letters B [6, 7, 8], and recently reviewed in [9]. The properties of axions, such as their bosonic nature, little couplings to SM and small masses, allow them to form structures from stellar up to galactic scale. First of all, if we consider the fundamental principle of quantum mechanics - the particle-wave duality - we can think of DM structures as waves. These waves naturally have some wavelength, using de Broglie's formula in the non-relativistic limit we have

$$\lambda = \frac{h}{mv}. \tag{2.5}$$

Relatively, heavy particles such as electrons have wavelengths of the order of nanometers. Because of that, in most of day-to-day life phenomena we experience electrons as particles, with their wave nature revealing on the appropriate length scale, such as diffraction on a crystalline lattice. However, for light DM we expect these waves to be very long, up to even hundreds of light years, with very low frequencies. Such waves can be seen as DM forming the web-like structures on the large scale.

Another argument for usefulness of axion as DM is its bosonic nature. As it is widely known bosons do not follow the Pauli exclusion principle. This means that many bosonic particles can occupy the same quantum state. If this number is large, and so macroscopic, the particles can be described with classical field theory, rather than quantum. Moreover, under specific circumstances, bosons can form Bose-Einstein condensate, which grants them new collective properties. As an illustration, Helium-4 atoms in superfluid state occupy the ground state and grant ability of collective movement without viscosity.

Bosonic condensates are especially interesting, as they might appear in gravitational setups. There are two types of them. First are hairy black holes, which are black hole solutions with additional external structures of matter fields, such as scalar condensates. This case is not only reserved to a black hole, as other objects such as neutron stars or regular stars might possess such hairy configurations too. I will return to this topic in the following sections of the thesis. Second setting are the so-called boson stars, or more precisely axion stars in this case. They constitute a self-gravitating droplet of a (pseudo-)scalar field, which is cold and macroscopic. Having in mind these ideas, axions might not only form large scale DM structures but also local aggregates of DM on sub-galactic distances.

Axionlike particles

Dark matter theory also considers axion-like particles (ALPs), which share similar physical foundations and the theoretical construction as QCD axions, however they are free from the PQ theory related constrains [10, 11].

First of all, mass range of ALPs is much broader, as it does not depend on the energy scale of spontaneous symmetry breaking of PQ symmetry. Therefore we talk about very broad range from 10^{-22} up to 10^{-2} eV. This naturally adds a lot of nuances to the large picture. For instance the ultralight, so called fuzzy dark matter made of 10^{-22} eV ALPs cannot be the only DM we need, as it would give only few percent to the total mass of DM the Universe needs to look like it looks. On the other hand, heavy ALPs could be spotted in nuclear interactions, especially in fierce environments, like inside supernovas. The production of ALPs adds an additional cooling channel to the system, which gives some observational possibilities.

The couplings of ALPs to the SM particles are also more untied. While QCD axions have a bound, originating from effective field theory, saying that the axion couplings are proportional to its mass, ALPs generally do not have such constrains.

Finally there are other methods allowing to introduce axion-like particles to physics, different than solution to QCD of CP violation problem. The top-down approach of string theories allows to derive ALPs in the compactification procedure. In fact ALPs are quite common in string compactifications as they rise naturally as zero modes of antisymmetric tensor fields. These, on the other hand, are generally present in most string theories. For illustration, let us consider a compactification of a weakly coupled heterotic string theory. Here the axion emerges as the Poincare dual of the antisymmetric tensor field $B_{\mu\nu}$ [12]. The $E_8 \otimes E_8$ theory in $9+1$ dimensions is given by the action [13]

$$S_H = \frac{2\pi M_s^8}{g_s^2} \int d^{10}x \sqrt{-g} R - \frac{M_s^6}{2\pi g_s^2} \int \frac{1}{4} F \wedge^* F - \frac{2\pi M_s^4}{g_s^2} \int \frac{1}{2} H \wedge^* H + \dots, \qquad (2.6)$$

where R is the Ricci scalar, F the gauge field strength and H is the field strength of the aforementioned $B_{\mu\nu}$ field. This action describes the dynamics of the massless bosonic excitations of the heterotic string. Compactification of the above theory on a six-dimensional manifold with volume V_6 leads to the effective action in $3+1$ dimensions

$$S_{3+1} = \frac{M_P^2}{2} \int d^4x \sqrt{-g} R - \frac{1}{4g_{YM}^2} \int d^4x \sqrt{-g} F_{\mu\nu} F^{\mu\nu} - \frac{1}{4f_a^2} \int d^4x \sqrt{-g} H_{\mu\nu\rho} H^{\mu\nu\rho} + \dots, \quad (2.7)$$

with parameters provided by

$$M_P^2 = \frac{4\pi}{g_s^2} M_s^8 V_6; \qquad g_{YM}^2 = \frac{4\pi g_s^2}{M_s^6 V_6}; \qquad f_a^2 = \frac{g_s^2}{2\pi M_s^4 V_6}. \qquad (2.8)$$

Using the above dependencies one can rule out the volume V_6 and the string scale M_s and get the axion energy scale

$$f_a = \alpha_{YM} M_P / (2\pi\sqrt{2}) \simeq 1.1 \times 10^{16} \text{GeV}, \qquad (2.9)$$

with $\alpha_{YM} = g_{YM}^2/(4\pi) \sim 1/25$, we get the energy scale of PQ symmetry breaking close to GUT scale.

On the other hand, in string theories of type II we can reach different values of f_a and a pretty large range

$$f_a \sim \frac{M_P}{\sqrt{V_6 M_s^6}} \sim 10^{4-17}\text{GeV}, \tag{2.10}$$

spreading over 13 orders of magnitude. This example shows how diverse ALPs can be, with large ranges of possible values of parameters describing their physics, depending on the creating mechanism. The ongoing experiments shall place constrains on these ranges and consequently narrow them in upcoming iterations.

Experiments

Axions and ALPs have been widely theoretically discussed in the past years. Recent works can be split into two different categories. First one (the mainstream one) is focused on direct detection of these new particles in Earth-based experiments. The other, which seems minor so far, focuses on space-based indirect effects, with axions playing important part in.

Most of the ALP-oriented experiments utilize the hypothetical particle reaction, which is typical for ALPs. The annihilation of an axion and creation of two photons in magnetic field or vice versa is a natural consequence of the last term from equation (2.4). The hypothetical existence of such process yields a basis for experiments, which can be colloquially named as *shining through a wall.* In such setups [14] the laser beam, placed in the strong magnetic field, simply strikes towards a *wall.* The goal is to turn these photons into axions, which can travel freely through the obstacle. As they pass it, they once more enter the region with strong magnetic field and hopefully a pair of photons can be recovered, so they might be easily observed. In practice, it is obviously not that easy and such phenomenon has not been observed yet. Microwave cavities such as ADMX [15] aim at ALPs of sub-eV mass range of the cosmic origin. Once again it uses the resonant conversion of axions into microwave range photons. On the other hand, it was predicted that axions may cause a time-varying nucleon electric dipole moment, which results in precession of nuclear spins in the background electric field (the counterpart of the magnetic nuclear resonance).

There are also some space-oriented experiments that aim into detecting the axions, which were created by stars (such as the Sun). The so-called Primarkoff effect allows for the production of axions in the solar core. Analogically to the devices mentioned in the previous paragraph, helioscopes use strong magnetic field to convert hypothetical solar axions into photons. The probability of such conversion in homogeneous magnetic field B over the distance L is

$$P_{a\to\gamma} = \left(g_{a\gamma}B\frac{\sin(qL/2)}{q}\right)^2, \tag{2.11}$$

with $q = m_a^2/2E$ being the axion-photon momentum transfer in vacuum. The examples of such devices are International Axion Observatory (IAXO) [16], CERN Axion Solar Tele-

scope (CAST) [17] and the newest BabyIAXO [18, 19]. However, as these ideas are totally interesting they have not brought any substantial results yet.

Despite already realised experimental projects there are various theoretical propositions that can be put into flesh in near future. Last twenty years were generous for condensed matter physics, both in experimental and theoretical progress. The fruits of these scientific advances became our everyday comfort. Fast CPUs, large memories, this abundance of computer resources was merely a dream in the previous century. Apart from practical aspects of condensed matter physics, plenty of interesting ideas emerged, such as novel states of matter or topological materials. The dark matter community did not stay indifferent to new physical mechanisms and opportunities offered by novel states of matter. Plenty of theoretical proposals have been presented. The usage of superfluid helium and its interaction with hypothetical ultra-light bosons were considered in [20]. Absorption of ultra-light particles in superconductors was studied in [21]. Authors calculated the outcomes of hypothetical scattering of particles such as ALPs and dark photons off conduction electrons in Cooper pairs. In [22] polar materials were considered. Authors used density functional theory for modelling the condensed matter setup and calculating adequate matrix elements. Scattering of ultra-light bosons on electrons in different crystals such as GaAs or sapphire was studied. On the other hand, novel materials such as Weyl semi-metals could host phenomena, like axion originated charge density waves [23]. Although these ideas seem theoretically interesting, their experimental utilization looks rather challenging.

In the recent years, researchers were looking for axion-involved space-based phenomena. Adding ALP to different astrophysical and gravitational theories gave a plethora of interesting outcomes. Let me briefly mention some of them. Laser-like blasts of light caused by axionic superradiant instability were predicted around rotating black holes [24, 25]. It was shown that an unstable axionic cloud can emit electromagnetic radiation, exponentially in time. In [26] authors showed that the polarization of light might be twisted by axionic fields. This result was obtained by modelling light rays emitted from protoplanetary nebula, which emits polarized light (with polarization perpendicular to the plane of the nebular disc). Then as the light passes the axionic cloud somewhere in the space, its polarization angle appears to be different than before the passage. Authors also propose the measurements of this angle as an indirect method of ALP detection. Similar effect concerning cosmic microwave background (CMB) was predicted [27]. It appears that fuzzy axionic dark matter can influence the polarization of CMB both in the early stage of the Universe and in the late time. Surprisingly these effects can be distinguishable, as the early-time oscillations of the axion field wash out the polarization of the CMB produced at last scattering. Neutron stars [28, 29, 30] host a suitable environment for axionic configurations. It was shown that depending on pulsar frequency axions can form a stable condensate or radiate away. Moreover pulsars can also be used in polarimetry measurements. As their light is polarized, any fluctuations for the polarization angle might indicate some new physics originated from the hidden sector interactions.

2.1.2 Dark photons

Another kind of particle that I considered in my research is the dark photon. It is a particle originating from a $U(1)$ symmetry gauge group, that is kinetically mixed with the Maxwell field strength tensor. The hidden photon shares similar properties with its visible cousin. However, it might be massive and adds a lot of new physics into the consideration. The idea was initially introduced by Bob Holdom [31] and it was widely studied since that time [32, 13].

The motivation for dark photon is based on several clues. First is the so-called naturalness, based purely on particle physics arguments. Dark matter is thought to be, most likely, not a single kind of particle, but the whole new set of particles. This new sector can be as various as the SM itself. Given the extremely low interaction cross-section between SM and DM, most of the dark sector particles can be uncharged under SM gauge groups.

Most of experiments assume that some kind of interaction between SM and DM exist. In fact processes such as scattering of a heavy nuclei require the adequate non-zero interaction Hamiltonian terms

$$H_{int} \neq 0 \implies \langle f|H_{int}|i \rangle > 0, \tag{2.12}$$

where the transition amplitude from initial $|i\rangle$ to final $|f\rangle$ state is non-zero. In such picture the DM cannot be completely *dark*, as there is some weak coupling with SM particles. However this image can be totally false. The dark sector might exist as a parallel world, containing different particles - scalars, fermions - that are fully decoupled from the standard model.

This sad perspective, especially in its strong variant, can exclude any direct detection of a DM particle from our experimental planning. However there is a shade of hope if we assume that there might a portal to the dark world. A particle that is both coupled to the visible and the dark side. Theoretically such portal can take various forms: vector, fermionic (neutrino), scalar or previously introduced pseudo-scalar - axions.

From all these possibilities the vector solution looks most promising, as this kind of particles constitutes gauge bosons, which mediate the fundamental interactions between particles. By analogy, the dark sector might have its own interactions, with its own gauge bosons. Therefore the kinetic mixing between the dark photon and the visible photon (which is Abelian gauge boson - that is allowed for such mixing) can take place.

This addition opens a new spectrum of possibilities, which are two-fold. First, the dark photon itself can be investigated with its reaction with visible matter. On the other hand, it may allow to indirectly probe dark particles that are decoupled from SM. One way or another the consequences are quite serious.

The case of supernovae is an interesting example and simultaneously a second, phenomenological clue for dark photon. Surprisingly it appears that supernovae are colder than they should be. It means there occurs some kind of excessive cooling mechanism, which allow them to reach lower temperatures. This new mechanism can be related to the dark sector particles, as new channels for thermal energy evaporation.

Dark photons are thought to be produced in the core of a supernova. From there they can escape from the star area and decay into an electron and positron pair. Later on, these pairs can produce 511keV photons, which are naturally measurable and can be registered as an excess of annihilation radiation. The bounds on this phenomenon were placed using the Raffelt criterion in the measurements of SN 1987a [33, 34]. The new particle cannot carry more energy than $3 \times 10^{52} erg/s$ out of the system. On the other hand, the over abundance of galactic positrons can not occur. This conditions place specific constraints on the coupling parameter and the dark photon mass.

These γ-ray flashes are also predicted in different astrophysical systems. For instance binary neutron star mergers are also high energy physics labs, which can host phenomena related to physics beyond SM [35]. When the merging occurs a metastable remnant, similar to a protoneutron star after the supernova, is formed. As this extremely hot body cools down it can produce new weakly coupled particles.

Similarly to ALPs dark photon also can be derived from strings. A compactification of $E_8 \otimes E_8$ heterotic string supergravity serves as an example. In this case the first exceptional Lie group E_8 contains Standard Model gauge groups, while the second E_8 group includes a hidden gauge group, which interacts with the first one only gravitationally. During compactification the second factor can be broken into non-Abelian and $U(1)$ gauge groups. For instance in the orbifold compactification of heterotic string, one obtains SM groups and two hidden sector symmetries, one non-Abelian and another $U(1)$ [36]

$$E_8 \otimes E_8 \to SU(3) \otimes SU(2) \otimes SU(1) \otimes [SU(6) \otimes U(1)]. \tag{2.13}$$

In low energy scales this results in an effective Lagrangian where the non-gravitational coupling occurs through kinetic mixing. This Lagrangian has the form

$$\mathcal{L}_{EM+DP} = -\frac{1}{4} F_{\mu\nu} F^{\mu\nu} - \frac{\alpha}{4} F_{\mu\nu} B^{\mu\nu} - \frac{1}{4} B_{\mu\nu} B^{\mu\nu} - m^2 B_\mu B^\mu, \tag{2.14}$$

where the Maxwell field strength tensor, is defined as $F_{\mu\nu} = 2\nabla_{[\mu} A_{\nu]}$. The other field B_μ is the vector potential of dark photon field, with corresponding field strength tensor, defined analogically $B_{\mu\nu} = 2\nabla_{[\mu} B_{\nu]}$. Finally m denotes the mass of the dark photon and α is the coupling parameter between two sectors.

In general case the mass of the dark photon might be non-zero, as it arises either from standard Higgs mechanism or the Stueckelberg mechanism. The mass range is quite large as values from meV up to GeV scales are expected. For the second parameter of the theory, the kinetic mixing, different sources (observational constraints and string predictions) expect the value of α to be in range

$$10^{-12} < \alpha < 10^{-2}. \tag{2.15}$$

Similarly to axions, dark photons have been intensively probed throughout two past decades. Most of the experiments focus on the detection of space-originated dark photons, however some aim at capturing particles created in hypothetical processes in accelerators. It is expected that dark matter particles can interact with nuclei or electrons in the detecting

materials. So far it was only DAMA/Libra collaboration that claimed to capture an excess modulation of the signal [37, 38]. However, their results have not been replicated for a long period of time [39]. The gamma rays incoming from dwarf galaxies were carefully studied by Dark Energy Survey [40] and other projects [41, 42, 43, 44]. Astronomers aim at registering excessive cosmic rays that can be related to non-gravitational dark matter-ordinary matter interactions. For instance regular photons can contain traces of past interactions with dark photons or dilaton-like particles. Moreover these interactions may cause oscillations of fine structure constant [45]. Recently authors in [46] revised the data from 1987A supernova. Many new effects were brought into consideration, such as finite temperature and density of coupling parameter. The final result brought a significant decrease of the previous upper limit on dark photon mass. It has been reduced below 15MeV, while previously it was over 100MeV.

Another experiment focused on direct detection (or even production) is BABAR, where researchers try to produce dark matter particles in accelerators. Precisely it is thought that positron-electron e^+e^- collisions can be a source of dark photons [47]. SENSEI (Sub-Electron-Noise Skipper CCD Experimental Instrument) collaboration created a device based on the idea of a CCD matrix. The electrons in the valence band of a semiconductor can be excited to the conductance band where the device can detect them. Possible dark photon-electron interaction can cause such process, leading to the measurement of the interaction. The detector is placed in an underground cave, which helps to eradicate different noises. Recent report on SENSEI's activity [48] shown no registered dark matter related events and provided constraints on the probed particles.

One of the most prominent experiments of our times is run by XENON collaboration. The Italy-based laboratory, deep under Gran Sasso d'Italia massif, is one of the best isolated from the outer world labs. Such level of isolation allows for conducting precise measurements of subtle phenomena. The heart of the laboratory's apparatus is the large tank filled with two tones of ultra-pure liquid xenon. Whole tank is surrounded by hundreds of photomultipliers. Such set up can remind the great Super-Kamiokande experiment, which successfully found the evidence for neutrinos oscillation. However XENON collaboration aims at detecting different beings. The WIMPs were the first target, as a photon emission was expected after a collision between a WIMP and a xenon nucelus. Although as the attention of the dark matter hunters turned towards lighter particles such as axions and dark photons, researchers realised that XENON1T might measure these particles too, but via absorption. It is expected that light dark matter particles can cause an analogue of photoelectric effect in a xenon atom. The measured energy would be then proportional to the dark particle mass.

Recently XENON collaboration reported an excess of events [49] in a possible mass range of dark matter particles. This paper caused an avalanche of papers by particle-oriented dark matter theorists in the autumn of 2020 in Physical Review Letters. So far it is not known what caused the excess. Plenty of ideas have appeared, with axions and dark photons as most probable culprits. However, sceptics indicate that it might have been a radioactive background issue. Upcoming experiments - LUX-ZEPLIN and PandaX, based in the US and China respectively, might hopefully replicate the result or falsify it.

The remaining two branches of dark matter are alternative theories of gravity and macroscopic objects.

2.1.3   Alternative theories of gravity

Alternative theories of gravity assume that the gravitational interaction behaves differently on different length scales. They do not deny the predictions of General Relativity (GR) in the Solar system, as there is too much experimental evidence that it is hard to overthrow. Starting from the famous Mercury perihelion, going through Sir Arthur Eddington's observation of light bending during the 1919 solar eclipse and ending with the newest gravitational waves detection. First try of modified physics for solving dark matter problem is the so-called MOND (MOdified Newtonian Dynamics). It was aimed to describe the flattening rotation curve of spiral galaxies. In fact the hypothesis added a slight modification to the Newton's second law of dynamics

$$\vec{F} = \left(\frac{a}{a + a_0} \right) m\vec{a}, \tag{2.16}$$

where a_0 is an arbitrary parameter of the acceleration dimension and is predicted to be very small $a_0 \sim 10^{-10}$m/s^2. The model seemed to describe well the rotational curves of galaxies given only the baryonic mass of a galaxy. However it miserably failed in different applications. First of all it does not eradicate the need for dark matter, as there is still the problem of missing mass in different galactic systems. Secondly, it does not describe correctly other phenomena, such as collisions of galaxies. Moreover, the idea can be considered inelegant and full of ad hoc assumptions.

Another, more general approaches are generalizations of the General Relativity. They assume that standard GR is valid in limited cases and the Einstein-Hilbert action

$$S_{EH} = \int d^4x \sqrt{-g} R, \tag{2.17}$$

where R is Ricci scalar, can include another gravity-related terms. As there are many ideas for extension of this action, let me shortly mention some of the most popular. Introducing higher order curvature terms into the Einstein-Hilbert action is a natural treatment. These terms are topological invariants which can consist not only of Ricci scalar, but different contractions of Ricci and Riemann tensors - the Gauss-Bonnet theory is an example here, with its term

$$\mathcal{G} = R^{\mu\nu\rho\sigma} R_{\mu\nu\rho\sigma} - 4R^{\mu\nu} R_{\mu\nu} + R^2. \tag{2.18}$$

More general extensions are named as $f(R)$ theories, with action

$$S_{f(R)} = \int d^4x \sqrt{-g} f(R), \tag{2.19}$$

where $f(R)$ is some generic function of the Ricci scalar. There is also even more general family called scalar-tensor theories, where an additional scalar field is introduced. The

example of such theory is the Brans-Dicke theory of gravitation, with action

$$S_{BD} = \int d^4x \sqrt{-g} \left(\phi R - \frac{\omega}{\phi} \nabla_\mu \phi \nabla^\mu \phi \right), \tag{2.20}$$

where ϕ is the scalar field and ω is a dimensionless coupling constant. In this theory ϕ plays the role of a spatially varying gravitational constant G.

To summarize, alternative theories of gravity bring a plethora of new physical phenomena. It considers various aspects of research - new black hole solutions, cosmological modifications and even changes of stellar evolution. However they do not fully remove the need for excessive mass in galaxies, therefore they cannot be considered a final solution to the dark matter problem.

2.1.4 Macroscopic objects

At last but not least let me briefly discuss the third branch of dark matter research - the macroscopic objects. This idea suggests the dark matter merely consists of non-shining objects, no new particles or new gravity are needed. The so-called MACHOs (Massive Astrophysical Compact Halo Objects) are the bodies that build the galactic halos and are hardly detectable. These can be black holes, neutron stars, brown dwarfs, jupiters (aka gas giants) or another hypothetical exotic objects such as boson stars, gravastars or quark stars. Moreover invisible structures formed on the visible objects can also be classified as macroscopic objects (I shall discuss this topic in the next subsection).

Finally, to summarize this subsection. I believe that the Nature does not really care about human's segmentation of ideas. Therefore it will rather not listen to our quarrels and prayers - the answer to the dark matter quest might be the golden mean between these seemingly separate branches. The macroscopic objects might be built from new particles that undergo modified laws of gravity.

2.2 Hairy black holes

Everyone who studies physics realize at some point that physicists truly adore the language of metaphors and hilarious names. Terms such as black hole, wormhole or hair sound rather funny to a stranger. However their symbolic meaning is enormous as they capture the depth and complication of the physical structure of these objects.

During the so-called golden age of General Relativity (roughly 1960s and 1970s) many fascinating and inspiring ideas were discovered and introduced. Among them was the famous no-hair conjecture, named by Jacob Bekenstein and advertised to broad auditorium by John Archibald Wheeler.

It states that solutions of Einstein-Maxwell equations (General Relativity with electromagnetism) can be fully described by merely three physical parameters - mass, angular momentum and electric charge. General Relativity predicts that any physical process of

gravitational collapse should lead to the emergence of a black hole. Apparently the end state of this process should be independent of the initial conditions. Naturally the values of these three parameters would depend on the initial conditions, but the functions describing the solution will belong to the same family and have the same form. This is the reason behind the statement *black holes have no hair*, as they seem to not have any structures that would alter the three-parameter picture, such as the outer configurations of some matter fields.

The conjecture inspired the truly rigorous formulation of the problem in question, the so called uniqueness theorem. First mathematically rigorous proof of the uniqueness theorem of the black hole solution was given by Werner Israel in his pioneering paper from 1967 [50]. He showed that the Schwarzschild metric is the unique static asymptotically flat solution of the Einstein vacuum field equations. Among all, in proving uniqueness theorems for black holes, the key role is played by Killing vectors describing symmetries of the underlying spacetimes. Moreover, the black hole event horizon is identified with a null hypersurface to which the aforementioned Killing vectors are tangent (orthogonal). Soon after, Israel generalized his concepts on the Reissner-Nordstrom solution in the realm of Einstein-Maxwell theory. Later on, the uniqueness was found for the rotating solutions - the stationary and axisymmetric Kerr and Kerr-Newman metrics - by Brandon Carter [51] and Stephen Hawking and George Ellis [52].

However it is not always the case, as going beyond the standard General Relativity brings the possibility of obtaining the hairy solutions. Such solutions are possible to obtain considering scalar fields, vector fields or non-abelian Yang-Mills fields (I will briefly review recent advances and examples below). Including new degrees of freedom to the theory of gravity can vastly change the structure of the obtained spacetimes. Because of that there are many examples that involve different stable matter field configurations emerging outside black hole event horizons. Non-trivial hair naturally appears in standard GR but in asymptotically anti-de Sitter (AdS) spacetimes. In asymptotically flat spacetimes obtaining hair requires a little bit more effort.

One of the first fields studied in gravitation was the scalar field, which is relatively simple to model and can phenomenologically mimic more complex matter contributions. The scalar fields gained on physical significance in 2012, when the Large Hadron Collider at CERN found the evidence for the Standard Model Higgs boson. This discovery has shown that scalar fields can exist fundamentally in nature and their meaning seems bigger than just toy models.

Depending on the specific construction of the Langrangian, field composition, couplings and symmetries the analysis of the solution could provide three distinct outcomes [53].

1. A strict no-hair theorem - giving the lack of possibility for the formation of a non-trivial scalar.

2. A no-hair theorem under some set of assumptions, but hairy solutions if any of these assumptions are broken.

3. A hairy solution, where the scalar profile is always non-trivial.

Let me now list a couple of examples of theories belonging to each group. The Lagrangian

$$\mathcal{L} = \frac{1}{4}R - \frac{1}{2}\nabla_\mu\Phi\nabla^\mu\Phi - \frac{1}{2}\mu^2\Phi^2, \tag{2.21}$$

corresponds to scalar-vacuum ($\mu = 0$) and massive-scalar-vacuum ($\mu \neq 0$) theories. Both of them belong to the first group, as they exhibit clean no-hair behaviours, which were proved by Chase [54] and Bekenstein [55], respectively. Second class contains theories such as V-scalar-vacuum

$$\mathcal{L} = \frac{1}{4}R - \frac{1}{2}\nabla_\mu\Phi\nabla^\mu\Phi - V(\Phi), \tag{2.22}$$

where except gravitational and kinetic term we have a generic potential. Massive-complex scalar-vacuum theory (with complex scalar field and $V(\Phi) = \mu^2\Phi^\dagger\Phi$) exhibits similar properties. These theories show both hairy and no-hair behaviours, depending on certain assumptions and parameter ranges. They were studied by Heusler and Straumann [56], Bekenstein [57], Pena and Sudarsky [58]. Finally the example of the third class is Einstein-Skyrme theory

$$\mathcal{L} = \frac{1}{4}R - \frac{1}{2}\nabla_\mu\Phi^a\nabla^\mu\Phi^a - \kappa|\nabla_{[\mu}\Phi^a\nabla_{\nu]}\Phi^b|^2, \tag{2.23}$$

where only hairy solutions are present, such as Droz-Heusler-Straumann [59] and its generalizations.

The pure scalar hair is not the only option that is being considered by researchers. The simplest generalization is the addition of electromagnetic field and granting the scalar field electric charge by including it in the covariant derivative

$$\mathcal{L} = \frac{1}{4}R - \frac{1}{4}F_{\mu\nu}F^{\mu\nu} - \frac{1}{2}(\nabla_\mu\Phi - iqA_\mu\Phi)^\dagger(\nabla^\mu\Phi - iqA^\mu\Phi) - \mu^2\Phi^\dagger\Phi, \tag{2.24}$$

with q being the charge of the scalar field. In this theory, hairy solutions emerge naturally in asymptotically AdS spacetimes. This feature has been widely used in the realm of holography aka AdS/CFT correspondence., which I will describe in the following section. If one wishes to obtain a hairy solution within this theory in an asymptotically flat spacetime, the usage of the so-called box boundary conditions is imminent.

Recently it was shown that rotating black holes can undergo a process of spontaneous scalarization in the Gauss-Bonnet gravity

$$\mathcal{L} = R - \frac{1}{2}\nabla_\mu\Phi\nabla^\mu\Phi + \frac{1}{8}\eta\Phi^2\mathcal{G}, \tag{2.25}$$

where η is a coupling constant and $\mathcal{G}$ is the Gauss-Bonnet invariant defined before in equation (2.18). Moreover the scalarization appears to be induced by the black hole spin, which was investigated by several authors [60, 61].

One may notice this abundance of theories can serve as a motivation to test various scenarios of matter composition. The same situation takes place in searches for dark matter candidates. One can wonder how many hypothetical terms and couplings may be attached

to standard GR gravity (or extended) and elaborated under various circumstances. This is one of the main targets of the research conducted for this thesis.

The particle oriented dark matter theory gives a birth to various candidates and moreover there are some experimental clues for the correctness of these models. However, it is the space where dark matter was originally observed and serves as the main theatre of its evolution. Seeking for new space-oriented dark matter physics is truly necessary. The exoticism of these new fields can be a source of interesting phenomena, such as new stellar objects and black hole hair like clouds and condensates. Hairy black holes are usually considered as theoretical concepts, but can dark matter fields form condensates on the compact objects in astrophysical environment? Moreover the black holes can serve as a high energy physics laboratories, which can host subtle dark matter related effects. Building this theoretical literature will allow astronomers and other experimentalists to conduct observations and precise measurements of space based phenomena, that can carry the traces of dark matter in imaginable future.

2.3 AdS/CFT correspondence

One of contributions collected in this thesis utilizes the AdS/CFT correspondence in modelling of the dark matter related physics. Therefore I consider it justified to briefly describe fundamental concepts of the gauge/gravity duality.

The anti-de Sitter/Conformal Field Theory (AdS/CFT) correspondence is a duality originating from the string theory, which links a n-dimensional gravitational theory with a $(n-1)$-dimensional quantum field theory. On the first side one has a theory of (quantum) gravity, which apart from gravitational components can contain different matter fields. Such Lagrangian possesses a set of symmetries, which are of the key importance, because they persist on both sides of the correspondence. This gravitational theory lives in the bulk of the n-dimensional AdS spacetime. It should be noted that this family of spacetimes has the asymptotic boundary, which naturally has the dimensionality reduced by one. On the second side, there is a quantum field theory, living in the Minkowski spacetime, on the aforementioned boundary of the AdS spacetime. Depending on the specific set of fields, their symmetries and couplings the weakly coupled gravitational theory may refer to boundary field theory that can describe different strongly coupled many-body systems.

This incredible idea was proved by Juan Maldacena in his famous 1998 paper [62], which is one of the most cited papers in high energy theoretical physics. The proof itself is complicated, but simply speaking it relies on the thermodynamical properties of both theories presented in the language of path integrals. One ought to consider the partition function, which gives a complete description of the field theory, as it is possible to produce different relevant quantities from it. For both sides of the duality we can compute separate partition functions, one for the bulk theory and another for the boundary. Finally it appears, if the bulk partition function is taken to the limit of the AdS boundary it is equal to the boundary

theory partition function, in other words

$$Z_{CFT}[\eta_{\mu\nu}] = Z_{AdS}[g_{\mu\nu}|_{\partial}] \simeq e^{S_g[g_{\mu\nu}|_{\partial}]}, \tag{2.26}$$

where S_G is the action of the gravitational bulk theory and ∂ represents the boundary of the AdS spacetime. This fact leads to the conclusion that both theories describe systems which share the same physical properties and behaviours.

Such observation can be utilized in various ways. The most important is the overcoming the problem of solving a strongly coupled theory. Instead of struggling with a correlated many-body system, one can find the gravitational weakly coupled counterpart, which can be solved even in the perturbative regime. The gauge/gravity correspondence guarantees that the easily computed quantities on the gravitational side can be translated to relevant parameters in the boundary field theory. The adequate correlation functions can be obtained via standard path integral relation

$$\langle \mathcal{O}_1(x_1)...\mathcal{O}_n(x_n) \rangle = \frac{\delta^n \log Z}{\delta J_1(x_1)...\delta J_n(x_n)}, \tag{2.27}$$

where functional derivatives are taken with respect to specific sources.

The gauge/gravity duality found many applications, just to mention a few disciplines - in modelling condensed matter systems, neutron star matter and even in collider nuclear physics.

As an illustrative example let us take a simple holographic superconductor [64]. On the gravitational side of the theory we consider a charged complex scalar field

$$S = \int_{\mathcal{M}} d^4x \sqrt{-g} \left(R - 2\Lambda - \frac{1}{4}F_{\mu\nu}F^{\mu\nu} - \frac{1}{2}(\nabla_\mu \psi - iqA_\mu \psi)^\dagger (\nabla^\mu \psi - iqA^\mu \psi) - \mu^2 |\psi|^2 \right), \tag{2.28}$$

where Λ is the cosmological constant and is naturally negative, which guarantees that the resulting spacetime will be asymptotically AdS. If one varies the above action with respect to the fields, the equations of motion will be the result. For a certain set of conjectures and parameters a Schwarzschild-AdS hairy or hairless black holes are the solutions.

Now if one wishes to interpret such system with the AdS/CFT toolbox, the whole problem should be taken to the asymptotic boundary of the AdS spacetime. In terms of a radial coordinate, that is $r \to \infty$. After such operation the equations of motion reach their asymptotic forms and the asymptotic solutions can be computed. By virtue of the gauge/gravity duality the behaviours of the bulk fields are related to the operators and currents which are present in dual field theory. In this example, the scalar field asymptotic form corresponds to the condensation operator (order parameter) of the superconducting condensate.

Detailed relations between physical quantities of the bulk gravitational theory and the boundary CFT are collected in the holographic dictionary. For example the metric tensor in the bulk corresponds to the stress-energy tensor of the boundary theory. Similarly gauge field potential corresponds to some currents.

By using this machinery one can compute relevant quantities, that describe the boundary strongly coupled field theory using only the computations from the gravitational bulk. In this way one can note that the scalar condensation operator undergoes a phase transition of the second kind and the conductivity reveals characteristic patterns being the result of the superconducting gap.

Chapter 3

Methods

In the previous section I described the physical foundations of problems I was dealing with during my doctoral research. Now I shall focus on the technical side of the research. I will briefly explain the theoretical methods I used to model considered systems and then the numerical ones that helped me to extract viable physical information from the theory.

3.1   Theoretical methods

Below I list several theoretical methods which were used for establishing the problems considered in all papers included in this thesis. I give a basic description of these methods, that allowed me to set up the model, derive the equations of motion, introduce the boundary conditions and analyse the solutions.

3.1.1   Equation of motion

The research collected in this thesis utilizes rather standard methods of contemporary theoretical physics in the field of gravitation. I start with defining a theoretical set up, by writing down the action

$$S = \int d^n x \sqrt{-g}(R + \mathcal{L}_M), \tag{3.1}$$

where R is the Ricci scalar and $\mathcal{L}$ is the matter Lagrangian density. At this point one defines the composition of the physical space, namely the fields that take part in the theory. Moreover the dimensionality n of the space is defined, too. Here the gravitational part of the action comes from standard General Relativity, no other curvature terms were used in this research. At this point some general properties of the theory might be investigated such as symmetries.

Using the widely known variational principle,

$$\delta S = 0, \tag{3.2}$$

we calculate adequate functional derivatives, and we derive equations of motion, that define the behaviour of the matter fields.

Obtaining the gravitational part requires varying the action with respect to the metric tensor $g_{\mu\nu}$. With few transformations we obtain the Einstein equation

$$R_{\mu\nu} - \frac{1}{2}g_{\mu\nu}R = T_{\mu\nu}, \tag{3.3}$$

which gives us a complete set describing both the spacetime and the fields dynamics.

At this point the problem needs to be precisely specified. Depending on the physical problem and other theoretical justifications one should make a series of assumptions on what the final solution should look like. This requires us to select a form of the metric and fields, which should be put into the generic equations of motion in order to obtain a solveable system of differential equations.

For example an ansatz for static and spherically symmetric spacetime is given by

$$ds^2 = g_{\mu\nu}dx^\mu dx^\nu = f(r)dt^2 + g(r)dr^2 + r^2d\theta^2 + r^2\sin^2\theta d\phi^2 \tag{3.4}$$

and a sample dynamical scalar field would take a form

$$\Psi = \psi(r)Y_{lm}(\theta, \phi)e^{-i\omega t}, \tag{3.5}$$

where Y_{lm} are spherical harmonics. Substituting this ansatz into the equations of motion gives us a set of differential equations which sometimes can be solved analytically, but more often numerically.

3.1.2 Boundaries and asymptotics

Solving a differential equation requires providing boundary conditions on both ends of the domain. Usually, some of these boundary conditions are straightforward, like $g_{tt} = 0$ on the event horizon. On the other hand, they can originate from the properties of the spacetime, for example axial symmetry of the spacetime forces the axial symmetry of the fields inside.

However there are situations where the boundary conditions are not given by physics right away. Instead one has to find an analytical behaviour of the solution in some certain limits and then impose it on the numerical solution.

Such cases take place in many black hole physics scenarios. Let us consider a few examples.

First when we have several fields in the vicinity of a black hole. If one of the fields is precisely bound, but the remaining are not, one ought to take a limit of the equations of motion, introduce the known boundary conditions and then after several mathematical transformations obtain some conditions on the remaining functions.

In the second case, we have a similar situation to the first one. However one of the equations of motion has a singularity in a spatial point, for instance the event horizon. If adjust to zero value, a field on a horizon brings regularity of the system and eradicates the singularity from the equation then this is the boundary condition we were looking for.

Third example is a bit more complex and for an illustration we will take the case of the holographic superconductor from one of the contributions contained in this thesis. The equation will be stripped from physical constants that are irrelevant in this explanation. In the asymptotically AdS spacetime the metric behaves like

$$g_{tt} \sim r^2, \tag{3.6}$$

when $r \to \infty$. Therefore by taking a simple limit of an equation of motion, we are guaranteed to obtain infinite terms. This is not something that we are looking for. However the Frobenius method comes with a rescue. The equation of motion for the scalar field in this particular case yields

$$\psi'' + \left(\frac{f'}{f} + \frac{2}{r}\right)\psi' + \left(\frac{\phi^2}{f} - m^2\right)\frac{\psi}{f} = 0, \tag{3.7}$$

where $g_{tt} = f(r) = r^2(1 - (r_h/r)^3)$, ϕ is the electric potential, m is the mass of the scalar and prime denotes a derivative with respect to r.

If one takes the limit $r \to \infty$ of the above equation to the leading order terms, we get

$$\psi'' + \frac{4}{r}\psi' - \frac{m^2}{r^2}\psi = 0. \tag{3.8}$$

Having an equation in such form allows us to use the Frobenius method and using the expansion

$$\psi(r) = r^\rho \sum_n c_n r^{-n}. \tag{3.9}$$

By differentiating the series and substituting it into the equation we obtain the characteristic equation for leading order exponents ρ,

$$(\rho - n)(\rho - n - 1) + 4(\rho - n) - m^2 = 0, \tag{3.10}$$

with final solutions

$$\rho_\pm = \frac{1}{2}\left(-3 \pm \sqrt{9 + 4m^2}\right), \tag{3.11}$$

which provides us with asymptotic solution

$$\psi = \frac{\psi_1}{r^{-\rho_+}} + \frac{\psi_2}{r^{-\rho_-}} + \mathcal{O}\left(\frac{1}{r^{-\rho_-+1}}\right). \tag{3.12}$$

At the end of the day such analysis delivers us the boundary conditions for the numerical attempts. Moreover it gives the constrains on the physical parameters, such as scalar mass. In this particular case in order to obtain a stable scalar condensate one requires it to vanish in infinity, therefore $\rho_\pm$ must be negative. On the other hand, the exponents also must be real, so the scalar does not have oscillating modes. This requires the term under the square root in (3.11) to be positive and gives the bounds on the mass parameter

$$m^2 \geqslant -\frac{9}{4}. \tag{3.13}$$

Such limitation in these theories is called Breitenlohner-Freedman limit for tachyonic fields in AdS spacetimes.

Summarizing this subsection. The analysis of boundary behaviour of the equation in question brings not only the clues for selecting the boundary conditions, but also useful information about the role of some physical parameters in the theory.

3.1.3 Other quantities and benchmarks

Finding the precise solution of the equations of motion is definitely not the final goal of most of research projects. It is necessary to study the behaviour of relevant physical quantities. In this short paragraph I will discuss the calculation of free energy of the physical state of the system, as it is the most used benchmark in all research conducted for this thesis.

Helmholtz free energy, or simply free energy, is a thermodynamical potential that was introduced for gas related processes, where the temperature and volume can be controlled. Free energy also sets the equilibrium conditions and plays a key role in phase transitions. The preferable physical state is the one where free energy is minimal, which is an obvious analogy to the least action principle in the realm of field theory.

Classically free energy is defined as

$$F = U - TS_E, \tag{3.14}$$

where U is the internal energy, T is the temperature and S_E is the entropy.

Surprisingly this definition is still valid in black hole physics. However the right-hand side components have different definitions and meanings. Let us start one by one, the internal energy counterpart for a gravitational system is the quasilocal energy introduced by Brown and York in their famous work on conserved quantities derived from the gravitational action [63]. The definition of the energy in the gravity is a vast problem itself, here however the authors define it relatively with respect to the flat Minkowski spacetime. It takes the form of

$$U = -\frac{1}{8\pi} \lim_{r \to r_b} \oint_{\mathcal{S}^2} (k - k_0)\sqrt{\sigma}d^2x, \tag{3.15}$$

where k is the external curvature of the studied metric, while k_0 is the external curvature of the flat spacetime. Next, σ is the determinant of a metric on a time-like hypersurface $\mathcal{S}^2$ with radius r_b, which is present in the limit.

Following quantities such as temperature and entropy are well defined in black hole thermodynamics. The definition of gravitational analogue for temperature requires the surface gravity evaluated on the event horizon of the black hole [65]

$$\kappa^2 = -\frac{1}{2}(\nabla^a \chi^b)(\nabla_a \chi_b)\Big|_{Horizon}, \tag{3.16}$$

where χ^a is the Killing field of the considered spacetime. Then the Hawking temperature is simply defined as

$$T_H = \frac{\kappa}{2\pi}. \tag{3.17}$$

On the other hand, the black hole entropy is simply proportional to the area of the even horizon

$$S_E = \frac{1}{4} \oint_{\mathcal{S}_H^2} \sqrt{h} d^2 x, \tag{3.18}$$

with h being the metric determinant on the event horizon.

By using these quantities one can obtain the free energy for different black hole solutions. However it is not a fully general method. Unfortunately it is unable to capture non-trivial configurations of fields present in the vicinity of a black hole, such as scalar (or more complicated) hair. Therefore for such research it is recommended to compute free energy straight from the basis of the theoretical set up, using the classical action

$$F = TS_{cl}. \tag{3.19}$$

The term *classical* refers to the signature of the metric. In relativistic physics the time component of the spacetime always has the different sign than the other, spatial, components. Depending on the convention, it might be negative or positive. Nevertheless the goal is to impose the Euclidean signature to the metric, so all coordinates have the same sign. To achieve such goal one has to perform the Wick rotation on the time coordinate

$$t \rightarrow i\tau, \tag{3.20}$$

with τ being the imaginary time.

3.2 Numerical methods

Most of the field theory research I dealt with can be brought down to boundary value problems (BVPs). These however are not easily solvable, especially if one considers a more sophisticated gravitational set up, such as Kerr metric, or if the problem is non-linear. Some of them, can be solved using analytic methods such as Sturm-Liouville approach. Nevertheless in general, it requires making some assumptions that are not always possible and we have to use numerical approximations to the problem.

The core philosophy of various numerical methods is the same in most cases – translating a differential problem into an algebraic one. Below, I briefly discuss the methods I used in works being the part of this thesis and illustrate them with simple examples.

3.2.1 Pseudo-spectral collocation method

The key idea of (pseudo-)spectral methods is to approximate the sought function in a differential equation with a combination of spectral functions [66]. We require such functions ϕ_i to be orthogonal

$$\int_{\mathcal{M}} \phi_i(x) \phi_j(x) dx = \delta_{ij}. \tag{3.21}$$

The most popular choices are sines and cosines, where we talk about Fourier spectral methods, or Chebyshev polynomials. Chebyshev polynomials of the first kind can be defined in the following, recursive way

$$T_0(x) = 1,$$
$$T_1(x) = x,$$
$$T_{n+1}(x) = 2xT_n(x) - T_{n-1}(x),$$

or with a more general formula

$$T_n(x) = \cos(n \arccos(x)). \tag{3.22}$$

Second formulation reveals that Chebyshev polynomials are in fact cosines in a disguise. However they are used in problems that do not require the solution to be periodic. The domain of Chebyshev polynomials is the interval $[-1, 1]$. Therefore if one wants to use this technique, appropriate transformations of the independent variable are required. After preparing the equation to a Chebyshev-eligible form, we can solve it. For illustrative purpose, we use a standard second order ordinary differential equation as an example

$$y'' + g(x)y' + h(x)y = s(x), \tag{3.23}$$

where $g(x)$, $h(x)$ and $s(x)$ are generic functions of x. To solve a BVP with the Chebyshev pseudo-spectral method one has to substitute a series of Chebyshev polynomials

$$y(x) \approx \sum_i^N a_i T_i(x), \tag{3.24}$$

into the given equation, where a_i are the series coefficients (and become the values, which we want to compute as a solution to the problem). Mind that N is the number of polynomials used and it also denotes its highest order. The great advantage of this method is that the derivatives can be computed analytically, as it is naturally straightforward to compute a derivative of a polynomial. Then comes a crucial point, where one has to collocate the equation on a grid. For the sake of convergence one should not use any uniform grids. Instead natural grids for this method are Chebyshev-related ones – either zeros (aka Gauss-Lobatto grid) or extremes of the highest N-order polynomial. The former one is defined as

$$x_n = \cos(n\pi/N), \tag{3.25}$$

and it gives a high density of points near the edges of the numerical domain, while the central part remains significantly less dense. After substituting these points into the master equation we achieve the goal of translating a differential problem into an algebraic one. We obtain a set of N algebraic equation with N unknowns

$$\begin{cases} f_1(a_1, a_2, \cdots, a_n) = s_1, \\ f_2(a_1, a_2, \cdots, a_n) = s_2, \\ \vdots \\ f_n(a_1, a_2, \cdots, a_n) = s_n, \end{cases} \tag{3.26}$$

where the a_i coefficients ought to be found.

The next problem is to solve such system. In case of a linear differential equation it is only a matter of computing an inverse of the matrix. However in physical applications we usually deal with non-linear differential equation. In such case one has to use iterative schemes for minimizing the equations, for instance Newton-Raphson method.

One of the greatest advantages of the pseudo-spectral method is its convergence. Although it requires only a few points in a spatial discretization in order to achieve high accuracy. Moreover a properly constructed algorithm should demonstrate exponential convergence with exponentially decreasing error with an increase of N. This method was used in the contribution [72].

3.2.2 Shooting method

A BVP is usually defined as a second order differential equation with its values (Dirichlet boundary conditions) specified on the boundaries or the values of the derivatives (Neumann boundary conditions). The idea of the shooting method can be brought down to translating a BVP into an initial value problem (IVP).

Let us proceed with an exemplar ODE, exactly the same as in the previous paragraph

$$y'' + g(x)y' + h(x)y = s(x), \tag{3.27}$$

with Dirichlet boundary conditions

$$y(x_L) = a, \qquad y(x_R) = b, \tag{3.28}$$

denoting values of the solution on the left and right-hand side of the numerical domain.

We can reconsider equation (3.27) and instead of using boundary conditions (3.28), utilize an alternative pair

$$y(x_L) = a, \qquad y'(x_L) = \eta, \tag{3.29}$$

which describes the value of the solution and its derivative on the left-hand side of the numerical domain. The parameter η is arbitrary at the moment. Our second order ODE can be rewritten into a set of two first order ODEs

$$y' = u,$$
$$u' + g(x)u + h(x)y = s(x),$$

which allows us to utilize a variety of solvers for IVPs and integrate these equations from x_L to x_R. We can use standard Runge-Kutta schemes, Adams-Bashford method or more sophisticated adaptive stepsize algorithms such as Dormand-Prince or Fehlberg methods.

After the integration we check if the solution fulfills the right-hand side boundary condition 3.28. The odds that our initial guess of η will bring the desired behaviour of our function are rather small. Therefore our goal is to minimize the objective function

$$F(\eta) = |b - y(x_R; \eta)|, \tag{3.30}$$

which is the absolute error between computed and target value of the solution. Alternatively one can use different error, such as squared error. Having the objective function defined we have to minimize it with a chosen algorithm. It can be a simple bisection search, gradient descent or Newton-Raphson procedure. After several iterations we should obtain the value η, for which the solution fulfills the BVP boundary conditions. This numerical method was used in contributions [70, 71].

3.2.3 Spectral differentiation

Spectral differentiation relies on constructing a differentiation matrix, which is applied to a function discretized on a grid. This method is thoroughly described in [67], here I only briefly describe its usage.

It sounds similar to techniques such as finite differences method (FDM) and from the outside it really is, especially in the simple usage of this method. At the end of the day a differential equation can be translated to a matrix equation, with specific differentiation matrices as the components.

One of the greatest advantages of this method is the accuracy of the computed derivative. In case of FDM, usually the differentiation error is proportional to the stepsize of the grid. Because of that it is necessary to exploit relatively large grids, sometimes containing thousands of points, in order to achieve acceptable results. However this is not the case of spectral differentiation, where only few grid points are required for obtaining satisfying results.

Suppose we can interpolate any function in our domain $x \in [-1, 1]$ with a polynomial, e.g. Chebyshev polynomial. Let $p(x)$ be an interpolant of v_i values of some function, defined on the Chebyshev points (3.25). On a small grid, with $N = 2$ (three points in the grid $x_0 = 1$, $x_1 = 0$ and $x_2 = -1$), we have a quadratic polynomial

$$p(x) = \frac{1}{2}x(1 + x)v_0 + (1 - x)(1 + x)v_1 + \frac{1}{2}x(x - 1)v_2. \tag{3.31}$$

The derivative of the interpolant yields

$$p'(x) = (x + \frac{1}{2})v_0 - 2xv_1 + (x - \frac{1}{2})v_2. \tag{3.32}$$

The differentiation operation can be rewritten as a matrix equation

$$w = D_2 v, \tag{3.33}$$

where w is a vector of values of the derivatives of v, defined on the grid and the differentiation matrix is defined as

$$D_2 = \begin{pmatrix} \frac{3}{2} & -2 & \frac{1}{2} \\ \frac{1}{2} & 0 & -\frac{1}{2} \\ -\frac{1}{2} & 2 & -\frac{3}{2} \end{pmatrix}. \tag{3.34}$$

This result can be generalized to N number of grid points and used in discretization of differential equations.

Taking the equation from previous paragraphs (3.27) as an example, we write

$$D_N^2 y + I_g D_N y + I_h y = I_s, \tag{3.35}$$

where y is a solution vector and I are diagonal matrices containing the values of the functions g, h and s. These matrices can be collected into a single operator

$$L = D_N^2 + I_g D_N + I_h. \tag{3.36}$$

At this point one should introduce the boundary conditions to the system by substituting adequate rows and columns of the L matrix and right-hand side of the equation. Finally, this allows us to straightforwardly solve the equation

$$y = L^{-1} I_s, \tag{3.37}$$

where we invert the L matrix with a preferred method. In case of a non-linear equation the algorithm gets only little more complicated. One can assume the form of the solution and substitute it into the non-linearity as the initial guess. Then one ought to solve the problem (3.37) iteratively until stopping conditions are fulfilled. This method was used in contributions [73, 74].

Chapter 4

Original contributions

In this chapter I include the copies of the articles that were co-authored by me during my doctoral studies. They do not present a strict cycle, but they are oriented around the issue of interactions between visible and dark sectors. For every article I present a short summary listing the theoretical basis of the article and its most important results.

4.1   Summary of articles

4.1.1   Ultra-compact spherically symmetric dark matter charged star objects

Reference

B. Kiczek and M. Rogatko, *Ultra-compact spherically symmetric dark matter charged star objects*, JCAP 09 (2019) 049.

Motivation

As it was mentioned in the previous chapters, the addition of dark sector fields to the known systems may change interestingly their behaviour. In this work, the goal was to study the influence of the additional dark sector U(1) gauge group on the solutions describing ultra-compact starlike objects. Naturally the dark photon is mixed with the Maxwell field via kinetic mixing, therefore we expect new dependencies on some kind of effective charge, being a mixture of the electric charge and a hypothetical charge originating form the dark sector group.

Therefore we wish to obtain the solution of the spacetime around a compact spherically symmetric object charged, in general, with electric charge, the *dark charge* and some mixture of both. After obtaining such solution it is interesting to see what properties it has.

Methods

We start with the definition of action

$$S = \int d^4x \sqrt{-g} \left(R - \frac{1}{4}F_{\mu\nu}F^{\mu\nu} - \frac{\alpha}{4}B_{\mu\nu}F^{\mu\nu} - \frac{1}{4}B_{\mu\nu}B^{\mu\nu} \right), \tag{4.1}$$

where $F_{\mu\nu} = 2\nabla_{[\mu}A_{\nu]}$ is the ordinary Maxwell field while $B_{\mu\nu} = 2\nabla_{[\mu}B_{\nu]}$ is the U(1) gauge field related to the dark sector.

By varying the action over all fields we get the equations of motion,

$$G_{\mu\nu} = T_{\mu\nu}, \tag{4.2}$$

$$\nabla_\mu F^{\mu\nu} + \frac{\alpha}{2}\nabla_\mu B^{\mu\nu} = 0, \tag{4.3}$$

$$\nabla_\mu B^{\mu\nu} + \frac{\alpha}{2}\nabla_\mu F^{\mu\nu} = 0. \tag{4.4}$$

In the first approximation we pick the spherically symmetric ansatz for the line element given by

$$ds^2 = -e^{2\phi(r)}dt^2 + e^{2\lambda(r)}dr^2 + r^2(d\theta^2 + \sin^2\theta d\phi^2), \tag{4.5}$$

with gauge fields in form

$$A_t = -\frac{Q}{r}, \quad B_t = -\frac{Q_d}{r}. \tag{4.6}$$

By plugging these quantities into Einstein equations and solving them we get

$$e^{-2\lambda(r)} = 1 - \frac{2M}{r} + \frac{Q_c^2}{4r^2}, \quad \lambda(r) = -\phi(r), \tag{4.7}$$

with the effective charge $Q_c^2 = Q^2 + Q_d^2 + \alpha Q Q_d$, which constitutes the solution of the metric outside spherically symmetric ultra-compact starlike object.

Using this derived spacetime we considered a fluid sphere, with Tolman-Oppenheimer-Volkoff (TOV) equations derived in the end

$$p'(r) = \frac{Q_c(r)'Q_c(r)}{2r^4} - \frac{(\rho + p(r))}{r^2} \left[m(r) + \frac{\mathcal{F}_c(r)}{2} + \frac{r^3 p(r)}{2} - \frac{Q_c(r)^2}{8r} \right] \left[1 - \frac{2m(r)}{r} - \frac{\mathcal{F}_c(r)}{r} \right]^{-1}. \tag{4.8}$$

In the fifth section of the paper we numerically investigated the emergence of scalar hair and the influence of the dark charge on their distribution.

Results

First of all, we derived the gravitational metric of the outside of spherically symmetric ultra-compact starlike object. The metric can be seen as a generalised Reisner-Nordstrom solution, with an effective charge being a composition of electric charge, the dark sector related charge and a mixing term.

Then we considered a dark matter charged fluid sphere, where TOV equations have been derived. Solving them was beyond of the scope of this article, however, we hope to return to these calculations elsewhere, as the dark sector impact on the stellar evolution constitutes a fascinating problem.

Next, the stability bounds on mass and charge for ultra-compact object were found. It was revealed that the compact object with hidden sector charge can reach smaller size than the object made from the visible components only.

Finally we investigated the possibility of emergence of the visible scalar hair. We checked what are the conditions and how these solutions behave. It was found that the large quantity of dark sector charge in the system results with shrunk and smaller scalar condensate.

4.1.2 Influence of dark matter on black hole scalar hair

Reference

B. Kiczek and M. Rogatko, *Influence of dark matter on black hole scalar hair*, Phys. Rev. D **101**, 084035 (2020).

Motivation

In the previous paper we have studied scalar hair around an ultra-compact object influenced by U(1) dark matter sector. This work is a natural continuation of it. We have already seen that in the probe limit, where the gravitational background and both gauge fields are fixed, the visible scalar hair was shrinking with the growth of *dark charge* in the system. In this work we quit the probe limit scenario and solve the fully backreacting system.

Methods

We start with the action

$$S = \int_{\mathcal{M}} d^4x \sqrt{-g} \Big(R - \frac{1}{4}F_{\mu\nu}F^{\mu\nu} - \frac{\alpha}{4}B_{\mu\nu}F^{\mu\nu} - \frac{1}{4}B_{\mu\nu}B^{\mu\nu} - |D\psi|^2 - m^2\psi^2 \Big) - \int_{\partial\mathcal{M}} d^3x \sqrt{-\gamma}\mathcal{K},$$
(4.9)

as in the previous case $F_{\mu\nu}$ is a Maxwell field strength tensor, $B_{\mu\nu}$ is a strength tensor of a hidden sector vector boson. The complex scalar field $\Psi = \psi e^{i\theta}$, where θ denotes the phase, is coupled only to the ordinary electromagnetic field by the covariant derivative $D_\mu = \nabla_\mu - iqA_\mu$. The last term of the action is the Gibbons-Hawking boundary term of our box, where the considered objects are contained. The box is a 3-dimensional hypersurface with γ metric and the extrinsic curvature $\mathcal{K}$.

Varying the action gives us the equations of motion, for our fields we choose following ansatz

$$ds^2 = -g(r)h(r)dt^2 + \frac{dr^2}{g(r)} + r^2(d\theta^2 + \sin\theta^2 d\phi^2), \qquad (4.10)$$

$$A_\mu dx^\mu = \phi(r)dt, \qquad (4.11)$$

$$B_\mu dx^\mu = \chi(r)dt, \qquad (4.12)$$

$$\Psi = \psi(r), \qquad (4.13)$$

where the metric is spherically symmetric and matter fields depend only on the radial coordinate. Finally we get the equations of motion

$$h' - rh\psi'^2 - \frac{q^2 r\phi^2\psi^2}{g^2} = 0, \qquad (4.14)$$

$$g' + g\left(\frac{1}{r} + \frac{1}{2}r\psi'^2\right) + \frac{q^2 r\phi^2\psi^2}{2gh} - \frac{1}{r} + \frac{r}{2h}(\phi'^2 + \alpha\chi'\phi' + \chi'^2 + m^2 h\psi^2) = 0, \qquad (4.15)$$

$$\phi'' + \left(\frac{2}{r} - \frac{h'}{2h}\right)\phi' - \frac{2q^2\phi\psi^2}{\tilde{\alpha}g} = 0, \qquad (4.16)$$

$$\psi'' + \left(\frac{2}{r} + \frac{h'}{2h} + \frac{g'}{g}\right)\psi' + \left(\frac{q^2\phi^2}{gh} - m^2\right)\frac{\psi}{g} = 0, \qquad (4.17)$$

$$\chi'' + \left(\frac{2}{r} - \frac{h'}{2h}\right)\chi' + \frac{\alpha q^2\chi\psi^2}{\tilde{\alpha}g} = 0. \qquad (4.18)$$

We solve these equations simultaneously using the shooting method. In simple words, we integrate the fields from the inner boundary to the outer one using the standard Runge-Kutta 4 method. At the outer boundary we check if the boundary conditions are fulfilled. If not we pick new initial conditions using the bisectional search and repeat the procedure until reaching the convergence.

After obtaining adequate solutions we analyse the system using the thermodynamical framework. Apparently the theory has three phases:

- Generalised Reisner-Nordstrom (RN) black hole (the analytic result of the previous work),

- Hairy black hole (HBH),

- Boson star (BS).

We adopt thermodynamical treatment by calculating the free energy of the system

$$F = T_H S_{cl}, \qquad (4.19)$$

with S_{cl} being the classical action, and checking what are physical implications of the presence of the *dark charge* in the system.

Results

We have investigated the influence of the dark sector U(1) gauge group related charge on the possible configurations in the Einstein-Maxwell-dark photon-scalar theory. The main result of this calculation is the phenomenon of shifting phase boundaries caused by the presence of the *dark charge*. This process can be seen on the schematic phase diagram presented below.
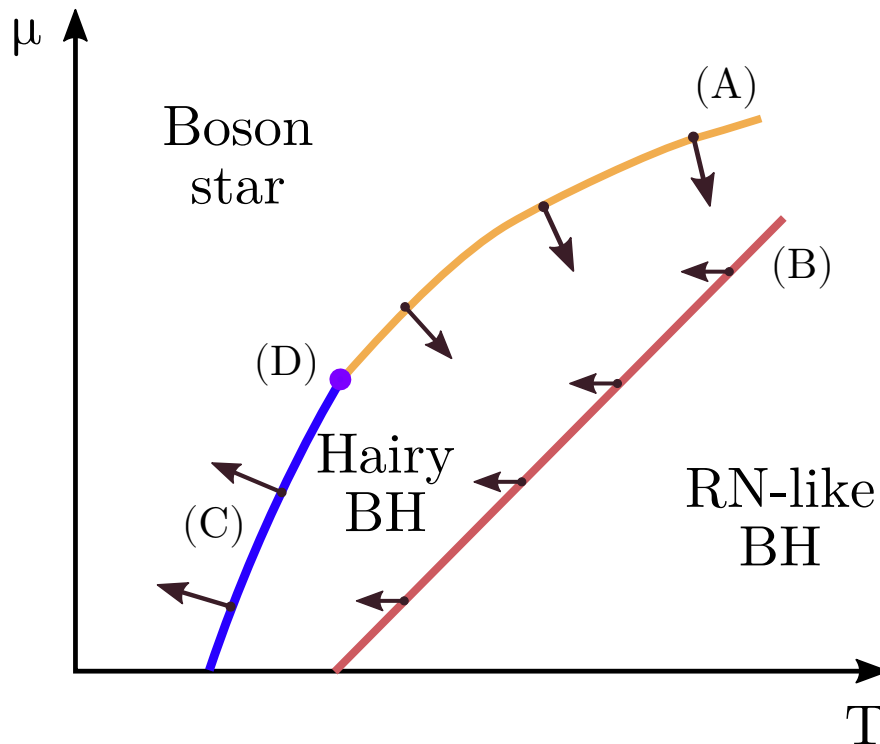

Figure 4.1: The schematic phase diagram of the Einstein-Maxwell-dark photon-scalar theory wit spherically symmetric asymptotically flat solutions.

The diagram is basically a plot on the μ-T plane, which stand for the chemical potential (which is a boundary value of the Maxwell field on the box boundary, the name is a loose analogy to the AdS/CFT rigorously defined chemical potential) and the Hawking temperature.

We found that adding more *dark charge* to the system significantly shrinks the parameter space available for hairy black hole solutions to emerge. It happens both on the HBH-RN boundary (second kind phase transition) and on the BS-HBH boundary (first kind phase transition).

We also noted a very interesting thing. Namely there are points in the parameter space that are completely immune to the presence of dark sector, as the system with these particular parameters remains invariant under the change of *dark charge* amount. These are so-called isosbestic points, which appeared to be well-known in the realm of condensed matter physics.

4.1.3 Holographic DC SQUID in the presence of dark matter

Reference

B. Kiczek, M. Rogatko and K. I. Wysokiński, *Holographic DC SQUID in the presence of dark matter*, JCAP 01 (2021) 063.

Motivation

Superconducting quantum interference devices or simply SQUIDs constitute one of the most sensitive sensors constructed by humans. They are able to detect a slightest change of the magnetic field, a.k.a. magnetic flux quantum.

A SQUID is a loop made of two Josephson junctions. A Josephson junction (JJ) consists of two superconductors divided by a thin layer of non-superconducting material, i.e. a metal or an insulator. Its characteristic feature is the flow of a direct current, which magnitude depends on the phase difference between the Cooper pair wave functions in both superconductors

$$I = I_{max} \sin \phi. \tag{4.20}$$

Where $\phi = \phi_R - \phi_L$, with $\phi_{L(R)}$ being the phases of the superconductor order parameter on the left (right) side of the junction. If one applies external magnetic field to a SQUID, the maximal current which can flow through it is given by

$$I_{max} = I_c \left| \cos \frac{\pi \Phi}{\Phi_0} \right|, \tag{4.21}$$

where Φ is the magnetic flux and $\Phi_0 = \frac{h}{2e}$ is the magnetic flux quantum.

The sensitivity of SQUIDs and interesting progress in the usage of superconductors in the dark matter search [20, 21, 22] motivates us to pursue in that direction. We discuss the usage of SQUID in possible dark sector searches.

In this work we used the AdS/CFT correspondence to build a holographic SQUID, where we modelled an injection of a DM particle into one of Josephson junctions. To show the effect of this interaction we compare the DM case with a DM-free scenario.

Methods

The first ingredient of the AdS/CFT based model is the adequate gravitational background, which naturally must be asymptotically anti de Sitter. For this purpose we use the gravitational action

$$S_g = \int \sqrt{-g} \, d^4x \left(R - \Lambda \right), \tag{4.22}$$

with a negative cosmological constant $\Lambda = -6/L^2$. Later on we use the AdS-Schwarzschild black hole line element as a gravitational background

$$ds^2 = -f(r)dt^2 + f^{-1}(r)dr^2 + r^2(d\xi^2 + dy^2). \tag{4.23}$$

With $f(r) = \frac{r^2}{L^2}(1 - r_0^3/r^3)$ and the corresponding Hawking temperature of the BH is $T_H = \frac{3r_0}{4\pi L^2}$, which is a very important quantity for the model in question.

The matter part of the action is the Abelian-Higgs sector with additional U(1) gauge field belonging to the hidden sector

$$S_{dm+EM+H} = \int \sqrt{-g}\ d^4x \left(-\frac{1}{4}F_{\mu\nu}F^{\mu\nu} - [\nabla_\mu\psi - i\ A_\mu\psi]^\dagger [\nabla^\mu\psi - i\ A^\mu\psi] - m^2|\psi|^2 \right.$$
$$\left. -\frac{1}{4}B_{\mu\nu}B^{\mu\nu} - \frac{\zeta}{4}F_{\mu\nu}B^{\mu\nu} \right). \tag{4.24}$$

We model the presence of the dark sector in one of Josephson junctions by using a spatially dependent kinetic mixing parameter

$$\zeta(\xi) = \alpha_0 e^{-(\xi-\xi_0)^2/\lambda^2}. \tag{4.25}$$

With ξ_0 being the centre of the affected JJ and λ a Gaussian broadening, which can be loosely interpreted as a de Broglie's wavelength of a DM particle. By varying the action and substituting all relevant quantities into the obtained formulas we get our system of equations of motion

$$\partial_r^2|\psi| + \frac{1}{r^2\ f}\partial_\xi^2|\psi| + \left(\frac{2}{r} + \frac{\partial_r f}{f}\right)\partial_r|\psi| + \left[\frac{1}{f^2}\ M_t^2 - \frac{1}{r^2\ f}\ M_\xi^2 - M_r^2 - \frac{m^2}{f}\right]|\psi| = 0, \tag{4.26}$$

$$\tilde\zeta\left[\partial_r^2 M_t + \frac{2}{r}\ \partial_r M_t + \frac{1}{r^2\ f}\ \partial_\xi^2 M_t\right] - \frac{2}{f}\ M_t\ |\psi|^2 + \frac{1}{2}\partial_\xi\zeta\frac{\zeta}{2}\frac{1}{r^2 f}\partial_\xi M_t = 0, \tag{4.27}$$

$$\tilde\zeta\left[\partial_\xi^2 M_r - \partial_\xi\partial_r M_\xi\right] - 2\ r^2\ M_r\ |\psi|^2 - \frac{1}{2}\partial_\xi\zeta\frac{\zeta}{2}\left(\partial_\xi M_r - \partial_r M_\xi\right) = 0, \tag{4.28}$$

$$\tilde\zeta\left[\partial_r^2 M_\xi - \partial_r\partial_\xi M_r + \frac{\partial_r f}{f}\left(\partial_r M_\xi - \partial_\xi M_r\right)\right] - \frac{2\ M_\xi}{f}\ |\psi|^2 = 0, \tag{4.29}$$

which is a set of non-linear second order partial differential equations. By using the Frobenius method we obtain asymptotic forms of the fields on the AdS boundary

$$|\psi| = \frac{|\psi^{(1)}(\xi)|}{r^{\Delta_{(1)}}} + \frac{|\psi^{(2)}(\xi)|}{r^{\Delta_{(2)}}} + \mathcal{O}(r^{-3}), \tag{4.30}$$

$$M_t = \mu(\xi) - \frac{\rho(\xi)}{r} + \mathcal{O}(r^{-2}), \tag{4.31}$$

$$M_r = \mathcal{O}(r^{-3}), \tag{4.32}$$

$$M_\xi = \nu(\xi) + \frac{J(\xi)}{r} + \mathcal{O}(r^{-2}). \tag{4.33}$$

These expansions carry parameters such as μ, ρ, ν, J and $\psi^{(i)}$, which are of key importance as they constitute relevant physical quantities of the CFT living on the boundary of the bulk AdS spacetime. They denote respectively the chemical potential, charge density, velocity of the super current carriers, electric current and the condensation parameter (with $i = 1$ or $i = 2$, depending on the particular choice of the model). By solving the EOMs and using these expansions we can obtain the information about the strongly coupled boundary quantum field theory.

To solve these complicated equations we use a numerical method based on spectral methods. Precisely it is a pseudo-spectral Chebyshev collocation method. In brief, we assume that our fields are combinations of Chebyshev polynomials with some factors. We substitute this assumption into the EOMs and collocate the equations on a Gauss-Lobato grid. In such way we translate a calculus problem into an algebraic one. Then we solve a nonlinear system of algebraic equations using the iterative Newton-Raphson method, until we reach convergence.

Results

As a warm up we check the simplified case of a homogeneous holographic superconductor under the influence of the dark sector field. We find that its critical quantities such a critical temperature and critical chemical potential are shifted due to the presence of the coupling. This gives us a clue for further investigation in the full problem.

When we move to solving the equation of the holographic SQUID we start with the DM-free scenario. We suppose that both Josephson junctions are identical, considering every parameter from shape to chemical potential. In such case the SQUID is trivial, as no interference is observed.

As we add the hidden sector into the consideration we observe an interference pattern, which is generated due to the current imbalance between junctions, that finally causes an effective magnetic flux. This gives us a criterion for a possible detection of such particle.

We also tested the dependence of the Gaussian width λ on the *signal strength* - the maximal current. It can be seen on a figure below.

The strongest *signal* is seen when λ is very close to the width of the gap in the Josephson junction. It is also an interesting clue for some possible experiments, as the gap width might be engineered for a particular wavelength, corresponding to the mass, of a sought particle.

Naturally our considerations cannot be treated as some blueprint for an experiment. A relevant calculations in a realm of conventional condensed matter and high energy physics should be conducted. However they might be a bit challenging, as considering such phenomenon on the holographic ground is much easier than in quantum field theory based approach.
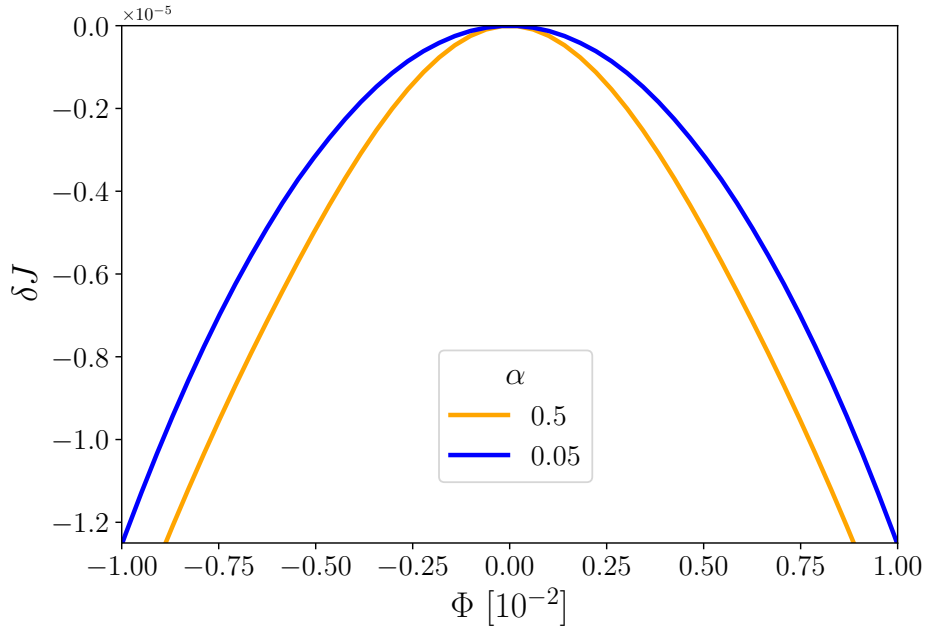
Figure 4.2: A dependence of a current difference as a function of magnetic flux. Two curves represent different couplings of the hidden sector.
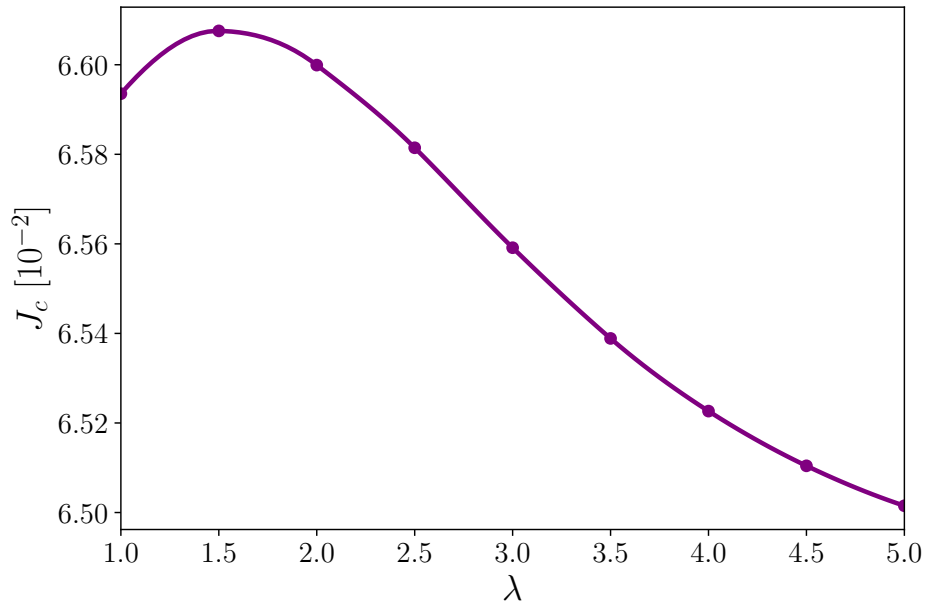

Figure 4.3: Critical current vs. width of the Gaussian incursion.

Erratum

During the collection of materials for this thesis an essential typos have been spotted in the original article. After the equation (4.11) on page 18 following definitions shall be corrected:

$$\tilde{F}_{\mu\nu} = 2\nabla_{(\mu}\tilde{A}_{\nu)} \quad \rightarrow \quad \tilde{F}_{\mu\nu} = 2\nabla_{[\mu}\tilde{A}_{\nu]},$$
$$\tilde{B}_{\mu\nu} = 2\nabla_{(\mu}\tilde{B}_{\nu)} \quad \rightarrow \quad \tilde{B}_{\mu\nu} = 2\nabla_{[\mu}\tilde{B}_{\nu]}.$$

4.1.4 Axionlike dark matter clouds around rotating black holes

Reference

B. Kiczek and M. Rogatko, *Axionlike dark matter clouds around rotating black holes*, Phys. Rev. D**103**, 124021 (2021).

Motivation

There is no doubt that axions constitute one of the most prominent candidates for dark matter. Their physical properties such as stability and their ability to form large scale structures, due to they possible low masses, have granted them this status. However, it is interesting to evaluate if there are any chances on the emergence of axionlike DM structures on the stellar scale.

The studies of dark matter at the stellar scale can be theoretically performed in the black hole, as well as other compact object, surroundings. Conclusions from these investigations can be used to apply similar calculations for regular stars, such as the Sun. Lessons learnt from these considerations can be very beneficial for planning future experiments, as it is not excluded that dark matter may form some kind of structures even in the Solar System. The questions is what kind of structures are these and what do they look like?

In a recent paper Boskovic with collaborators [25] have shown, using an analytical approximation, that axions may form stationary configurations around slowly rotating black holes. In our paper we generalise this result on different masses of axions and angular momentum of the hosting black holes.

Methods

We start with the action of the theory

$$\mathcal{S} = \int d^4x \sqrt{-g} \left[R - \frac{1}{4} F_{\mu\nu} F^{\mu\nu} - \frac{1}{2} \nabla_\mu \Psi \nabla^\mu \Psi - \frac{\mu^2}{2} \Psi^2 - \frac{k}{2} \Psi * F^{\mu\nu} F_{\mu\nu} \right],$$

where R is the Ricci scalar, $F_{\mu\nu} = 2\nabla_{[\mu} A_{\nu]}$ is the Maxwell field strength tensor and Ψ is the scalar field (axion) with mass μ. The respective equation of motion for the axion field is following

$$\nabla_\mu \nabla^\mu \Psi - \mu^2 \Psi - \frac{k}{2} * F^{\mu\nu} F_{\mu\nu} = 0.$$

The obtained equation of motion (EoM) is a generalised Klein-Gordon equation with a source term, being the invariant of the Maxwell field. This particular source term plays a very important role in this scheme, because if it vanishes (when the magnetic field is zero or when the spacetime is spherically symmetric) the equation then undergoes a no-hair theorem and no axionic configurations can be established. Thus, in this situation we can speak of magnetically induced axionlike hair.

We consider the above EoM in two gravitational backgrounds in the probe limit scenario.

1. Kerr black hole immersed in uniform magnetic field using Wald's technique,

$$ds^2 = -\left(1 - \frac{2Mr}{\Sigma}\right)dt^2 - \frac{4Mra\sin^2\theta}{\Sigma}dtd\phi + \frac{\Sigma}{\Delta}dr^2 + \Sigma d\theta^2 + \frac{\Xi\sin^2\theta}{\Sigma}d\phi^2,$$

2. Kerr-Newman black hole,

$$ds^2 = -\left(1 - \frac{2Mr}{\Sigma} + \frac{Q^2}{\Sigma}\right)dt^2 - \frac{2a(2Mr - Q^2)\sin^2\theta}{\Sigma}dtd\phi + \frac{\Sigma}{\Delta}dr^2 + \Sigma d\theta^2 + \frac{\Xi\sin^2\theta}{\Sigma}d\phi^2,$$

with auxiliary functions given by

$$\Sigma(r,\theta) = r^2 + a^2\cos^2\theta,$$

$$\Delta(r) = r^2 - 2Mr + a^2,$$

$$\Xi(r,\theta) = (r^2 + a^2)^2 - a^2\Delta\sin^2\theta,$$

where all parameters have their standard textbook definitions. Naturally, in KN case $\Delta(r) = r^2 - 2Mr + a^2 + Q^2$ is enriched with the electric charge of the black hole. For every considered point in the parameter space we also compute the free energy of the system as a benchmark of thermodynamical stability of the cloud.

To solve these problems we use a numerical method based on the spectral differentiation using Chebyshev polynomials. We build up a differentiation matrix for a two dimensional Gauss-Lobatto grid. From this basic matrix, we are able to construct other differentiation matrices - the second and mixed derivatives, and the whole left-hand side operator in the end. In this way we are able to translate a differential problem into an algebraic one and solve it by calculating the inverse of the system matrix.

Results

We have found that axions, indeed, can have stationary solutions around Kerr black holes immersed in magnetic field and Kerr-Newman black holes. Moreover these solutions exist in the whole range of parameter space, as they are magnetically induced.

The mass of the axions significantly influences the spatial distribution of the cloud. For ultralight axions the cloud spreads from polar areas down almost to $\theta \simeq 80°$. As one increases the mass of the axionic field we find out that their angular localisation shifts to $\theta \simeq 45°$, leaving polar areas depleted. It should also be noted that larger mass decreases the spatial extent of the cloud, which is a quite expected result.

From the thermodynamical point of view, the free energy of axionic cloud happens to be the smallest (the strongest binding) as the hosting black hole is nearly extreme ($a \to 1$) and the mass is tiny (the ultralight case). This theoretical clue allows to think that black holes in the galaxies (which are naturally rotating and have some magnetic field around them) may host axionlike dark matter structures that can spread over a large distance from them.

4.1.5 Static axionlike dark matter clouds around magnetized rotating wormholes - probe limit case

Reference

<u>**B. Kiczek**</u> and M. Rogatko, *Static axionlike dark matter clouds around magnetized rotating wormholes - probe limit case*, Eur. Phys. J. C **82**, 586 (2022).

Motivation

In this work we return to the issue of axionlike clouds, but this time in the vicinity of wormholes. Previously we studied axionlike clouds around rotating black holes and found their stationary solutions.

Wormholes are tunnel-like structures that can link two separate regions of the Universe, or even different universes. Their origins are in early works of Einstein and Rosen [68] on their bridge. This discovery resulted in a blossom of interest in these objects, from their mathematical structure up to their possible usage in space travels. Later on Morris and Thorne [69] gave the contemporary understanding of wormholes using the survivability of human travellers as a criterion for calling a wormhole traversable.

In modern physics, wormholes can be seen as black hole mimickers in many cases and from large distances it is truly difficult to distinguish one from another. So far there is no a reliable criterion that could surely exclude a possibility if the observed compact object is not a wormhole. Therefore the primary objective of this paper was to study the possible axionlike dark matter halos around a wormhole and compare the achieved results with aforementioned black hole solutions.

Methods

For the matter part we use exactly the same Einstein-Maxwell-axion theory as in the previous work on black holes, therefore I do not write it here again. What is essential for these computations are the gravitational background we used. Let me briefly comment on them.

The Kerr-like wormhole is the wormhole extension of the standard Kerr black hole solution. Its line element is following

$$ds^2 = -\left(1 - \frac{2Mr}{\Sigma}\right)dt^2 - \frac{4Mar\sin^2\theta}{\Sigma}dtd\phi + \frac{\Sigma}{\tilde{\Delta}}dr^2 + \Sigma d\theta^2 \qquad (4.34)$$
$$+\left(r^2 + a^2 + \frac{2Ma^2r\sin^2\theta}{\Sigma}\right)\sin^2\theta d\phi^2,$$

where $\tilde{\Delta}(r) = r^2 + a^2 - 2M(1 + \lambda^2)r$, with λ being the deviation parameter. If one puts $\lambda = 0$ we return to a plain Kerr black hole. However, using this gravitational background is bittersweet. The sweet part is that it allows us to test the behaviour of axionlike clouds both in wormhole and black hole regimes. The bitter part is that it is not an exact vacuum

solution of Einstein field equations, thus we should treat it as a toy model. In the end we immerse the Kerr-like wormhole in uniform magnetic field using the Wald method.

During the work on this project we came to the conclusion that the comparison between a black hole and one type of a wormhole is not enough, and an additional wormhole should be included into the consideration. The axionlike cloud requires the gravitational object to be axially symmetric, and therefore rotating. We decided to include a rotating counterpart of the well-known (and typical solution) Morris-Thorne wormhole, which is Teo wormhole. It serves as a benchmark for observed phenomena, if they are tied to only one solution or they might be rather more generally wormhole related. The used background is described by a line element

$$ds^2 = -N^2 dt^2 + \frac{dr^2}{1 - \frac{b}{r}} + K^2 r^2 \left[d\theta^2 + \sin^2\theta (d\phi - \omega dt)^2 \right], \tag{4.35}$$

with functions provided by

$$N = \exp\left[-\frac{r_+}{r} \right], \qquad b(r) = r_+ \left(\frac{r_+}{r} \right)^\gamma, \qquad \omega = \frac{2ar_+}{r^3}, \qquad K = 1, \tag{4.36}$$

which are quite common choices in the literature.

To solve obtained field equations we used the same method as in the *Axionlike dark matter clouds around rotating black holes* paper.

Results

The main results of this work are the spatial distributions of axionic clouds. Once again, we found that they are magnetically induced and stationary. However their distribution significantly differs from the black hole scenario. Specifically, there appears a gap between the surface of wormhole's throat and the axionic cloud itself. For a black hole the axionic field had a non-zero finite value on the horizon. In case of a Kerr-like wormhole the axionic field vanishes, then grows to some maximal value and fades away with the growth of radius.

We checked this also for the Teo wormhole and found a very similar result. In that case the field did not vanish totally, as there was a little value on the throat. However the overall tendency was similar, and probably if we used $\psi(r_{th}) = 0$ boundary condition, we could have reached a similar picture.

Nevertheless, a significant difference, with respect to black holes, in the shape of axionlike dark matter structures has been found. Naturally this finding is only a tip of the iceberg as it can become now a starting point in finding some observable imprints caused by the axionic condensate, like some possible influence on the trajectory of light. We hope to return to these problems in future investigations.

4.2 Attached articles

JCAP09(2019)049

Ultra-compact spherically symmetric dark matter charged star objects

Bartłomiej Kiczek and Marek Rogatko

Institute of Physics, Maria Curie-Skłodowska University.
pl. Marii Curie-Skłodowskiej 1, 20-031 Lublin, Poland

E-mail: bkiczek@kft.umcs.lublin.pl, rogat@kft.umcs.lublin.pl

Abstract. We study the properties of ultra-compact spherically symmetric *dark matter* sector star objects, being the solution of Einstein equations with two U(1)-gauge fields. One of them is the ordinary Maxwell field, while the auxiliary gauge field pertains to the *hidden* sector, and mimics the properties of *dark matter*. The *visible* and *hidden* sectors are coupled by a kinetic mixing term with a coupling constant α. We also investigate the possibility of condensation of charged scalar field around the reflecting *dark matter* star object. It happens that *dark matter* sector, both *dark matter* charge and coupling constant, cause shrinking of the star radius for which the condensation may occur.

Contents

1 Introduction

The pursuit for an illusive ingredient of our Universe constituting over 23 percent of its mass, non-baryonic *dark matter*, authorizes of the most important topic of the astronomy and physics [1]. *Dark matter* builds a thread-like structure of the so-called cosmic web being a scaffolding for the ordinary matter to accumulate [2, 3]. For the first time Hubble Space Telescope, revealed images of the structure in question, a giant filament of *dark matter*, being the part of the comic web extending from one of the most massive galaxy clusters MACS J071 [3].

The contemporary understanding of the creation of structures in the Universe, the so-called ΛCDM model, envisages that galaxies are embedded in extended massive halos composed of *dark matter*. They are surrounded by smaller *dark matter* sub-halos, which are large enough to accumulate gas and dust and form satellite galaxies, orbiting around the host ones. However, smaller galaxies can be circled by much smaller sub-halo *dark matter* satellites, almost invisible to telescopes [4]. It can be concluded that in the proximity of the Milky Way we can suppose that such kind of structures may also exist.

On the other hand, *dark matter* interaction with the Standard Model particles is one of the main theoretical investigations of the particle physics in the early stages of our Universe [5, 6]. Several new types of fundamental particle have been claimed as candidates for *dark matter* sector, which are expected to interact with nuclei in suitable detecting materials on Earth. It was claimed only by the DAMA collaboration [7, 8] that they observed modulation in the rate of interaction events in their detectors which might be the trace of *dark matter* sector. Several groups want to reproduce the DAMA results but in vain [9]. This situation triggers the discussion concerning the composition, interaction with ordinary matter, the self-interaction and the possible ways to discriminate between various models of *dark matter* [10].

One also tries to implement physics beyond the Standard Model for the explanation of *dark matter* non-gravitational interactions. This fact resurgences interests in gamma rays

emissions coming from dwarf galaxies, possible dilaton-like coupling to photons caused by ultra-light *dark matter*, and oscillations of the fine structure constant [11]–[13]. The Earth experiments are also exploited for the detection of possible low-energy mass of *dark matter* sector, especially in $e^+ \, e^-$ colliders [14]. BABAR detector set some energy range for *dark photon* production, i.e., $0.02 < m < 10.2 \, \text{GeV}$, but in vain. No significant signal has been observed. However the new experiments are planned to cover the energy region $15 \leq m \leq 30 \, \text{MeV}$. Recently, the revision of the constraints on *dark photon* with masses below $100 \, \text{MeV}$ was proposed based on the observation of supernova 1987A event [15]. Collisions among galaxy clusters can also provide new tools for testing non-gravitational forces acting on *dark matter* [16].

Collapse of neutron stars and emergence of the first star generations [17]–[19], alternative theories [20]–[22], or compact objects studies [23]–[26], can deliver some other hints for these researches in question. The existence of *dark matter* can affect black hole growth during the early stages of our Universe. The numerical studies of *dark matter* and dark energy collapse and their interactions with black holes and wormholes were investigated in [27, 28].

Because of the absence of evidences for the most popular particle candidates for *dark matter*, it was claimed the growing sense of 'crisis' in the *dark matter* particle community, and necessity of diversifying the experimental efforts. The efforts in question should accomplish upcoming astronomical surveys, gravitational wave observatories, to deliver us some complimentary information about the *dark matter* sector [1].

1.1 Dark matter model

Having all the above arguments in mind, we shall examine the problem of the influence of *dark matter* on the properties of spherically symmetric static charged star-like solution. In our research we shall consider the model of *dark matter* sector in which the additional U(1)-gauge field is coupled to the ordinary Maxwell one. The action describing Einstein-Maxwell *dark matter* gravity yields [29, 30]

$$S = \int d^4 x \sqrt{-g} \left(R - \frac{1}{4} F_{\mu\nu} \, F^{\mu\nu} - \frac{1}{4} B_{\mu\nu} \, B^{\mu\nu} - \frac{\alpha}{4} \, F_{\mu\nu} B^{\mu\nu} \right), \tag{1.1}$$

where $F_{\mu\nu} = 2\nabla_{[\mu} A_{\nu]}$ is the ordinary Maxwell field while $B_{\mu\nu} = 2\nabla_{[\mu} B_{\nu]}$ stands for the auxiliary U(1)-gauge field mimicking the dark matter sector coupled to Maxwell one. The coupling constant is denoted by α. Predicted values of α-coupling constant, being the kinetic mixing parameter between the two U(1)-gauge fields, for realistic string compactifications range between 10^{-2} and 10^{-16} [31]–[34]. It turns out that astrophysical observations of $511 \, \text{eV}$ gamma rays [35], experiments detecting the electron positron excess in galaxies [36, 37], as well as, possible explanation of muon anomalous magnetic moment [38], strongly advocate the idea of *dark matter* sector coupled to the Maxwell one. Moreover, the *kinetic mixing term* between ordinary boson and relatively light one (the *dark* one) arising from U(1)-gauge symmetry connected with a *hidden sector*, may cause a low energy parity violation [39]. The low energy gauge interaction in the hidden sector may manifest itself by the Higgs boson decays, and a relatively light vector boson with mass $m \geq 10 \, \text{GeV}$ can be produced [40].

The presented model has also its justification in string/M-theory, where the mixing portal (term which couples Maxwell and the additional U(1)-gauge field) arises in open string theory. Both gauge states are supported by D-branes separated in extra dimensions [41], in supersymmetric Type I, Type II A, Type II B models, where the massive open strings stretch between two D-branes. The massive string/brane states existence connect the different gauge sectors.

The other cognizance of the above scenario can be achieved by M2-branes wrapped on surfaces which intersect two distinct codimension four orbifolds singularities. It happened that the natural generalization can be carried out in M, F-theory and heterotic string models.

In the considered action (1.1) the auxiliary gauge field is connected with some *hidden sector* [41]. For the first time such a model was introduced [42], in order to describe the existence and subsequent integrating out of heavy bi-fundamental fields charged under the U(1)-gauge groups. In general, such kind of terms emerge in the theories having in addition to some *visible* gauge group, the other one in the *hidden sector*. Such scenario is realized e.g., in compactified string or M-theory solutions generically possess *hidden sectors* which contain the gauge fields and gauginos, due to the various group factors included in the gauge group symmetry of the *hidden sector*.

The *hidden sector* in the low-energy effective theory contains states which are uncharged under the Standard Model gauge symmetry groups. They are charged under their own groups and interact with the *visible* ones via gravitational interaction. We can also think out other portals to our *visible sector* [43, 44]. For the consistency and supersymmetry breaking [32], the realistic embeddings of the Standard Model in $E8 \times E8$ string theory, as well as, in type I, IIA, or IIB open string theory with branes, require the existence of the *hidden sectors*.

The organization of the paper is as follows. In section 1 we give some introduction to the presented model of *dark matter* sector. In section 2 we present the direct derivation of static spherically symmetric solution of Einstein — *dark matter* equations of motion. Section 3 is devoted to the analysis of *dark matter* charged fluid sphere, while in section 4 we derive the bound on the gravitational mass and charges for a stable *dark matter* compact star-like object. In section 5 we considered the problem of hair growing of charged under *visible* sector scalar field, on the ultra-compact reflecting star. In section 6 we concluded our investigations.

2 Ultra-compact charged star-like object in hidden sector

In this section we consider the spherically symmetric static solution of Einstein *dark matter* sector equations of motion, being a model of ultra-compact charged *dark matter* star-like object.

The components of energy momentum tensor defined as $T_{\mu\nu} = -\delta S/\sqrt{-g}\delta g^{\mu\nu}$, devoted to Maxwell, *dark matter* U(1)-gauge field and the mixture of them, may be written as

$$T_{\mu\nu} = T_{\mu\nu}(F) + T_{\mu\nu}(B) + \alpha T_{\mu\nu}(F, \ B), \tag{2.1}$$

where the adequate energy momentum tensors are given by

$$T_{\mu\nu}(F) = \frac{1}{2}F_{\mu\gamma}F_{\nu}{}^{\gamma} - \frac{1}{8}g_{\mu\nu}F_{\alpha\beta}F^{\alpha\beta}, \tag{2.2}$$

$$T_{\mu\nu}(B) = \frac{1}{2}B_{\mu\gamma}B_{\nu}{}^{\gamma} - \frac{1}{8}g_{\mu\nu}B_{\alpha\beta}B^{\alpha\beta}, \tag{2.3}$$

$$T_{\mu\nu}(F, \ B) = \frac{1}{2}F_{\mu\gamma}B_{\nu}{}^{\gamma} - \frac{1}{8}g_{\mu\nu}F_{\alpha\beta}B^{\alpha\beta}. \tag{2.4}$$

In what follows we suppose that the existence of t-component of the gauge field potentials

$$A_t = -\frac{Q}{r}, \qquad B_t = -\frac{Q_d}{r}, \tag{2.5}$$

where Q is the ordinary Maxwell charge while Q_d is connected with *dark matter* sector.

The line element of spherically symmetric spacetime implies

$$ds^2 = -e^{2\phi(r)}dt^2 + e^{2\lambda(r)}dr^2 + r^2(\sin^2\theta d\phi^2 + d\theta^2).\tag{2.6}$$

Having in mind (2.5) and (2.6), the $(t\ t)$ and $(r\ r)$ components of Einstein equations $G_{\mu\nu} = T_{\mu\nu}$, are provided by

$$-e^{2\phi(r)}\left[\frac{1}{r^2} - \frac{e^{2\lambda(r)}}{r^2} - \frac{2\lambda'(r)}{r}\right] = \frac{Q_c^2}{4r^4},\tag{2.7}$$

$$\frac{1}{r^2} - \frac{e^{2\lambda(r)}}{r^2} + \frac{2\phi'(r)}{r} = -\frac{Q_c^2}{4r^4 e^{2\phi}},\tag{2.8}$$

where the total charge $Q_c^2 = Q^2 + Q_d^2 + \alpha Q Q_d$, the prime denotes taking derivative with respect to r-coordinate. Consequently, analyzing the above equations, we draw a conclusion that $\lambda(r) = -\phi(r)$, and the metric tensor component yields

$$e^{-2\lambda(r)} = 1 - \frac{2M}{r} + \frac{Q_c^2}{4r^2},\tag{2.9}$$

where M is the total gravitational mass and Q_c the total charge, measured by the observer at future timelike infinity.

3   Dark matter charged fluid sphere

This section will be devoted to the examination of the charged *dark sector* fluid sphere and the Tolmann-Openheimer-Volkov (TOV) equation for the object under inspection. In order to derive the relativistic hydro and electro-*dark matter* dynamic equation for the charged sphere let us consider the action for *visible* and *hidden* sector U(1)-gauge fields with current sources. It is provide by the relation of the form as

$$S_{EM+dm+cur}(F,\ B) = \int d^4x \sqrt{-g}\left[-\frac{1}{4}F_{\mu\nu}F^{\mu\nu} - \frac{1}{4}B_{\mu\nu}B^{\mu\nu} - \frac{\alpha}{4}F_{\mu\nu}B^{\mu\nu} - 2A^\mu j_\mu(F) - 2B^\mu \tilde{j}_\mu(B)\right].\tag{3.1}$$

Varying the underlying action with respect to the adequate gauge fields we arrive at the following equations of motion

$$\nabla_\mu F^{\mu\nu} + \frac{\alpha}{2}\nabla_\mu B^{\mu\nu} = 2j^\nu(F),\tag{3.2}$$

$$\nabla_\mu B^{\mu\nu} + \frac{\alpha}{2}\nabla_\mu F^{\mu\nu} = 2\tilde{j}^\nu(B).\tag{3.3}$$

It can be shown that for the Maxwell field it implies

$$\tilde{\alpha}\nabla_\mu F^{\mu\nu} = 2j^\nu(F) - \alpha\tilde{j}^\nu(B),\tag{3.4}$$

where $\tilde{\alpha} = 1 - \alpha^2/4$ and on the right-hand side we get currents responsible both for visible and *dark matter* sector. The adequate components of the energy momentum tensor imply

$$T_{\mu\nu}(F) = \frac{1}{2}F_{\mu\gamma}F_\nu{}^\gamma - \frac{1}{8}g_{\mu\nu}F_{\alpha\beta}F^{\alpha\beta} - g_{\mu\nu}\ A_\delta j^\delta(F) + 2A_{(\mu}j_{\nu)}(F),\tag{3.5}$$

$$T_{\mu\nu}(B) = \frac{1}{2}B_{\mu\gamma}B_\nu{}^\gamma - \frac{1}{8}g_{\mu\nu}B_{\alpha\beta}B^{\alpha\beta} - g_{\mu\nu}\ B_\delta\tilde{j}^\delta(B) + 2B_{(\mu}\tilde{j}_{\nu)}(B),\tag{3.6}$$

$$T_{\mu\nu}(F,\ B) = \frac{1}{2}F_{\mu\gamma}B_\nu{}^\gamma - \frac{1}{8}g_{\mu\nu}F_{\alpha\beta}B^{\alpha\beta}.\tag{3.7}$$

Moreover, for the charged sphere we shall consider perfect fluid component of the energy momentum tensor. It yields

$$T_{\mu\nu}(p,\ \rho) = (\rho + p)u_\mu u_\nu + pg_{\mu\nu}, \tag{3.8}$$

where $p(r)$ is the fluid pressure while ρ stands for the total mass density of the sphere in question.

Having in mind that the considered ultra compact object has the spherical symmetry, the elaborated electric Maxwell field ought to posses the radial symmetry. Just the electromagnetic strength tensor will be of the form as $F_{rt} = E(r)$. Then using equation (3.4) we get the following relation:

$$E(r) = \frac{1}{r^2}e^{\phi(r)+\lambda(r)}Q_c(F,\ B)(r), \tag{3.9}$$

where $Q_c(F,\ B)(r)$ yields

$$Q_c(F,\ B)(\zeta) = \int d\zeta\ \zeta^2\ e^{\phi(\zeta)+\lambda(\zeta)}j^t(F,\ B)(\zeta), \tag{3.10}$$

while the currents for the mixture of Maxwell and *dark matter* fields is written in the form as follows:

$$j^t(F,\ B) = \alpha_1 j^t(F) - \alpha_2 \tilde{j}^t(B), \tag{3.11}$$

with the adequate coefficients $\alpha_1 = 2/\tilde{\alpha}$ and $\alpha_2 = \alpha/\tilde{\alpha}$.

Using the Einstein equation (tt)-component provided by the equation

$$-\frac{e^{-2\lambda(r)}}{r^2} + \frac{1}{r^2} + \frac{2\lambda(r)'e^{-2\lambda(r)}}{r} = \rho + \frac{Q_c^2(r)}{4r^4}, \tag{3.12}$$

we arrive at the final expression for the metric tensor component describing *dark sector* ultra compact charged sphere of a radius r

$$e^{-2\lambda(r)} = 1 - \frac{2m(r)}{r} - \frac{\mathcal{F}_c(r)}{r}, \tag{3.13}$$

where we set

$$m(\zeta) = \int d\zeta\ \frac{\rho\ \zeta^2}{2}, \qquad \mathcal{F}_c(\zeta) = \int d\zeta\ \frac{Q_c(\zeta)}{4\zeta^2}. \tag{3.14}$$

$m(r)$ stands for the interior mass accumulated in a sphere of r-radius. It will be also necessary to introduce the notion of gravitational mass. To commence with, let us match the exterior and interior solutions of the considered field equations. Namely at the distance $R = r$, we have equality

$$1 - \frac{2M}{R} + \frac{Q_c^2}{4R^2} = 1 - \frac{1}{R}\int_0^R d\zeta\rho\zeta^2 - \frac{1}{R}\int_0^R d\zeta\frac{Q_c(\zeta)^2}{4\zeta^2}, \tag{3.15}$$

which provides the explicit relation for gravitational mass M at the distance equal to R

$$M = \frac{Q_c^2}{8R} + m(R) + \frac{\mathcal{F}_c(R)}{2}. \tag{3.16}$$

Just the definition of gravitational mass at any radius r implies

$$m_g(r) = m(r) + \frac{\mathcal{F}_c(r)}{2} + \frac{Q_c(r)^2}{8r}. \tag{3.17}$$

All the above lead to the conclusion that the gravitational mass will modify the metric function $e^{-2\lambda(r)}$. Now, consequently with the help of the aforementioned notion, we obtain that the following relation:

$$e^{-2\lambda(r)} = 1 - \frac{2m_g(r)}{r} + \frac{Q_c(r)^2}{4r^2}, \tag{3.18}$$

where the metric component depends on the gravitational mass and the total (Maxwell and *dark matter* charges) of the examined sphere.

3.1 TOV equation

In order to find the Tolmann-Oppenheimer-Volkov equation for the *dark sector* ultra-compact charged star we have to use the conservation of the energy momentum tensor, $\nabla_\mu T^{\mu\nu} = 0$. Namely having in mind this relation

$$\nabla_r \Big[T_r{}^r(F,\ B) + T_r{}^r \rho,\ p) \Big] = -\frac{Q_c(r)'Q_c(r)}{2r^4} + p(r)' + \phi(r)'\Big(\rho + p(r)\Big) = 0, \tag{3.19}$$

and the G_{rr} component of the Einstein equation, as well as, relation (3.13), we arrive at the following form of the equation binding pressure, density and charge of the *dark sector* star-like object

$$p'(r) = \frac{Q_c(r)'Q_c(r)}{2r^4} - \frac{\Big(\rho + p(r)\Big)}{r^2} \left[m(r) + \frac{\mathcal{F}_c(r)}{2} + \frac{r^3 p(r)}{2} - \frac{Q_c(r)^2}{8r} \right] \left[1 - \frac{2m(r)}{r} - \frac{\mathcal{F}_c(r)}{r} \right]^{-1}. \tag{3.20}$$

4 Bound on the gravitational mass and charge of stable dark matter sector compact object

In this section we look for the upper bound on gravitational mass for given radius and total charge, for the ultra-compact *dark matter* sector star objects. It turns out that following the procedure presented in [45, 46], after some algebra, one can get almost the same result. Namely for sphere of radius r the inequality implies

$$\sqrt{m_g(r)} \le \frac{\sqrt{r}}{3} + \sqrt{\frac{r}{9} + \frac{Q_c^2(r)}{12r}}. \tag{4.1}$$

On the other hand, in order to derive the inequality for the case when $r \ge R$, let us suppose that $\psi_k = m_g(r) + r^3 p(r) - Q_c^2(r)/4r$ is a sequence of regular solutions with support in the range $[R_k,\ R]$ of the Tolmann-Oppenheimer-Volkov equation (3.20). Moreover, we suppose that $\lim_{k\to\infty} R_k/R = 1$. Then, following the steps presented in [46], one arrives at the inequality among $M,\ R,\ Q_c$ valid for the exterior solution of the Einstein equations with two U(1)-gauge fields. Namely, it implies

$$\sqrt{M} \le \frac{\sqrt{R}}{3} + \sqrt{\frac{R}{9} + \frac{Q_c^2}{12R}}. \tag{4.2}$$

However, an interesting problem was suggested in [47], i.e., it was posed a question if the addition of some characteristics of horizonless object could improve the upper bound on its gravitational mass. The refinement of the bounds derived in [46] was presented in [47].

On the other hand, geodesic motion determines important features of the spacetime and objects in it. Namely, null unstable geodesics are closely connected with the appearance of a compact object visible by the external observer. They are also bounded with the characteristic modes of black holes, i.e., computing the Lyapunov exponent one can prove that, in the eikonal limit, quasi-normal modes of black holes are determined by parameters of the circular null geodesics [48]. Circular geodesics are of special interests. For example in Kerr spacetime the binding energy of the last stable circular timelike geodesics is related to gravitational binding energy that can be radiated to infinity. This fact can be implemented to the estimation of a spin of astrophysical black objects through observations of the accretion discs surrounded the compact object in question [49].

Circular null orbits (photonspheres) were also analyzed in the background of a regular horizonless ultra-compact stars [47, 50], where it was revealed that photonspheres attributed to the aforementioned objects possessed an upper bound expressed in terms of mass and charge.

To proceed further, let us discuss the upper bound of the gravitational mass allowed for the ultra-compact spherical *dark matter* sector star objects. To begin with, one finds that the Lagrangian describing the geodesics in the spacetime of *dark matter* ultra-compact star yields

$$2\mathcal{L} = -e^{2\phi(r)}\dot{t}^2 + e^{2\lambda(r)}\dot{r}^2 + r^2\dot{\theta}^2 + r^2\sin\theta\dot{\phi}^2, \tag{4.3}$$

where the dot means taking derivate with respect to the proper time. We shall restrict our considerations to the equatorial orbits. Then, following the methods of classical mechanics, the generalized momenta with respect to the coordinates $(t, \ r, \ \phi)$

$$p_t = -e^{2\phi(r)}\dot{t} = -E, \qquad p_r = e^{2\lambda(r)}\dot{r} = L, \qquad p_\phi = r^2\dot{\phi}, \tag{4.4}$$

where the constants E and L are attributed to the total energy and orbital momentum of the system, respectively. The Legendre transformation leads to the Hamiltonian of the form

$$2H = -E\dot{t} + L\dot{\phi} + e^{2\lambda(r)}\dot{r}^2 = \epsilon = const. \tag{4.5}$$

If $\epsilon = 0$, one obtains null geodesics, whereas $\epsilon = 1$ we have to do with the timelike ones. Consequently from equation (4.5) we get

$$(\dot{r})^2 = \frac{1}{e^{2\lambda(r)}}\left[E^2 e^{-2\phi(r)} - \frac{L^2}{r^2} - \epsilon\right]. \tag{4.6}$$

The right-hand side of the above relation authorizes the effective potential which will be denoted by $V_r(r)$.

The condition for the circular null orbits, $V_r = V_r' = 0$, implies

$$\frac{E^2}{L^2} = \frac{e^{-2\lambda(r)}}{r^2}, \qquad 1 + r \ \lambda'(r) = 0, \tag{4.7}$$

which gives us the characteristic relation $N(r = r_c) = 0$, with the definition

$$N(r) = 3e^{-2\lambda(r)} - 1 - r^2\left(p(r) - \frac{Q_c(r)^2}{8r^4}\right). \tag{4.8}$$

One can see that the light rings of the spherically symmetric ultra-compact *dark matter* sector object, which line element is provided by (2.6), are characterized by the functional (4.8). The

dimensionless function $N(r)$ determines the discrete radii of the null circular geodesics of the spacetime in question. It has the following boundary conditions

$$N(r \to 0) = 2, \qquad N(r \to \infty) = 2. \tag{4.9}$$

The above feature implies that spherically regular horizonless compact objects are characterized by an even number of null circular geodesics. Let us remark that in [51, 52] it is derived that horizonless matter configurations having a light ring must have pairs of them. For such regular configurations one of the closed light ring is stable. However, in the spherical symmetric case being subject to the equation $\sim r_c \, (\rho + p_T) = 1$, where r_c is the radius of the light ring and p_T tangential pressure, we have odd number of the light rings [53].

For the exterior region of the ultra-compact object in question, one has that

$$r \geq R, \qquad p(r) = \rho = 0. \tag{4.10}$$

Further suppose that the spatially regular charged *dark matter* sector compact object, has the external light ring for $r_c > R$. Inspection of the equations (2.9) and (4.8) reveals that

$$r_c(out) = \frac{6 + \sqrt{36M^2 - 7Q_c^2}}{4}, \tag{4.11}$$

which gives us the stronger bound for mass and the total charge. Namely, we arrive at the condition

$$\frac{\sqrt{Q^2 + Q_d^2 + \alpha Q Q_d}}{M} \leq \frac{6}{\sqrt{7}}. \tag{4.12}$$

Let us analyze the derived condition for the specific choice of the charges from *visible* and *hidden* sectors. Namely, if $Q = Q_d$ we get

$$\frac{Q}{M} \leq \frac{6}{\sqrt{7(2 + \alpha)}}. \tag{4.13}$$

The larger α one takes into account, the smaller value of the ratio we get. On the other hand, when $Q_d = \beta Q$ and $\alpha = const$, we obtain

$$\frac{Q}{M} \leq \frac{6}{\sqrt{7(1 + \beta^2 + \alpha\beta^2)}}. \tag{4.14}$$

Just the bigger multiplying factor β one takes, the smaller value of Q/M we have.

In principle the presence of the light ring outside the surface of a spherically regular horizonless compact star object, may cause the appearance of the another light ring which is included inside the outer one. It was revealed [54] that the existence of the inner stable null circular geodesic, might show that the ultra-compact object under consideration was nonlinearly unstable to perturbations massless fields. Therefore we draw a conclusion that spherically symmetric horizonless spacetimes describing a compact object within the theory with *dark matter* sector has to have no light rings. It implies that the lower on the radii of the stable *dark matter* star-like object yields

$$R > \frac{6 + \sqrt{36M^2 - 7Q_c^2}}{4}. \tag{4.15}$$

Having in mind the exact form of the total charge, from (4.15), one can remark that the radius of ultra-compact *dark matter* sector star object will be smaller that this without *hidden sector*.

One has that the larger *dark charge* Q_d (M, Q, $\alpha = const$) we consider, the smaller radius one obtains. Consequently, if we assume that mass and the charges of the object are constant, and the bigger value of α one takes, the smaller radius of ultra-compact *dark matter* sector we receive.

5 Scalar hair on dark matter compact star

The no-hair theorem for asymptotically flat horizonless neutral compact star being subject to the reflecting boundary conditions, with the influence of scalar field with potential, was derived in [55]. Then the problem was elaborated in [56], implementing the spacetime with a positive cosmological constant. The case of the massless scalar field non-minimally coupled to gravity was studied in [57].

On the other hand, the charged reflecting sphere influenced by scalar field was examined in [58], while the analytical formulae for the discrete spectrum of star radii were revealed in [59]. It turns out that the low frequency scalar perturbations in the spacetime of a black hole in a box can lead to the superradiant instability, as well as, formation of a quasi-local hair [61]. It is believed that box boundary may enforce fields to bounce back and trigger the condensation around the black object. This kind of a problem was analyzed in the case of scalar field configurations near charged compact reflecting star [62], where the lower and upper bounds for the radii of the object were provided.

5.1 Model of scalar field configuration

To find out the possibility of formation of the scalar hair we start our considerations with the following action:

$$S_{EM+dm+sc} = \int d^4x \sqrt{-g} \left(-\frac{1}{4} F_{\mu\nu} F^{\mu\nu} - \frac{\alpha}{4} B_{\mu\nu} F^{\mu\nu} - \frac{1}{4} B_{\mu\nu} B^{\mu\nu} - D_\alpha \psi D^\alpha \psi - \mu^2 \psi^2 \right), \quad (5.1)$$

where the covariant derivative is given by $D = \nabla_\mu - q A_\mu$. q and μ are respectively charge and mass of the scalar field $\psi(r)$. The scalar field in question is charged with respect to *visible* sector.

For the brevity of further notation we rename the left-hand side of the relation (2.9), i.e., $e^{-2\lambda(r)} = f(r)$. Moreover, for the convenience of numerical calculations we also rescale charges in the line element describing *dark matter* charged static line element

$$\frac{Q_{(i)}}{2} \rightarrow Q_{(i)}, \quad (5.2)$$

where the subscript (i) denotes charges bounded with *visible* and *hidden* sectors.

Having in mind the form of the action (5.1), we get equation of motion for the scalar field, $\delta S / \delta \psi = 0$, which is provided by

$$\nabla_\mu \nabla^\mu \psi - \left(q^2 A_\mu A^\mu + \mu^2 \right) \psi = 0. \quad (5.3)$$

Its explicit for the static background implies the second order ordinary differential equation of the form as follows:

$$\psi'' + \left(\frac{f'}{f} + \frac{2}{r} \right) \psi' + \left(\frac{q^2 Q^2}{r^2 f^2} - \frac{\mu^2}{f} \right) \psi = 0, \quad (5.4)$$

where prime denotes derivative with respect to r-coordinate. It can be noticed that the relation (5.4) reveals the scaling symmetry of its parameters. Namely, one has that

$$r \to sr, \ M \to sM, \ Q_{(i)} \to sQ_{(i)}, \ q \to q/s, \ \mu \to \mu/s. \tag{5.5}$$

In order to solve the differential equation we have to establish the adequate boundary conditions imposed on $\psi(r)$. In what follows we implemet the reflecting boundary conditions, which means that at the surface of the *dark matter* star the scalar field will vanish, $\psi(r_s) = 0$. Moreover, one supposes that the timelike box boundary conditions should to be satisfied in the considered spacetime. It means that at $r = r_b$ the scalar field in question is reflected back, $\psi(r_b) = 0$.

The function describing the scalar field has to have at least one extremum point in the range from r_s to r_b. At the aforementioned point the function $\psi(r_{\text{ext}})$ should satisfy the following conditions:

$$\psi'(r_{\text{ext}}) = 0, \qquad \psi(r_{\text{ext}})\psi''(r_{\text{ext}}) \le 0. \tag{5.6}$$

Following the procedure presented in [62], we apply the transformation $\tilde{\psi} = \sqrt{r}\psi$ in the equation (5.4) and then collecting terms with $\tilde{\psi}$ derivatives, we use the extremum condition (5.6) in order to achieve the inequality valid for $r = r_{extr}$

$$\mu^2 r^2 f \le -\frac{1}{4}f^2 - \frac{1}{2}f'fr + q^2 Q^2. \tag{5.7}$$

In the next step we check the monotonicity and the sign of each term on the right-hand side of the inequality, because of the fact that both $f(r)$ and $rf'(r)$ are descending and greater than zero, and moreover left-hand side is a descending function for the distance greater than the radius of the star. Consequently, one concludes that

$$\mu^2 r_s^2 f(r_s) \le \mu^2 r^2 f(r) \le q^2 Q^2. \tag{5.8}$$

Neglecting the middle term we solve the inequality

$$\mu^2 r_s^2 \left(1 - \frac{2M}{r_s} + \frac{Q_c^2}{r_s^2}\right) \le q^2 Q^2 \tag{5.9}$$

treating μr_s as the variable in the quadratic inequality. Finally it leads to the possible range where r_s lies within. It is provided by

$$\mu M + \sqrt{\mu^2(M^2 - Q_c^2)} \le \mu r_s \le \mu M + \sqrt{\mu^2(M^2 - Q_c^2) + q^2 Q^2}. \tag{5.10}$$

The lower bound is a Schwarzschild radius for charged *dark matter* sector black hole and the upper one is connected with the larger solution of the inequality (5.9).

5.2 Numerical results

Integrating from r_s to r_b, we numerically solve the ordinary differential equation (5.4) governing the motion of the scalar field ψ in the spacetime of ultra-compact *dark matter* star-like object. By virtue of the shooting method, we have found the adequate radius of the star surface r_s, with previously set r_b fulfilling the auxiliary condition $\psi(r_b) = 0$ on the second boundary. We perform our shooting by bisection method in the range derived from the maximum point analysis (5.10). The algorithm may find more than one value of r_s, corresponding to the boundary condition in a given interval. If such situation takes place, we choose the largest solution.
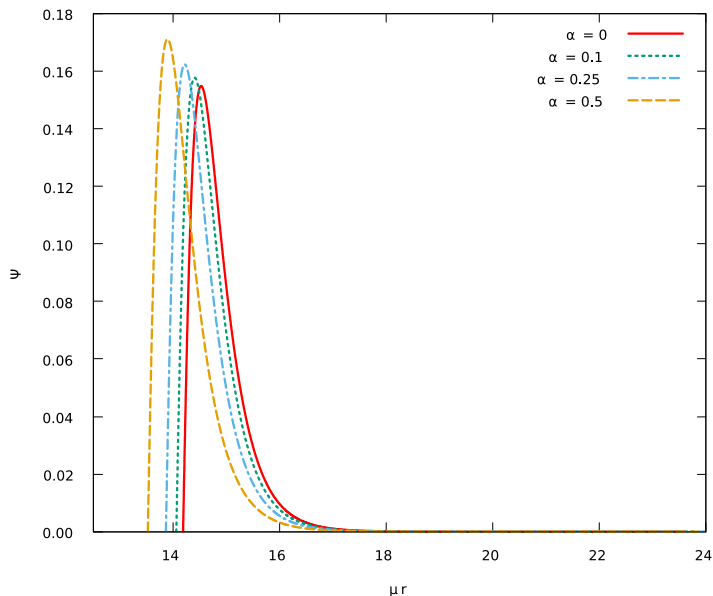
Figure 1. The distribution of the condensed scalar field ψ around a compact charged star-like object. The calculation was carried out for parameters $M = 8$, $Q = 4$, $Q_d = 4$, $q = 1$ (normalized to the mass μ).

After obtaining solution of the equation of motion satisfying the aforementioned requirements, we shall investigate the influence of the *dark matter* charge and the coupling strength on the possibility of the scalar hair formation in the vicinity of ultra-compact star-like object. In figure 1 one depicts the value of ψ scalar field versus μr, for the fixed values of mass of the star and charges of *visible* and *hidden* sectors equal to 4. The physical parameters of the system have been normalized to μ due to the scaling symmetry (5.5). One can observe that the larger α-coupling constant we examine, the smaller radius of the hairy compact star we arrive at. The influence of *dark matter* causes that the condensation takes place for the smaller objects. On the other hand, the maximal value of ψ also depends on the α-coupling constant. If α increases the maximal value of the scalar field that form hair also grows.

To proceed further, let us take a closer look on the scenario when one of the charges dominates the other. We set one of them to $Q_{(i)} = 3$ and plot the star radius for condensing scalar, for different values of the other kind of charge. In figure 2 the dependence of the star radius on the charges, the electric and the *dark matter* one, is envsaged respectively. One can see that increasing the charge forces the star to be smaller in order to hold the condensed scalar. Every curve separately shows similar parabolic behavior, but when we are aware of the coupling presence there are some differences to be spotted. The effect of the coupling is similar in the change of both charges. The splitting distance between line of interest and baseline scales more or less linear with α. Both plots tend to the same final value of r_s when the charges are equal ($Q = 3$, $Q_d = 3$) but the curves differ quantitatively. The initial value of r_s from the left panel of figure 2 is smaller than the one from the right panel. In such a case the increase of Q_d causes more steep drop of r_s than in case of increasing Q.

The larger value of α-coupling constant we consider, the smaller μr_s we get. This leads to the conclusion that the both charges result in shrinking the star radius so the scalar hair may occur.
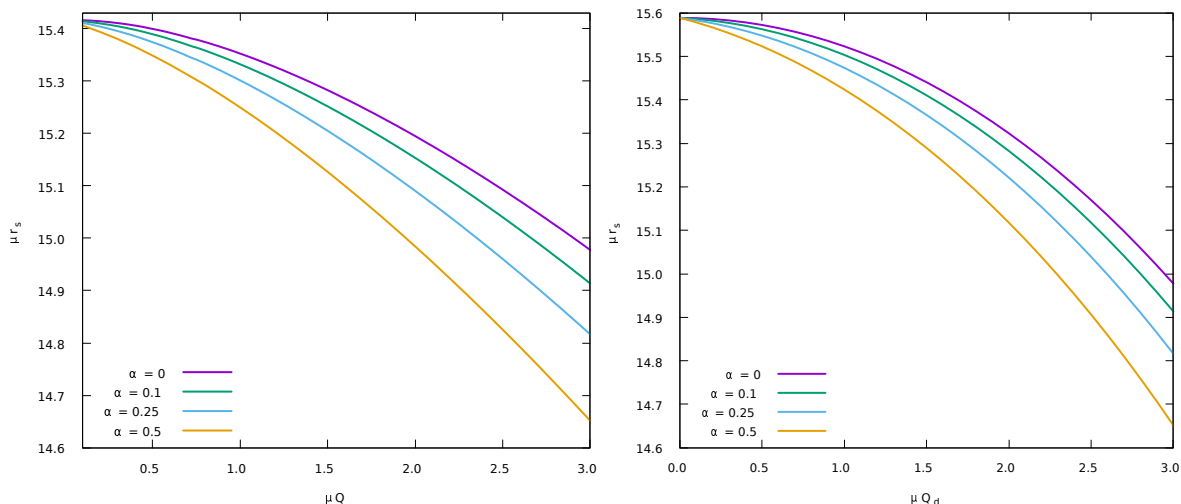
Figure 2. Star radius dependence on an electric charge (left panel), *dark matter* charge (right panel) and the dark matter coupling constant. For this plot $M = 8$, $q = 1$. The unvaried charge is equal $Q_{(i)} = 3$, in both panels.
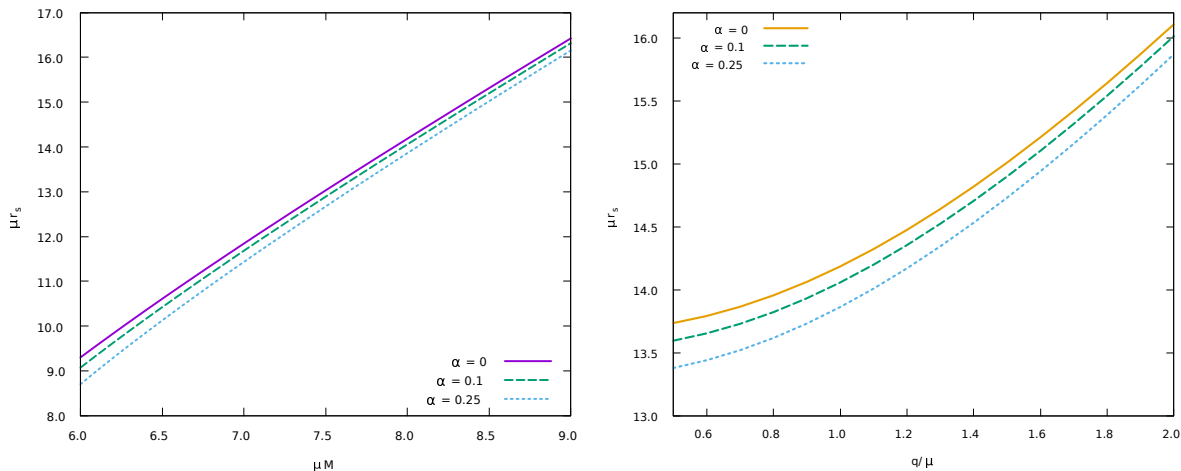

Figure 3. Star radius dependence on the star mass with different *dark matter* coupling (left panel) and on the scalar field charge (right panel). In both plots $Q = 4$, $Q_d = 4$, in the left panel $q = 1$ and in the right panel $M = 8$.

The left panel of the figure 3 depicts the hairy star radius as a function of its mass. Adding the *dark matter* coupling to the system shrinks the obtained radius. A similar behavior is also shown on in the right panel of the figure 3, where the radius versus scalar field charge is plotted. Both of these plots are presented for equal charges $Q = Q_d = 4$.

6 Discussion and conclusions

In our paper we have studied the charged spherically horizonless solution of Einstein *dark matter* sector equation of motion, being the two U(1)-gauge theory in which the ordinary Maxwell field pertain to the *visible* sector while the auxiliary $U1$)-gauge field is responsible for the *hidden* one. The solution in question models the ultra-compact star-like object in the underlying theory.

We have found the lower bound on the radius of the charged *dark matter* sphere, which takes place for any solutions satisfying the condition of pressure being less than the density of the object. However, it is possible to derive some refinement on the bound in question. Namely, the investigations of photonsphere in the background of the spherically symmetric ultra-compact *dark matter* sector star objects reveals the fact that it has an upper bound expressed in terms of the ADM mass and total charge, which in turn gives us some additional condition binding the total charge and mass.

Due to the fact that spherically symmetric horizonless ultra-compact star-like object may be unstable to perturbations of massless fields, we obtain another restriction on its radius. It turns out that the larger *dark charge* is considered, the smaller radius of the compact object we get. When the charge and mass of the *dark matter* object are constant, the increase of the α-coupling constant value, binding the *hidden* and *visible* sectors, causes the decrease of the radius of *dark star*.

We have also investigated the possibility of condensation of scalar field around compact reflecting stars in a box-boundary regime. The presented model includes the *dark matter* charge and its influence on the condensing scalar through the background metric. From every plot presented in this article we can conclude that the *dark matter*-electromagnetic field coupling decreases the largest star radius which is capable of holding hair. Moreover this effect is stronger when both charges are present in the system and when they are sufficiently large, so the mixing term makes significant contribution in the metric function. On the other hand the effective charge may not be too large so the square root in (5.10) remains real. We are aware of the restraints of the probe limit and that the problem requires a full study with back reaction and solving the Maxwell equations. Also it is interesting to see the stability of the scalar condensate when the charged dark matter would be dropping into the system in a time-dependent approach. We take it as an inspiration to further research to be presented elsewhere.

References

[1] G. Bertone and M.P. Tait, Tim, *A new era in the search for dark matter*, *Nature* **562** (2018) 51 [arXiv:1810.01668] [INSPIRE].

[2] R. Massey et al., *Dark matter maps reveal cosmic scaffolding*, *Nature* **445** (2007) 286 [astro-ph/0701594] [INSPIRE].

[3] J.P. Dietrich et al., *A filament of dark matter between two clusters of galaxies*, *Nature* (2012) [arXiv:1207.0809] [INSPIRE].

[4] T.K. Starkenburg, A. Helmi and L.V. Sales, *Dark influences II: gas and star formation in minor mergers of dwarf galaxies with dark satellites*, *Astron. Astrophys.* **587** (2016) A24 [arXiv:1508.06281] [INSPIRE].

[5] M. Regis, J.-Q. Xia, A. Cuoco, E. Branchini, N. Fornengo and M. Viel, *Particle dark matter searches outside the Local Group*, *Phys. Rev. Lett.* **114** (2015) 241301 [arXiv:1503.05922] [INSPIRE].

[6] Y. Ali-Haïmoud, J. Chluba and M. Kamionkowski, *Constraints on Dark Matter Interactions with Standard Model Particles from Cosmic Microwave Background Spectral Distortions*, *Phys. Rev. Lett.* **115** (2015) 071304 [arXiv:1506.04745] [INSPIRE].

[7] R. Bernabei et al., *Searching for WIMPs by the annual modulation signature*, *Phys. Lett.* **B 424** (1998) 195 [INSPIRE].

[8] R. Bernabei et al., *Final model independent result of DAMA/LIBRA-phase1*, *Eur. Phys. J.* **C 73** (2013) 2648 [arXiv:1308.5109] [INSPIRE].

[9] COSINE-100 collaboration, *An experiment to search for dark-matter interactions using sodium iodide detectors*, *Nature* **564** (2018) 83 [arXiv:1906.01791] [INSPIRE].

[10] N. Masi, *Dark matter: TeV-ish rather than miraculous, collisionless rather than dark*, *Eur. Phys. J. Plus* **130** (2015) 69 [INSPIRE].

[11] A. Geringer-Sameth et al., *Indication of Gamma-ray Emission from the Newly Discovered Dwarf Galaxy Reticulum II*, *Phys. Rev. Lett.* **115** (2015) 081101 [arXiv:1503.02320] [INSPIRE].

[12] K.K. Boddy and J. Kumar, *Indirect Detection of Dark Matter Using MeV-Range Gamma-Ray Telescopes*, *Phys. Rev.* **D 92** (2015) 023533 [arXiv:1504.04024] [INSPIRE].

[13] K. Van Tilburg, N. Leefer, L. Bougas and D. Budker, *Search for ultralight scalar dark matter with atomic spectroscopy*, *Phys. Rev. Lett.* **115** (2015) 011802 [arXiv:1503.06886] [INSPIRE].

[14] BABAR collaboration, *Search for a Dark Photon in e^+e^- Collisions at BaBar*, *Phys. Rev. Lett.* **113** (2014) 201801 [arXiv:1406.2980] [INSPIRE].

[15] J.H. Chang, R. Essig and S.D. McDermott, *Revisiting Supernova 1987A Constraints on Dark Photons*, *JHEP* **01** (2017) 107 [arXiv:1611.03864] [INSPIRE].

[16] D. Harvey, R. Massey, T. Kitching, A. Taylor and E. Tittley, *The non-gravitational interactions of dark matter in colliding galaxy clusters*, *Science* **347** (2015) 1462 [arXiv:1503.07675] [INSPIRE].

[17] J. Bramante and T. Linden, *Detecting Dark Matter with Imploding Pulsars in the Galactic Center*, *Phys. Rev. Lett.* **113** (2014) 191301 [arXiv:1405.1031] [INSPIRE].

[18] J. Fuller and C. Ott, *Dark Matter-induced Collapse of Neutron Stars: A Possible Link Between Fast Radio Bursts and the Missing Pulsar Problem*, *Mon. Not. Roy. Astron. Soc.* **450** (2015) L71 [arXiv:1412.6119] [INSPIRE].

[19] I. Lopes and J. Silk, *A particle dark matter footprint on the first generation of stars*, *Astrophys. J.* **786** (2014) 25 [arXiv:1404.3909] [INSPIRE].

[20] S.I. Blinnikov and M.Y. Khlopov, *On possible effects of 'mirror' particles*, *Sov. J. Nucl. Phys.* **36** (1982) 472 [INSPIRE].

[21] S.I. Blinnikov and M.Y. Khlopov, *Possible astronomical effects of mirror particles*, *Sov. Astron.* **27** (1983) 371 [INSPIRE].

[22] M.Y. Khlopov, G.M. Beskin, N.E. Bochkarev, L.A. Pustylnik and S.A. Pustylnik, *Observational Physics of Mirror World*, *Sov. Astron.* **35** (1991) 21 [INSPIRE].

[23] J.P.S. Lemos and E.J. Weinberg, *Quasiblack holes from extremal charged dust*, *Phys. Rev.* **D 69** (2004) 104004 [gr-qc/0311051] [INSPIRE].

[24] N. Dadhich, *On compactness limit of static charged object*, arXiv:1903.03436 [INSPIRE].

[25] S. Chakraborty and S. Sengupta, *Packing extra mass in compact stellar structures: An interplay between Kalb-Ramond field and extra dimensions*, *JCAP* **05** (2018) 032 [arXiv:1708.08315] [INSPIRE].

[26] N. Dadhich and S. Chakraborty, *Buchdahl compactness limit for a pure Lovelock static fluid star*, *Phys. Rev.* **D 95** (2017) 064059 [arXiv:1606.01330] [INSPIRE].

[27] A. Nakonieczna, M. Rogatko and R. Moderski, *Dynamical Collapse of Charged Scalar Field in Phantom Gravity*, *Phys. Rev.* **D 86** (2012) 044043 [arXiv:1209.1203] [INSPIRE].

[28] A. Nakonieczna, M. Rogatko and Ł. Nakonieczny, *Dark sector impact on gravitational collapse of an electrically charged scalar field*, *JHEP* **11** (2015) 012 [arXiv:1508.02657] [INSPIRE].

[29] T. Vachaspati and A. Achucarro, *Semilocal cosmic strings*, *Phys. Rev.* **D 44** (1991) 3067 [INSPIRE].

[30] A. Achucarro and T. Vachaspati, *Semilocal and electroweak strings*, *Phys. Rept.* **327** (2000) 347 [hep-ph/9904229] [INSPIRE].

[31] S.A. Abel and B.W. Schofield, *Brane anti-brane kinetic mixing, millicharged particles and SUSY breaking*, *Nucl. Phys.* **B 685** (2004) 150 [hep-th/0311051] [INSPIRE].

[32] S.A. Abel, J. Jaeckel, V.V. Khoze and A. Ringwald, *Illuminating the Hidden Sector of String Theory by Shining Light through a Magnetic Field*, *Phys. Lett.* **B 666** (2008) 66 [hep-ph/0608248] [INSPIRE].

[33] S.A. Abel, M.D. Goodsell, J. Jaeckel, V.V. Khoze and A. Ringwald, *Kinetic Mixing of the Photon with Hidden* U(1)*s in String Phenomenology*, *JHEP* **07** (2008) 124 [arXiv:0803.1449] [INSPIRE].

[34] NA64 collaboration, *Search for invisible decays of sub-GeV dark photons in missing-energy events at the CERN SPS*, *Phys. Rev. Lett.* **118** (2017) 011802 [arXiv:1610.02988] [INSPIRE].

[35] P. Jean et al., *Early SPI/INTEGRAL measurements of* 511 keV *line emission from the 4th quadrant of the Galaxy*, *Astron. Astrophys.* **407** (2003) L55 [astro-ph/0309484] [INSPIRE].

[36] J. Chang et al., *An excess of cosmic ray electrons at energies of* 300–800 GeV, *Nature* **456** (2008) 362 [INSPIRE].

[37] PAMELA collaboration, *An anomalous positron abundance in cosmic rays with energies* 1.5–100 GeV, *Nature* **458** (2009) 607 [arXiv:0810.4995] [INSPIRE].

[38] MUON G-2 collaboration, *Final Report of the Muon E821 Anomalous Magnetic Moment Measurement at BNL*, *Phys. Rev.* **D 73** (2006) 072003 [hep-ex/0602035] [INSPIRE].

[39] H. Davoudiasl, H.-S. Lee and W.J. Marciano, *'Dark' Z implications for Parity Violation, Rare Meson Decays and Higgs Physics*, *Phys. Rev.* **D 85** (2012) 115019 [arXiv:1203.2947] [INSPIRE].

[40] H. Davoudiasl, H.-S. Lee, I. Lewis and W.J. Marciano, *Higgs Decays as a Window into the Dark Sector*, *Phys. Rev.* **D 88** (2013) 015022 [arXiv:1304.4935] [INSPIRE].

[41] B.S. Acharya, S.A.R. Ellis, G.L. Kane, B.D. Nelson and M.J. Perry, *The lightest visible-sector supersymmetric particle is likely to be unstable*, *Phys. Rev. Lett.* **117** (2016) 181802 [arXiv:1604.05320] [INSPIRE].

[42] B. Holdom, *Two* U(1)*'s and* ϵ *Charge Shifts*, *Phys. Lett.* **166B** (1986) 196 [INSPIRE].

[43] D. Lüst, *Intersecting brane worlds: A Path to the standard model?*, *Class. Quant. Grav.* **21** (2004) S1399 [hep-th/0401156] [INSPIRE].

[44] S. Abel and J. Santiago, *Constraining the string scale: From Planck to weak and back again*, *J. Phys.* **G 30** (2004) R83 [hep-ph/0404237] [INSPIRE].

[45] P. Karageorgis and J.G. Stalker, *Sharp bounds on 2m/r for static spherical objects*, *Class. Quant. Grav.* **25** (2008) 195021 [arXiv:0707.3632] [INSPIRE].

[46] H. Andreasson, *Sharp bounds on the critical stability radius for relativistic charged spheres*, *Commun. Math. Phys.* **288** (2009) 715 [arXiv:0804.1882] [INSPIRE].

[47] S. Hod, *Upper bound on the gravitational masses of stable spatially regular charged compact objects*, *Phys. Rev.* **D 98** (2018) 064014 [arXiv:1903.10530] [INSPIRE].

[48] V. Cardoso, A.S. Miranda, E. Berti, H. Witek and V.T. Zanchin, *Geodesic stability, Lyapunov exponents and quasinormal modes*, *Phys. Rev.* **D 79** (2009) 064016 [arXiv:0812.1806] [INSPIRE].

[49] R. Narayan, *Black holes in astrophysics*, *New J. Phys.* **7** (2005) 199 [gr-qc/0506078] [INSPIRE].

[50] Y. Peng, *Upper bound on the radii of regular ultra-compact star photonspheres*, *Phys. Lett.* **B 790** (2019) 396 [arXiv:1812.04257] [INSPIRE].

[51] V. Cardoso, L.C.B. Crispino, C.F.B. Macedo, H. Okawa and P. Pani, *Light rings as observational evidence for event horizons: long-lived modes, ergoregions and nonlinear instabilities of ultracompact objects*, *Phys. Rev.* **D 90** (2014) 044069 [arXiv:1406.5510] [INSPIRE].

[52] P.V.P. Cunha, E. Berti and C.A.R. Herdeiro, *Light-Ring Stability for Ultracompact Objects*, *Phys. Rev. Lett.* **119** (2017) 251102 [arXiv:1708.04211] [INSPIRE].

[53] S. Hod, *On the number of light rings in curved spacetimes of ultra-compact objects*, *Phys. Lett.* **B 776** (2018) 1 [arXiv:1710.00836] [INSPIRE].

[54] J. Keir, *Slowly decaying waves on spherically symmetric spacetimes and ultracompact neutron stars*, *Class. Quant. Grav.* **33** (2016) 135009 [arXiv:1404.7036] [INSPIRE].

[55] S. Hod, *No-scalar-hair theorem for spherically symmetric reflecting stars*, *Phys. Rev.* **D 94** (2016) 104073 [arXiv:1612.04823] [INSPIRE].

[56] S. Bhattacharjee and S. Sarkar, *No-hair theorems for a static and stationary reflecting star*, *Phys. Rev.* **D 95** (2017) 084027 [arXiv:1704.02873] [INSPIRE].

[57] S. Hod, *No nonminimally coupled massless scalar hair for spherically symmetric neutral reflecting stars*, *Phys. Rev.* **D 96** (2017) 024019 [arXiv:1709.01933] [INSPIRE].

[58] S. Hod, *Charged massive scalar field configurations supported by a spherically symmetric charged reflecting shell*, *Phys. Lett.* **B 763** (2016) 275 [arXiv:1703.05333] [INSPIRE].

[59] S. Hod, *Marginally bound resonances of charged massive scalar fields in the background of a charged reflecting shell*, *Phys. Lett.* **B 768** (2017) 97 [arXiv:1806.06831] [INSPIRE].

[60] C.A.R. Herdeiro, J.C. Degollado and H.F. Rúnarsson, *Rapid growth of superradiant instabilities for charged black holes in a cavity*, *Phys. Rev.* **D 88** (2013) 063003 [arXiv:1305.5513] [INSPIRE].

[61] N. Sanchis-Gual, J.C. Degollado, P.J. Montero, J.A. Font and C. Herdeiro, *Explosion and Final State of an Unstable Reissner-Nordström Black Hole*, *Phys. Rev. Lett.* **116** (2016) 141101 [arXiv:1512.05358] [INSPIRE].

[62] Y. Peng, *Scalar field configurations supported by charged compact reflecting stars in a curved spacetime*, *Phys. Lett.* **B 780** (2018) 144 [arXiv:1801.02495] [INSPIRE].

Influence of dark matter on black hole scalar hair

Bartlomiej Kiczek[*] and Marek Rogatko[†]

Institute of Physics, Maria Curie-Sklodowska University,
20-031 Lublin, pl. Marii Curie-Sklodowskiej 1, Poland

Searches for *dark matter* sector field imprints on the astrophysical phenomena are one of the most active branches of the current researches. Using numerical methods, we elaborate the influence of dark matter on the emergence of black hole hair and formation of boson stars. We explore thermodynamics of different states of the system in Einstein-Maxwell-scalar dark matter theory with box boundary conditions. Finally, we find that the presence of dark sector within the system diminishes a chance of formation of scalar hair around a black hole.

I. INTRODUCTION

The astrophysical evidence of the illusive ingredient of our Universe, *dark matter*, is overwhelming and authorizes the galaxy rotation curves, gravitational lensing, a thread-like structure (cosmic web) on which ordinary matter accumulates [1,2]. On the contrary, the absence of the evidence of the most popular particle candidates for baryonic dark matter stipulates the necessity of diversifying experimental efforts [3]. Black holes and ultracompact horizonless objects being the ideal laboratories for dark matter studies may help us to answer the tantalizing question of how dark matter sector leaves its imprint in the physics of these objects. However, it happens that Schwarzschild black hole has a negative specific heat and it cannot be in equilibrium with thermal radiation. To overcome this difficulty, the idea of enclosing the black hole within a box was proposed [4,5]. Einstein-Maxwell systems with box boundary conditions were elaborated in [6], where it was established that the phase structure of the models was similar to AdS gravity. Inclusion of the additional scalar field to the theory in question envisages the correspondence of phase transitions in gravity in a box with s-wave holographic superconductor [7–9]. The thermodynamical studies of Einstein-Maxwell scalar systems in the asymptotically flat spacetime with reflecting boundary conditions were conducted in [10]. A certain range of parameters allows to obtain stable black hole solution, giving a way to circumvent no-hair theorem.

The next compact objects studied in our paper, from the point of view of the influence of dark matter on their physics, are boson stars. Boson stars being a self-gravitating solution of massive scalar field with a potential coupled to gauge

fields and gravity [11] are widely studied in literature [12–16] for a quite long period of time.

The purpose of our paper is to examine thermodynamical properties and stability of the black holes and horizonless objects-boson stars in Einstein-Maxwell-scalar system influenced by dark matter sector and envisage the role of the dark matter in the elaborated problems.

The organization of the paper is as follows. In Sec. II, we describe the basic features of the *hidden sector* model and derived the basic equations needed in what follows. Section III is devoted to the description of the obtained numerical results. In Sec. IV, we concluded our researches.

II. MODEL

We consider the spacetime manifold with timelike boundary $\partial\mathcal{M}$, which will be referred as a box. The action for Einstein-Maxwell scalar dark matter gravity is provided by

$$
S = \int_{\mathcal{M}} d^4x \sqrt{-g} \left(R - \frac{1}{4} F_{\mu\nu} F^{\mu\nu} - \frac{\alpha}{4} B_{\mu\nu} F^{\mu\nu} \right.
$$
$$
\left. - \frac{1}{4} B_{\mu\nu} B^{\mu\nu} - |D\Psi|^2 - m^2 |\Psi|^2 \right) - \int_{\partial\mathcal{M}} d^3x \sqrt{-\gamma} \mathcal{K}, \quad (1)
$$

where $F_{\mu\nu}$ is a Maxwell field strength tensor, $B_{\mu\nu}$ is a strength tensor of a hidden sector vector boson. The complex scalar field $\Psi = \psi e^{i\theta}$, where θ denotes the phase, is coupled only to the ordinary electromagnetic field by the covariant derivative $D_\mu = \nabla_\mu - iqA_\mu$. The theoretical justifications of the model in question originate from M/string theories, where such mixing portals coupling Maxwell and auxiliary gauge fields can be encountered [17]. The hidden sectors states are charged under their own groups and interact with the *visible* sector via gravitational interactions. The realistic string compactifications establish the range of values for α between 10^{-2} and 10^{-10} [18–21]. It seems that astrophysical

*bkiczek@kft.umcs.lublin.pl
†rogat@kft.umcs.lublin.pl

observations of gamma rays of energy 511 keV [22], positron excess in galaxies [23], and muon anomalous magnetic moment [24] argue for the aforementioned idea of coupling Maxwell field with dark matter sector. Recent experiments aimed at gamma ray emissions from dwarf galaxies [25], dilatonlike coupling to photons caused by ultralight dark matter [26], oscillations of the fine structure constant [27], revisions of the constraints on *dark photon* 1987A supernova emission [28], measurements of excitation of electrons in CCD-like detector [29], as well as the examinations in e^+e^- Earth colliders [30], give us some hints for the correctness of the proposed model. They and the future planned ballon d'essai will ameliorate the mass constraints on the hidden sector particles, especially for dark photons.

The second integral denotes the Gibbons-Hawking boundary term of our box with γ metric on the three-dimensional hypersurface ($r = r_b$), with the extrinsic curvature $\mathcal{K}$.

Varying the action (1), we get the equations of motion of the forms

$$(\nabla_\mu - iqA_\mu)(\nabla^\mu - iqA^\mu)\Psi - m^2\Psi = 0, \qquad (2)$$

$$\tilde{\alpha}\nabla_\mu F^{\mu\nu} = j^\nu, \qquad (3)$$

where $\tilde{\alpha} = 1 - \frac{\alpha^2}{4}$ and the current j^ν is provided by the relation

$$j^\nu = iq[\Psi^\dagger(\nabla^\nu - iqA^\nu)\Psi - \Psi(\nabla^\nu + iqA^\nu)\Psi^\dagger]. \quad (4)$$

In what follows, we use a time-independent spherically symmetric line element, with the metric coefficients being functions of r coordinate,

$$ds^2 = -g(r)h(r)dt^2 + \frac{dr^2}{g(r)} + r^2(d\theta^2 + \sin\theta^2 d\phi^2), \qquad (5)$$

and the adequate components of the fields in the theory will constitute radial functions of the forms

$$A_\mu dx^\mu = \phi(r)dt, \qquad B_\mu dx^\mu = \chi(r)dt, \qquad \Psi = \Psi(r). \quad (6)$$

In general, the scalar field can have harmonic time dependence which can be absorbed by a redefinition of the gauge field function. Having this in mind it can be seen that the r component of the equations of motion for the gauge and scalar fields leads to the conclusion that $\Psi(r) = \psi(r)$. By virtue of this, the following equations of motion are provided:

$$R_{\mu\nu} - \frac{1}{2}g_{\mu\nu}R = T_{\mu\nu}, \qquad (7)$$

$$\nabla_\mu \nabla^\mu \psi - q^2 A_\mu A^\mu \psi - m^2 \psi = 0, \qquad (8)$$

$$\nabla_\mu F^{\mu\nu} + \frac{\alpha}{2}\nabla_\mu B^{\mu\nu} - 2q^2 A^\nu \psi^2 = 0, \qquad (9)$$

$$\nabla_\mu B^{\mu\nu} + \frac{\alpha}{2}\nabla_\mu F^{\mu\nu} = 0. \qquad (10)$$

As in the case of Eq. (3), the last two equations can be rewritten as

$$\tilde{\alpha}\nabla_\mu F^{\mu\nu} - 2q^2 A^\nu \psi^2 = 0, \qquad (11)$$

$$\nabla_\mu B^{\mu\nu} + \frac{\alpha}{\tilde{\alpha}}q^2 A^\nu \psi^2 = 0. \qquad (12)$$

Consequently, the explicit forms of the equations of motion yield

$$h' - rh\psi'^2 - \frac{q^2 r\phi^2 \psi^2}{g^2} = 0, \qquad (13)$$

$$g' + g\left(\frac{1}{r} + \frac{1}{2}r\psi'^2\right) + \frac{q^2 r\phi^2 \psi^2}{2gh} - \frac{1}{r}$$
$$+ \frac{r}{2h}(\phi'^2 + \alpha\chi'\phi' + \chi'^2 + m^2 h\psi^2) = 0, \quad (14)$$

$$\phi'' + \left(\frac{2}{r} - \frac{h'}{2h}\right)\phi' - \frac{2q^2 \phi \psi^2}{\tilde{\alpha}g} = 0, \qquad (15)$$

$$\psi'' + \left(\frac{2}{r} + \frac{h'}{2h} + \frac{g'}{g}\right)\psi' + \left(\frac{q^2 \phi^2}{gh} - m^2\right)\frac{\psi}{g} = 0, \quad (16)$$

$$\chi'' + \left(\frac{2}{r} - \frac{h'}{2h}\right)\chi' + \frac{\alpha q^2 \chi \psi^2}{\tilde{\alpha}g} = 0. \qquad (17)$$

To solve the equations of the theory in question, one has to provide adequate boundary conditions. Namely, we can pick either a horizonless or a black hole solution. In case of a black hole, we expand the underlying functions in a Taylor series around the horizon of radius r_h,

$$\psi = \psi_0 + \psi_1(r - r_h) + \psi_2(r - r_h)^2 + \mathcal{O}(r^3), \qquad (18)$$

$$\phi = \phi_1(r - r_h) + \phi_2(r - r_h)^2 + \mathcal{O}(r^3), \qquad (19)$$

$$g = g_1(r - r_h) + g_2(r - r_h)^2 + \mathcal{O}(r^3), \qquad (20)$$

$$h = 1 + h_1(r - r_h) + \mathcal{O}(r^2), \qquad (21)$$

$$\chi = \chi_1(r - r_h) + \chi_2(r - r_h)^2 + \mathcal{O}(r^3). \qquad (22)$$

We set $g_0 = 0$ due to occurrence of the black hole event horizon. For the regularity of the $U(1)$-gauge fields on the event horizon, one also puts ϕ_0 and χ_0 equal to zero (in order to keep the terms with division by $g(r_h)$ in equations of motion finite). By implementing the expansions

(18)–(22) into the equations of motion, we find out that $\{r_h, \psi_0, \phi_1, \chi_1, \alpha\}$ comprise free parameters of the theory in question, while the remaining ones can be expressed by them.

As far as the boson star scenario is concerned, we perform a similar expansion. However, since the configuration in question is horizonless, the expansion accomplishes around the origin of the reference frame. At $r = 0$, we require that the derivatives of all the functions are set equal to zero, which ensures that there is no kink at this point. At $r = r_b$, we establish the Dirichlet boundary condition for the scalar field $\psi(r_b) = 0$ (the reflecting mirrorlike boundary conditions).

Asymptotic analysis of matter fields, at the box boundary, enables us to write

$$\psi \sim \psi^{(0)} + \psi^{(1)}(r_b - r) + \mathcal{O}(r^2), \qquad (23)$$

$$\phi \sim \phi^{(0)} + \phi^{(1)}(r_b - r) + \mathcal{O}(r^2), \qquad (24)$$

$$\chi \sim \chi^{(0)} + \chi^{(1)}(r_b - r) + \mathcal{O}(r^2). \qquad (25)$$

As was proposed in Refs. [10,16], because of the fact that the scalar field satisfies the reflecting mirrorlike boundary conditions $\psi(r_b) = 0$, one can fix $\psi^{(0)} = 0$ and the other parameter $\psi^{(1)}$ can be used for the phase transition description. This approach to the problem in question is widely exploited in holographic studies of superconductors and superfluids.

For the gauge fields, one has that $\phi^{(0)} = \mu$ and $\chi^{(0)} = \mu_d$ as chemical potentials for visible and hidden sector fields, treating the system as a grand canonical ensemble. In order to conduct the thermodynamical analysis, we calculate the free energy of the system, to see which phase is thermodynamically preferable, for a fixed temperature. In the case of a hairless solution, we take into account the classical formula $F = E - TS - \mu Q - \mu_d Q_d$, where E is Brown-York quasilocal energy [4,5]. Nevertheless, this approach may cause problems in hairy solution analysis, being insufficient to capture the mass of the scalar field. Therefore, we treat this problem evaluating the on shell action in Euclidean signature $F = TS_{cl}$, which enables to take into considerations the nontrivial profile of scalar field constituting the solution of the underlying system of differential equations.

Solution of Eqs. (13)–(17) with $\psi = 0$ can be achieved analytically, giving the Reissner-Nordstrom (RN) dark matter black object [31]. To proceed further and accomplish the complete numerical analysis of the underlying equations, we implement the shooting method, integrating the aforementioned relations from r_h to r_b, using the fourth order Runge-Kutta method. From the set of free parameters, we fix the scalar magnitude on the event horizon ψ_0 and pick r_h, ϕ_1, and χ_1 to be shooting parameters. Moreover, we impose values on both chemical potentials that serve as

constrains in our shooting procedure for ϕ_1 and χ_1. We set a domain of shooting parameters from the series expansion of the solutions near the horizon, then by using the iterative bisections one finds a solution that meets constrains, with a desired tolerance. Therefore, parameters $\{\mu_d, \alpha\}$, which are controlling, respectively, amount of *dark charge* and the coupling strength remain free; thus, they can be varied to see their impact on the system in question. For convenience, let us refer to the parameter $\psi^{(1)}$, as a *condensation*, which serves as a handy analogy to holographic theory. As mentioned above, in our numerical scheme, we treat μ_d as an input parameter in our code; however, one might not be interested in expressing these relations in a language of chemical potentials. Therefore, one might compute the total dark charge of the system

$$Q_d = \lim_{r \to r_b} \frac{1}{4\pi} \int_{\mathcal{S}^2} B_{\mu\nu} t^\mu n^\nu \sqrt{-g} d^2\theta, \qquad (26)$$

where t_μ is a unit timelike vector and n_μ is a normal vector to the boundary. In the similar manner, we compute electrical charge for $F_{\mu\nu}$.

III. RESULTS

We commence with the hairy black hole solution (HBH), i.e., a system with an event horizon and nontrivial scalar field profile. The parameter space of HBH can be illustrated on a plane of chemical potential and Hawking temperature (μ-T) as a triangular shape. That region is bound between boson star phase from the left-hand side and generalized RN solution from the right-hand side. A schematic phase diagram has been presented in the Fig. 1, where both mentioned lines are marked. Moreover, the influence of the dark sector on phase boundaries is visualized by arrows, showing the trend of the flow by increasing the hidden sector chemical potential.

The hairy configuration can be achieved for a specific value of the chemical potential. Below the value μ_{RN} scalar cannot condensate and we get RN-dark matter black hole. On the other hand, for the value greater than the critical one, μ_c, the system becomes unstable. By stable hairy solution, we mean a constrained solution of the equations of motion (13)–(17) that fulfils the boundary conditions with desired tolerance and its free energy is lower than the free energy of RN and BS, making it the ground state of the system. We can define μ_c as the chemical potential for which the phase transition driven by temperature is no longer of second order and the condensate collapses. In the range between μ_{RN} and μ_c, we contend a typical second order phase transition, depicted in Fig. 2. In the vicinity of critical temperature, condensation can be described by a function $\psi^{(1)} \sim (T_c - T)^{1/2}$. It should also be noted that establishing an HBH solution requires relatively a large value of the scalar charge. In our calculation, we used $q = 100$ and a small mass of $m = 10^{-6}$.
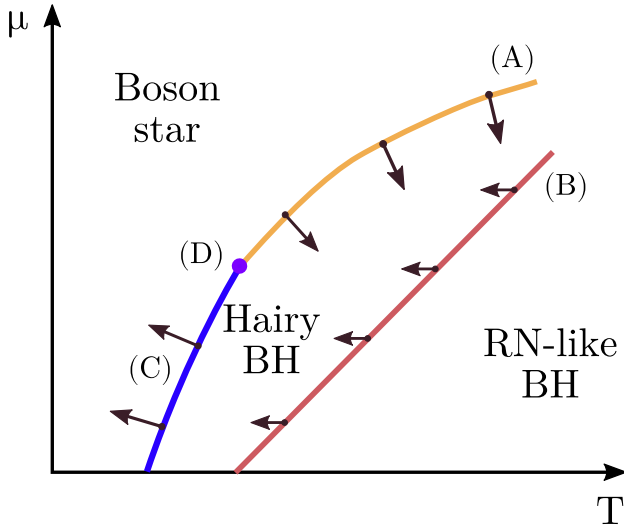
FIG. 1.   A scheme of phase diagram of the described system. Blue-yellow line indicates the border between boson star and hairy black hole parameter space, while the red line depicts hairy BH—generalized RN BH phase boundary. The arrows on the scheme show us the flow of phase boundaries driven by the chemical potential of dark matter. Lines have been split and labeled from A to C, with a point D being the center of rotation of left-hand side boundary.
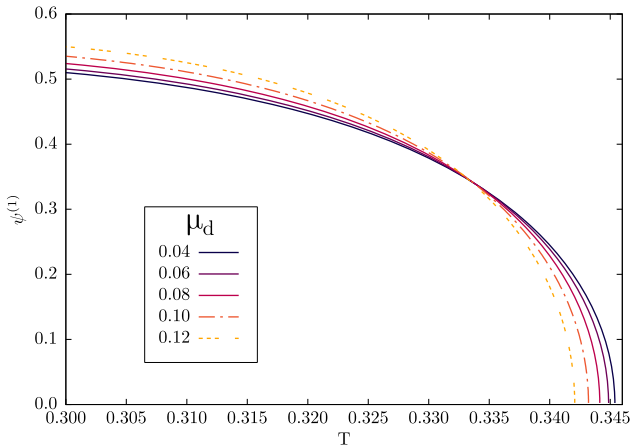

FIG. 3.   Double valued profiles of condensation as functions of Hawking temperature caused by an increasing amount of dark matter in the system with $\alpha = 10^{-3}$ and $\mu = 0.14$. While the first transition for $\mu_d = 0.08$ might still be considered as a regular, the another strictly not—the value of condensation becomes double valued for some range of temperatures. Moreover, these solutions obey the boundary conditions but their free energy is larger than both BSs and RNs; therefore, they cannot be considered as thermodynamically preferred.

FIG. 2.   Condensation $\psi^{(1)}$ as a function of temperature for the different values of μ_d and $\alpha = 10^{-3}$. For $\mu = 0.1$, a typical second order phase transition takes place, the dark matter presence influences the transition point and the condensation.

Let us now discuss physical mechanisms behind the phase boundaries flow from Fig. 1. When we cross the line of the critical chemical potential value μ_c, one encounters the *exotic phase*, where for one value of temperature we have two values of the condensation parameter $\psi^{(1)}$. Moreover, by evaluating its free energy, we can find it is so high that the hairy state is no longer stable—our

numerical method finds constrained solutions, but due to free energy leap, they are not thermodynamically preferred. The exotic phase effect occurs in case when scalar mass is close to or equal zero, for a mass away from this limit we do not obtain that phase. Instead, we have a sharp crossing, from stable solutions below μ_c to the situation when the equations of motion do not provide solutions with condensed scalar above the μ_c threshold at all. It is worth mentioning that a similar condensation-temperature profile has been shown in the so-called vector p-wave holographic superfluids [32], but a first order phase transition was hidden behind it. However, it was revealed that for the real value of the vector field, the model in question gave us the same description as holographic s-wave model with dark matter sector [33–34].

Dark matter gauge field plays an interesting role in this transition, as it accelerates the appearance, let us say, the exotic phase. For a larger value of dark sector chemical potential, $\psi^{(1)}$ becomes double valued for the lower chemical potential, which is depicted in Fig. 3, where μ_d has gradually increasing value. Moreover, when system enters the exotic phase, its free energy rises repeatedly and exceeds the free energy of RN black hole, so the hairy phase is no longer a preferred option. In this way, that effect restricts the range of chemical potential where the second order phase transition may occur, μ_c becomes a descending function of the dark charge [see curve (A) in the Fig. 1]. However, it cannot be increased without a limit. For every value of the electric charge, there exists a certain limit of dark charge, below which a formation of scalar hair is
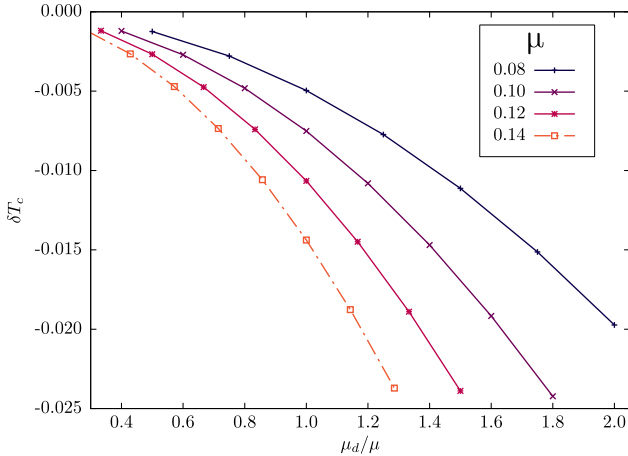
FIG. 4. Relative change of the critical temperature of hairy black hole—generalized RN black hole as a function of a ratio of chemical potentials. The temperature ratio has been normalized to the critical temperature of dark matter free solution, where $\mu_d = 0$.

FIG. 5. Quasirotation of the phase transition boundary between boson star and hairy black hole caused by dark sector charge with α coupling equal to 10^{-4}. It can be observed that the μ threshold for hairy BH solution is significantly lowered and some parameter space of boson star is taken for the advantage of hairy BH for lower values of the chemical potential.

possible. Above it, such condensation cannot take place and no stable solutions are found. This phenomenon adds up both gravitational influence of the charge on the metric and nongravitational coupling between both gauge fields.

Now, let us draw our attention to the HBH-RN BH (B) border. An interesting effect that hidden sector exerts on the hairy black hole system is the shifting of the critical temperature of the phase transition. The larger growth of dark matter charge (and also μ_d) we observe, the lower value of the transition temperature one achieves. Such effect has been depicted in the Fig. 4, where the critical temperature ratio described by the relation

$$\delta T_c = \frac{T_c(\mu_d) - T_c(0)}{T_c(0)}$$

is shown as a function of the chemical potential of hidden sector normalized to the visible sector chemical potential. One can notice that the shift of the critical temperature is proportional to the square of μ_d. Obviously, it cannot decrease as low as one wishes and a certain limit exists which has been discussed in analytic solution of dark matter charged RN-like black hole [31]. The descent of the critical temperature becomes steeper for larger value of the chemical potential of the visible sector. It can be explained by the nongravitational interaction between fields via *kinetic mixing* term, which plays a significant role when both fields are sufficiently strong.

To proceed further, we shed some light on the influence of dark matter sector on the black hole-boson star phase transition in the stable area of small values of the chemical
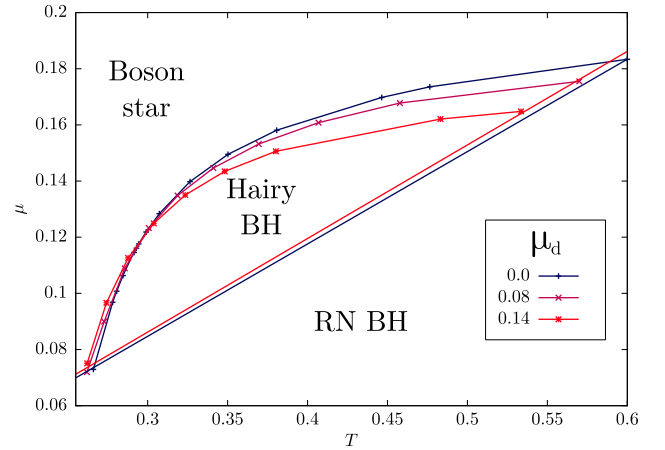
potential [line (C) in Fig. 1]. This process is depicted in Fig. 5, which asserts a phase diagram at the boundary between hairy black hole and boson star. While the boson star is a horizonless object, its Hawking temperature remains undefined. However, it is possible to calculate its characteristic—condensation and free energy as a function of chemical potential. Then to obtain the phase boundary curve, we start in the hairy black hole regime, then one moves toward lower Hawking temperatures and study the value of the free energy of the hairy black hole on the way. When it exceeds the free energy of a boson star, for the corresponding value of the chemical potential, the transition point is found. Both phases of the system are influenced by the hidden sector; nonetheless, the free energy of a boson star is affected much less than that of the black hole. Dark sector causes a significant drop of free energy of a hairy black hole. It means that the stability of a hairy solution is preserved for lower temperatures given the presence of the dark matter in the system. Such effect causes that hairy black hole solution is thermodynamically preferable for the lower Hawking temperatures and limits the emergence of boson star. The presence of α-coupling constant slightly diminishes the space of parameters for which boson star can emerge.

At last, it is sensible to mention some points that seem to be dark sector resistant. One of them appears on the phase boundary, labeled with (D) on the phase diagram scheme in Fig. 1. This point or rather its neighborhood does not seem to be susceptible on the dark charge presence in the system. For a particular numerical example, like in Fig. 5, it is placed around $\mu \approx 0.1160942$ and $T \approx 0.2929537$. Another one can be noticed in the condensation-Hawking temperature dependence presented in Fig. 2. All the curves
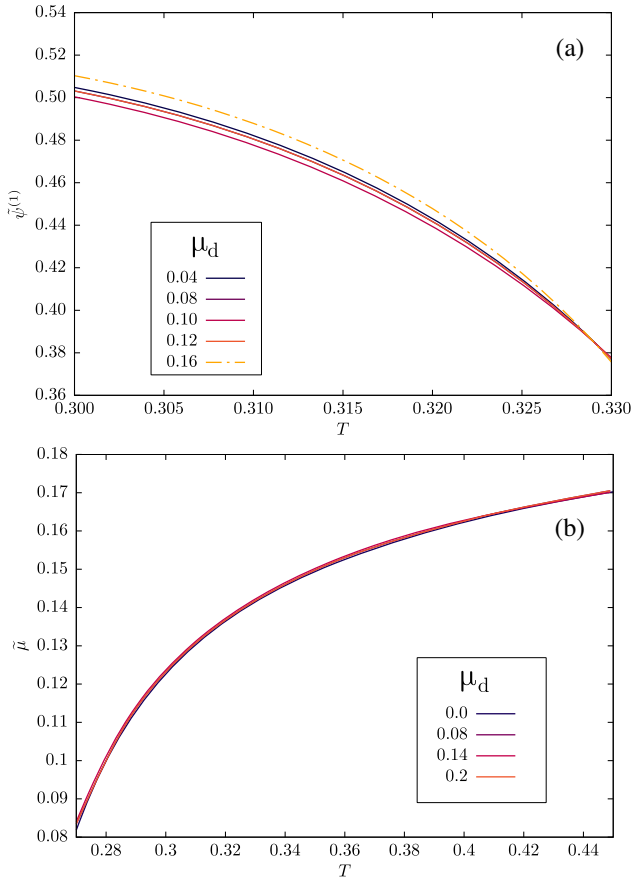
FIG. 6. Panel (a) presents condensation profile after the transformation performed in Eq. (29). The plot refers to the same data as in Fig. 2; however, it can be seen that the separation between curves is significantly smaller. In case of panel (b), which refers to Fig. 5, all curves appear to overlap with the dark matter free solution. The aforementioned transformation had removed the leading term of the dark sector influence.

certainly cross each other in one point, located at $\psi^{(1)} \approx 0.345$ and $T \approx 0.3325$. This interesting phenomenon shows that while the dark sector may modify the phase structure of the system and has an imprint on its critical quantities, there exists a specific configuration of the system, that remains completely untouched.

The points in question constitute the so-called *isosbestic* ones [35], where the curves dependent on temperature T and parametrized by values of dark matter chemical potential, intersect. They illustrate the influence of temperature on condensation $\psi^{(1)}$ and chemical potential of visible sector. At this point, we may perform a short analysis, which would reveal the leading order term of the dark sector influence. We take a following expansion of the condensate:

$$\psi^{(1)}(T, \mu_d) = \psi^{(1)}(T, 0) + \mu_d^2 \psi_1^{(1)}(T) + \mathcal{O}(\mu_d^3). \quad (27)$$

The second order term takes the approximated form

$$\psi_1^{(1)}(T) = \frac{\psi^{(1)}(T, \mu_{d1}) - \psi^{(1)}(T, \mu_{d2})}{\mu_{d1}^2 - \mu_{d2}^2}, \quad (28)$$

where in a certain example of curves from Fig. 2 we took $\mu_{d1} = 0.12$ and $\mu_{d2} = 0.08$. The zero of this function refers to the isosbestic point, where the contribution of μ_d is by definition none. By calculating the above function with help, the leading order of the influence of the dark sector may be subtracted from the main function

$$\tilde{\psi}^{(1)}(T, \mu_d) = \psi^{(1)}(T, \mu_d) - \mu_d^2 \psi_1^{(1)}(T). \quad (29)$$

In the similar manner, we can expand and analyze the chemical potential as a function of Hawking temperature, parametrized by μ_d from boson star-hairy black hole phase boundary,

$$\mu(T, \mu_d) = \mu(T, 0) + \mu_d^2 \mu_1(T) + \mathcal{O}(\mu_d^3). \quad (30)$$

We define $\mu_1(T)$ analogically to (28) with $\mu_{d1} = 0.2$ and $\mu_{d2} = 0.08$ and perform the same transformation for $\mu(T, \mu_d)$ curve as for $\psi(T, \mu_d)$ in (29). The effect of these transformations is depicted in Fig. 6, where all curves tend to be much closer to each other than before. Obviously, the total effect of μ_d is not ruled out completely, since it is much more complex than in the considered expansion.

IV. CONCLUSION

In our paper, based on Einstein-Maxwell scalar dark matter theory, where the hidden sector is mimicked by the auxiliary $U(1)$-gauge field coupled to the ordinary Maxwell one by the kinetic mixing term with a coupling constant α, we elaborate two scenarios of emergence of a hairy black hole or a boson star. The main motivation standing behind our research was to shed some light on the influence of dark matter sector on the physics and thermodynamics of these systems.

The obtained results reveal that the coupling between visible and hidden sectors plays a complex role in the behavior of scalar hair. The parameter space (μ-T), where these solutions constitute a thermodynamically favorable phase, is being narrowed on two boundaries and extended to another one. The dark sector's presence strongly reduces the value of critical chemical potential, above which the hairy solution becomes unstable. Moreover, the critical temperature of HBH-RN-like solution is shifted toward the lower value of Hawking temperature. However, the boundary between HBH and boson stars is shifted toward the latter. The presence of the dark sector lowers the free energy of HBH system, which broadens the parameter space available for the emergence of the object in question by a noticeable extent, i.e., leaving boson star as an adverse phase in the low μ regime. It appears that the free energy of boson stars in the considered configuration reacts faintly to

the presence of $U(1)$-gauge dark matter field. While the response of the system is visible, it is much smaller in magnitude than of the condensate around a black hole. However, we suppose that interesting results may be achieved for more robust model of a scalar field, e.g., containing self-interacting terms.

In the view of presented results, it seems that the hairy solutions are not only battled by no-hair theorems originating from the theory of black holes, but also by a factor that is commonly present in our Universe—the dark matter. Even if such formation would be possible despite different obstacles a significant abundance of dark matter may prevent hairy solutions from emerging.

To visualize the impact of dark sector, we compute the area of HBH parameter space between both phase boundaries. One can consider simple integration $\int(\mu_{BS}(T) - \mu_{RN}(T))dT$ of the curves from Fig. 5, which reveals that the dark sector with $\mu_d = 0.14$ takes away approximately 27% of the hairy black hole's parameter space, compared to dark matter free solution. It is indeed a significant difference, because even if such formation would be possible despite

different obstacles a significant abundance of dark sector may prevent hairy solutions from emerging.

The curves $\psi^{(1)}(T)$ and $\mu(T)$, parametrized by the values of dark matter chemical potential, reveal the isosbestic points, where they all intersect. One has the specific configurations of the considered system which is unaffected by the influence of hidden sector. At the points in question, we perform analysis revealing that the leading order influence of dark matter on the condensation $\psi^{(1)}$ and chemical potential of ordinary matter is quadratic in μ_d.

As a concluding remark, we present promising future research directions. We have elaborated the simple box-boundary models of a hairy black hole and a boson star (the so-called small boson star). The tantalizing question can be asked about the different boson star configurations with additional fields and potentials. Further investigations in this direction will be published elsewhere.

ACKNOWLEDGMENTS

[1] R. Massey *et al.*, Dark matter maps reveal cosmic scaffolding, Nature (London) **445**, 286 (2007).

[2] J. P. Dietrich, N. Werner, D. Clowe, A. Finoguenov, T. Kitching, L. Miller, and A. Simionescu, A filament of dark matter between two cluster of galaxies, Nature (London) **487**, 202 (2012).

[3] G. Bertone and T. M. P. Tait, A new era in the search for dark matter, Nature (London) **562**, 51 (2018).

[4] J. W. York, Black-hole thermodynamics and the Euclidean Einstein action, Phys. Rev. D **33**, 2092 (1986).

[5] H. W. Braden, J. D. Brown, F. B. Whiting, and J. W. York, Charged black hole in a grand canonical ensemble, Phys. Rev. D **42**, 3376 (1990).

[6] G. W. Gibbons and M. J. Perry, Black Holes in Thermal Equilibrium, Phys. Rev. Lett. **36**, 985 (1976).

[7] S. A. Hartnoll, C. P. Herzog, and G. T. Horowitz, Building a Holographic Superconductor, Phys. Rev. Lett. **101**, 031601 (2008).

[8] Y. Peng, B. Wang, and Y. Liu, On the thermodynamics of the black hole and hairy black hole transitions in the asymptotically flat spacetime with a box, Eur. Phys. J. C **78**, 176 (2018).

[9] Y. Peng, Studies of a general flat space/boson star transition model in a box through a language similar to holographic superconductors, J. High Energy Phys. 07 (2017) 042.

[10] P. Basu, C. Krishnan, and P. N. Bala Subramanian, Hairy black holes in a box, J. High Energy Phys. 11 (2016) 041.

[11] P. Jetzer, Boson stars, Phys. Rep. **220**, 163 (1992); S. L. Libling and C. Palenzuela, Dynamical boson stars, Living Rev. Relativity **15**, 6 (2012).

[12] B. Kleihaus, J. Kunz, C. Lammerzahl, and M.List, Charged boson stars and black holes, Phys. Lett. B **675**, 102 (2009).

[13] B. Hartmann, B. Kleihaus, J. Kunz, and I. Schaffer, Compact boson stars, Phys. Lett. B **714**, 120 (2012).

[14] D. Pugliese, H. Quevedo, J. A. Rueda, and R. Ruffini, Charged boson stars, Phys. Rev. D **88**, 024053 (2013).

[15] S. Kumar, U. Kulshreshtha, D. S. Kulsreshtha, S. Kahlen, and J. Kunz, Some new results on charged compact boson stars, Phys. Lett. B **772**, 615 (2017).

[16] Y. Peng, Large regular reflecting stars have no scalar field hair, Eur. Phys. J. C **79**, 309 (2019).

[17] B. S. Acharya, S. A. R. Ellis, G. L. Kane, B. D. Nelson, and M. J. Perry, Lightest Visible-Sector Supersymmetric Particle is Likely Unstable, Phys. Rev. Lett. **117**, 181802 (2016).

[18] S. A. Abel and B. W. Schofield, Brane-antibrane kinetic mixing, millicharged particles and SUSY breaking, Nucl. Phys. **B685**, 150 (2004).

[19] S. A. Abel, J. Jaeckel, V. V. Khoze, and A. Ringwald, Illuminating the hidden sector of string theory by shining light through a magnetic field, Phys. Lett. B **666**, 66 (2008).

[20] S. A. Abel, M. D. Goodsell, J. Jaeckel, V. V. Khoze, and A. Ringwald, Kinetic mixing of the photon with hidden U(1)s in string phenomenology, J. High Energy Phys. 07 (2008) 124.

[21] D. Banerjee *et al.*, Search for Invisible Decays of Sub-GeV Dark Photons in Missing-Energy Events at the CERN SPS, Phys. Rev. Lett. **118**, 011802 (2017).

[22] P. Jean *et al.*, Early SPI/INTEGRAL measurements of 511 keV line emission from the 4th quadrant of the Galaxy, Astron. Astrophys. **407**, L55 (2003).

[23] J. Chang *et al.*, An excess of cosmic ray electrons at energies of 300–800 GeV, Nature (London) **456**, 362 (2008).

[24] O. Adriani *et al.* (PAMELA Collaboration), An anomalous positron abundance in cosmic rays with energies 1.5–100 Gev, Nature (London) **458**, 607 (2009).

[25] A. Geringer-Sameth and M. G. Walker, Indication of Gamma-Ray Emission from the Newly Discovered Dwarf Galaxy Reticulum II, Phys. Rev. Lett. **115**, 081101 (2015).

[26] K. K. Boddy and J. Kumar, Indirect detection of dark matter using MeV-range gamma-rays telescopes, Phys. Rev. D **92**, 023533 (2015).

[27] K. Van Tilburg, N. Leefer, L. Bougas, and D. Budker, Search for Ultralight Scalar Dark Matter with Atomic Spectroscopy, Phys. Rev. Lett. **115**, 011802 (2015).

[28] J. H. Chang, R. Essig, and S. D. McDermott, Revisiting Supernova 1987A constraints on dark photons, J. High Energy Phys. 01 (2017) 107.

[29] M. Crisler, R. Essig, J. Estrada, G. Fernandez, J. Tiffenberg, M. S. Haro, T. Volansky, and T.-T. Yu (SENSEI Collaboration), SENSEI: First Direct-Detection Constraints on Sub-GeV Dark Matter from a Surface Run, Phys. Rev. Lett. **121**, 061803 (2018).

[30] J. P. Lees *et al.*, Search for a Dark Photon in $e^+ e^-$ Collisions at BABAR, Phys. Rev. Lett. **113**, 201801 (2014).

[31] B. Kiczek and M. Rogatko, Ultra-compact spherically symmetric dark matter charged star objects, J. Cosmol. Astropart. Phys. 09 (2019) 049.

[32] R.-G. Cai, L. Li, and L.-F. Li, A holographic p-wave superconductor model, J. High Energy Phys. 01 (2014) 032.

[33] M. Rogatko and K. I. Wysokinski, P-wave holographic superconductor/insulator phase transitions affected by dark matter sector, J. High Energy Phys. 03 (2016) 215.

[34] M. Rogatko and K. I. Wysokinski, Condensate flow in holographic models in the presence of dark matter, J. High Energy Phys. 10 (2016) 152.

[35] D. Vollhardt, Characteristic Crossing Points in Specific Heat Curves of Correlated Systems, Phys. Rev. Lett. **78**, 1307 (1997); S. Uchida, T. Ido, H. Takagi, T. Arima, Y. Tokura, and S. Tajima, Optical spectra of $La_{2-x}Sr_xCuO_4$: Effect of carrier doping on the electronic structure of the CuO_2 plane, Phys. Rev. B **43**, 7942 (1991); J. K. Freericks, T. P. Devereaux, and R. Bulla, Exact theory for electronic Raman scattering of correlated materials in infinite dimensions, Phys. Rev. B **64**, 233114 (2001).

Holographic DC SQUID in the presence of *dark matter*

Bartłomiej Kiczek, Marek Rogatko and Karol I. Wysokiński

Institute of Physics, Maria Curie-Sklodowska University,
pl. Marii Curie-Skłodowskiej 1, Lublin 20-031, Poland

E-mail: bkiczek@kft.umcs.lublin.pl, rogat@kft.umcs.lublin.pl,
karol.wysokinski@poczta.umcs.lublin.pl

Abstract. The gauge-gravity duality has been applied to examine the properties of holographic superconducting quantum device (SQUID), composed of two S-N-S Josephson junctions, influenced by *dark sector* modelled by the additional U(1)-gauge field coupled to the ordinary Maxwell one. The *dark matter* sector is known to affect the properties of superconductors and is expected to enter the current-phase relation. The kinetic mixing between two gauge fields provides a mechanism allowing for the conceivable observation of the effect. We find small but visible effect of the *dark matter* particle traversing the device, which shows up as a change of its maximal current.

Contents

1   Introduction

The quest for the *dark matter* in the Universe has been one of the most important topics of the current research in cosmology and physics [1]. Contemporary astronomical observations of galaxies and primordial radiation endorse the fact that our Universe is made mostly (over 23 percent of its mass) of non-luminous *dark matter*. Several new types of fundamental particles have been claimed as candidates for *dark matter* sector. They are expected to interact with nuclei in suitable detector materials on Earth. It was claimed only by the DAMA collaboration [2, 3] that they observed modulation in the rate of interaction events which might be the trace of *dark matter* sector. Several groups want to reproduce the DAMA results but in vain [4]. Recently the problem of *dark matter* identity and its detection has gained new impetus after the XENON1T experiment has reported the signal which source could not be explained [5]. This discovery has sparked intensive theoretical investigations of various scenarios which elucidate the observed effect [6–10]. This situation triggers the discussion concerning the composition, interaction with ordinary matter, the self-interaction and the possible ways to discriminate between various models of *dark matter* [11].

It was argued that due to the growing sense of 'crisis' in the *dark matter* particle community, arising from the absence of evidences for the most popular candidates for *dark matter* particles like WIMPs, axions and sterile neutrinos, diversifying the experimental effort should be paid attention to. These efforts ought to accomplish upcoming astronomical surveys, gravitational wave observatories which can provide us some complimentary information about the *dark matter* sector. They constitute our best hope for making progress in this direction. Unconventional experiments and techniques are also being looked for. One of the prospect directions is related to clever usage of molecular or condensed matter systems including superconductors or superconducting devices. Recent proposals authorise search for bosonic *dark matter via* absorption in superconductors [12], using superfluid helium [13] or optical phonons in polar materials [14] to detect light *dark matter*. More exotic proposals are based on the observations of color centres production in crystals [15], or the usage of bulk three-dimensional Dirac semi-metals [16] and other topological semiconducting compounds [17], as

well as, multilayered optical devices [18], for the detection of possible candidates for *dark matter* sector.

The theoretical approach we have been using in our research relies on the AdS/CFT correspondence [19, 20], which has been found to provide strong coupling description [21, 22] of many condensed matter models. In particular this gauge-gravity duality has been shown to describe U(1) and SU(2) symmetry breaking superconducting transitions. The applications of the holography to study various models of superconductivity have been recently reviewed in [23].

Our previous AdS/CFT studies [24]–[34] on holographic superconductors and superfluids reveal the influence of *dark matter* sector on various properties of them, e.g., superconducting transition temperature, Ginzburg-Landau ratio, vortices and condensation flow, viscosity bound for anisotropic superfluids and interacting currents in holographic Dirac fluid. These findings may in principle help to design future condensed matter experiments oriented on detection of *dark matter*. However, more sensitive probes are still searched for. One of them is proposed in the current paper, i.e., examination of the properties of DC SQUID device built of two Josephson junctions and influenced by *dark sector*.

The Josephson effect [35] is the well known quantum phenomenon observed in devices consisting of two superconductors separated by a thin layer of normal metal, insulator or a superconductor with much lower transition temperature. Such junctions, known as Josephson junctions, even without external bias sustain the direct current I which magnitude is related to the phase difference $\phi = \phi_L - \phi_R$

$$I = I_{\max} \sin \phi, \tag{1.1}$$

where ϕ_L and ϕ_R are the phases of the superconducting order parameter on the left and right hand side of the junction. When the external magnetic flux Φ penetrates the interior of SQUID its maximal current depends on the flux as $I_{\max}(\Phi) = I_c \left| \cos \frac{\pi \Phi}{\phi_0} \right|$, where $\phi_0 = \frac{h}{2e}$ is the magnetic flux quantum. This relation is at the heart of many devices able to detect tiny magnetic fields [36]. As it has already alluded to, our aim is to study the effect of the *dark sector* particle on the holographic SQUID. Recently the so-called second order Josephson effect has been proposed to detect axionic *dark matter* [37, 38].

The holographic model of Josephson junction was also paid attention to. In [39] a gravitational dual of S-N-S junction was constructed and the calculations on the gravity side reproduced the standard relation between the current across the junction and the phase difference of the considered condensate. In the probe limit, Maxwell field coupled to complex scalar one, was examined in the background of AdS-Schwarzschild black brane. The Josephson junction array was considered in [40], where a model was proposed in the background of multi-supergravity theories on products of distinct asymptotically AdS spacetimes coupled by mixed boundary conditions. Among all it was found that the Cooper-pair condensates were described by a discretised Schrödinger-like equation. In a continuum limit the relation in question became a generalised Gross-Pitajevski equation, known from the long-wavelength description of superfluids.

A holographic model of S-I-S junction constructed by examining a complex scalar field coupled to Maxwell one, in the background of four-dimensional AdS soliton was examined in [41]. The dependence of the maximal current on the dimension of the condensate operator and the width of the junction were presented. On the other hand, a holographic configuration including a chiral time-reversal breaking superconductors in $(2+1)$-dimensions was discussed in [42], where the ansatz for $p_x + ip_y$ superconductors [43] was implemented. Such kind of
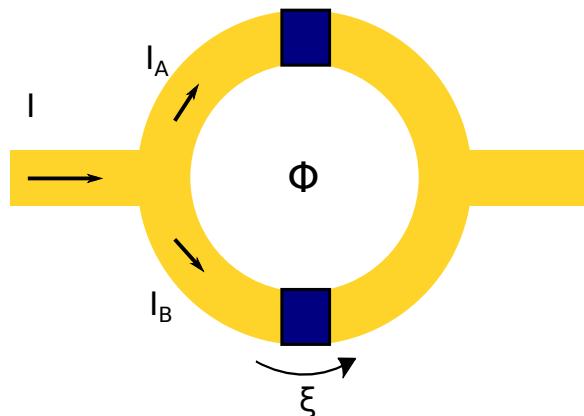
Figure 1. The schematic view of the condensed matter superconducting quantum interference device consisting of two Josephson junctions (dark-blue) embedded into the superconducting loop (yellow-bright). The current I flowing across the system is split into I_A in the upper and I_B in the lower branch of the device. The presence of the magnetic flux Φ induces the interference in the system. For the holographic setup see text for details.

superconductor is believed to support topologically protected gapless Majorana-Weyl edge modes. On the other hand, the model with two coupled vector fields, was also implemented in a generalisation of p-wave superconductivity, for the holographic model of ferromagnetic superconductivity [44].

The construction of a Josephson junction in non-relativistic case with a Lifshitz geometry as the dual gravity was discussed in [45], where the effect of the Lifshitz scaling was elaborated. Among all the standard sinusoidal relation between the current and phase difference was revealed for various values of scaling. The relation featuring exponential decreasing between condensate operator and the width of the weak link, as well as, the relation connected the critical current with the width were found.

Holographic s-wave and p-wave Josephson junctions with backreaction were studied in [46]. It turns out that the critical temperature of the considered junctions decreases with the increase of backreaction, while the tunnelling current and condensation also decrease with the growth of backreaction. However, the relation between current and phase difference remains in the form of a sine-function. On the other hand, the problems of holographic models of hybrid and coexisting both types of junctions, i.e., s- and p-wave were analysed in [47].

The studies of S-N-S junction in massive gravity theory unveil that the graviton mass parameter make it difficult for the normal metal-superconductor phase transition to occur [48]. Moreover the mass graviton parameter increase will cause the decrease of the maximal tunnelling current.

In recent years there has been also an interest in building holographic model of superconducting quantum interference device (SQUID) consisting of two appropriately connected Josephson junctions (see figure 1 for the condensed matter model). Consequently, in order to construct the holographic analog of SQUID one considers Einstein-Maxwell gravity with complex scalar field in $(3 + 1)$-dimensional AdS Schwarzschild black brane background. One of the spatial dimensions is compactified into a circle and with the properly chosen profiles of the chemical potential constitute the main building blocks of the holographic SQUID [49, 50].

Taking our main goal into account we interpret the relation $I = I_A + I_B$ for the total current in the SQUID, with the currents flowing across each of the junctions given by the

relation (1.1), in the slightly different manner. Namely suppose, that the phase difference, $\Delta\phi_A$ (or $\Delta\phi_B$), in one of the branches of the considered device has changed as a result of external factors. In the model under inspection we understand this phenomenon as a *hidden sector* particle appearing in one of the Josephson junctions of the SQUID. This means that the current phase relation changes in the same way as if the effective magnetic flux would appear. The large sensitivity of the device, rises the hope of detecting such transition of the *dark matter* particle, under the assumption of the validity of the coupling between *hidden* and *visible* sectors. In this paper we shall suppose that a single *dark matter* particle appears in one SQUID branch at a time, leaving aside the issue of possible fluctuations of the SQUID signal due to consecutive events. This problem will be studied in future publications.

The main motivation standing behind our consideration is to reinvestigate the holographic model of the Josephson junctions and the SQUID [39, 49, 50], in order to include the *hidden sector* particles responsible for the *dark matter* fields. In conventional physics the *hidden sector* should be added to the Standard Model. On the contrary, in our attitude we shall build holographic model in which *dark sector* naturally emerges from the string/M theory. In our research we shall consider the model in which the additional U(1)-gauge field is coupled to the ordinary Maxwell one. The action describing Maxwell *dark matter* sector is provided by [53, 54].

$$S_{\mathrm{dm+EM}} = \int \sqrt{-g} \; d^4x \left(-\frac{1}{4} F_{\mu\nu} F^{\mu\nu} - \frac{1}{4} B_{\mu\nu} B^{\mu\nu} - \frac{\alpha}{4} F_{\mu\nu} B^{\mu\nu} \right), \tag{1.2}$$

where $F_{\mu\nu} = 2\nabla_{[\mu} A_{\nu]}$ stands for the ordinary Maxwell strength tensor, while the hidden U(1)-gauge field $B_{\mu\nu}$ is given by $B_{\mu\nu} = 2\nabla_{[\mu} B_{\nu]}$. α is a coupling constant between two gauge fields. Predicted values of α-coupling constant, being the kinetic mixing parameter between the two U(1)-gauge fields, for realistic string compactifications range between 10^{-2} and 10^{-16} [55]–[58].

The compatibility with the current observations authorises its order up to 10^{-3}. It happens that some astrophysical phenomena like observations of $511\,\mathrm{eV}$ gamma rays [59], experiments connected with the detection of the electron positron excess in galaxies [60, 61], as well as, possible explanation of muon anomalous magnetic moment [62], strongly argue for the idea of *dark sector* coupled to the Maxwell one. Moreover, the *kinetic mixing term* between ordinary boson and relatively light one (the *dark* one) arising from U(1)-gauge symmetry bounded with a *hidden sector*, may be responsible for a low energy parity violation [63]. On the other hand, the low energy gauge interaction in the *hidden sector* may be envisaged by the Higgs boson decays, and a relatively light vector boson with mass $m \geq 10\,\mathrm{GeV}$ emergence [64].

As was mentioned the justifications of such kind of models might be obtained from the top-down perspective [65], starting from the string/M-theory. It is very important from the AdS/CFT correspondence point of view, because string/M-theory constitutes a fully quantum description and this guarantees that any phenomena envisaged by the top-down reduction are physical.

The second term in the above action is connected with some hidden sector [65], while the interaction of the visible and hidden sectors are described by the so-called *kinetic mixing term*, for the first time introduced in [66], in order to describe the existence and subsequent integrating out of heavy bi-fundamental fields charged under the U(1)-gauge groups. The term in question is characteristic for theories having in addition to some visible gauge group an additional one, in the hidden sector. The hidden sector describes states in the low-energy

effective theory, uncharged under the Standard Model gauge symmetry groups. On the contrary they are charged under their own groups.

It is gravity which enables interaction between those two sectors [67, 68]. It turns out that the realistic embeddings of the Standard Model in $E8 \times E8$ string theory, as well as, in type I, IIA, or IIB open string theory with branes, require the existence of the hidden sectors for the consistency and supersymmetry breaking [56, 69]. On the other hand, in string phenomenology [56] the dimensionless kinetic mixing term parameter can be produced at an arbitrary high energy scale and it does not deteriorate from any kind of mass suppression from the messenger introducing it. This fact is of a great importance from the experimental point of view, due to the fact that its measurement can provide some interesting features of high energy physics beyond the range of the contemporary colliders.

Moreover the mixing term of two gauge sectors are typical for states for open string theories, where both U(1)-gauge groups are advocated by D-branes that are separated in extra dimensions. It happens in supersymmetric Type I, Type IIA, Type IIB models and results in the existence of massive open strings which stretch between two D-branes [55].

The organization of the paper is as follows. In the next section we pay attention to the holographic model of DC SQUID composed of two Josephson junctions in Einstein-Maxwell gravity with complex scalar field affected by the *dark sector* particles modelled by the hidden U(1)-gauge field interacting with the ordinary Maxwell one. One considers the model of the junction, where a central part constitutes a normal metal (S-N-S). We also mentioned the case with an insulator (S-I-S). Section 3 is devoted to the numerical solutions of the adequate equations of motion, for the homogeneous case and the case of a *dark matter* beam. We propose an 'experiment' which helps to distinguish the presence of *dark matter* sector. In section 4 we concluded our investigations.

2 The holographic model and equations of motion

In this section we present the examined holographic model and the resulting equations of motion. We shall examine the holographic DC SQUID, composed of the two S-N-S Josephson junctions. We give some comments concerning the construction of holographic model of such a device.

2.1 How to build holographic SQUID influenced by *dark matter* sector?

As the SQUID is composed of two Josephson junctions we shall concentrate on the problem how to build holographic model of the S-N-S Josephson junction with the phase difference across the normal region, say γ. In order to simulate it one has to implement the holographic description of the superconductor, i.e., we should have the AdS background because of the fact that we describe an approximately conformal field theory.

In the next step we want to describe the conserved U(1) currents J_μ in the field theory. According to the AdS/CFT dictionary [22] in the gravity dual they correspond to gauge fields. In our case these gauge fields will be bounded with ordinary Maxwell field and the auxiliary one, pertaining to the *hidden sector*.

The superconducting state requires spontaneous symmetry breaking,[1] which on the gravity side corresponds to the condensation of the (complex) scalar field. The operator for which vacuum expectation value is non-zero will correspond to the scalar field in the bulk.

---

[1]The global symmetry of the boundary field theory is the conservation of the charge, which is precisely broken below the superconducting transition temperature. On the gravity side this is marked as an instability of the black hole which becomes hairy.

In order to incorporate temperature in the theory we take into account the black brane with Hawking temperature. On the other hand, to have $T_C \neq 0$, one incorporates the scale to generate it, which can be done by either introducing chemical potential μ or a non-zero charge density. In the AdS/CFT dictionary μ, on the field theory side, is correlated with the vacuum expectation value of the time component of gauge field. Thus if we take a non-zero chemical potential to generate superconductivity, one achieves a critical temperature proportional to it. All these points lead the holographic model of Josephson junction in which one should also have varying chemical potential $\mu(\vec{x})$ at fixed temperature (we have black brane at fixed Hawking temperature) such that in most of the space temperature T is below T_C connected with μ (the system in question is in a superconducting state) but in a narrow gap is above it, and the system is in a normal state.

For technical reasons we introduce gauge invariant fields described by $M_\mu = A_\mu - \partial_\mu \phi$, which have the adequate asymptotics at the boundary of AdS spacetime, i.e. for $r \to \infty$ proportional to chemical potential, charge density, superfluid velocity and current. Because of the fact that the ansatz for the scalar field has a quantum phase ϕ and $M_x = -\partial_x \psi + A_x$, the gauge invariant phase difference across the normal gap is given by

$$\gamma = - \int_{\text{gap}} dx M_x = \Delta \phi - \int_{\text{gap}} dx A_x. \tag{2.1}$$

It concludes, that from the boundary at infinity one obtains the following relation:

$$\gamma = - \int_{-\infty}^{+\infty} dx \left[\nu(x) - \nu(\infty) \right]. \tag{2.2}$$

Moreover, at the black brane event horizon we need to have the regularity conditions fulfilled, i.e., $M_t(r = r_0) = 0$. One also imposes that the junction is unbiased so $\mu(\infty) = \mu(-\infty)$ meaning that near the boundary μ approaches x-independent value.

Finally, in order to construct the holographic model of Josephson junction one demands the adequate profile for the chemical potential, for which we ought to obtain that $T_C \sim \mu(\infty)$ with $T_{\text{Hawking}} < T_C$, and also we demand that μ is much smaller in the junction leading to $T_C < T_{\text{Hawking}}$ there. All these conditions ensure that we arrive at superconductor for most of the range of $\vec{x}$, only in the thin region we shall get a normal state.

To conclude, the philosophy underlying our considerations is to incorporate *visible* and *hidden* sectors into AdS spacetime, apply the AdS/CFT machinery, and look if there are some implications of the auxiliary U(1)-gauge field at $r \to \infty$, at the boundary of the spacetime.

2.2 Equations of motion for the model

The holographic model of the 2+1 dimensional system in question relies on the 3+1 dimensional gravitation background of AdS static Schwarzschild black brane spacetime. One will work in the probe limit, which means that matter field do not cause the fluctuations of the gravitational one, we have no backreaction effects. In the probe limit approximation the dynamics of the gravitational part of the considered model will decouple from the rest, therefore one can elaborate gauge field perturbations on the fixed black brane background which is therefore uncharged.

The gravitational action in (3+1) dimensions is taken in the form

$$S_g = \int \sqrt{-g} \, d^4 x \, (R - \Lambda), \tag{2.3}$$

where $\Lambda = -6/L^2$ stands for the negative cosmological constant, while L is the radius of the AdS spacetime. In what follows we set $L = 1$.

We shall examine the Abelian-Higgs sector coupled to the *hidden* U(1)-gauge field, coupled to the *visible* one by the *kinetic mixing term*, with a coupling α

$$S_{\mathrm{dm+EM}+H} = \int \sqrt{-g}\ d^4x\ \left(-\frac{1}{4}F_{\mu\nu}F^{\mu\nu} - [\nabla_\mu\psi - i\ A_\mu\psi]^\dagger\ [\nabla^\mu\psi - i\ A^\mu\psi] - m^2|\psi|^2 \right.$$
$$\left. -\frac{1}{4}B_{\mu\nu}B^{\mu\nu} - \frac{\alpha}{4}F_{\mu\nu}B^{\mu\nu} \right). \tag{2.4}$$

In many analysis of the *hidden sector* in holographic approach [24]–[34], α is taken as a constant. In [44], where the generalisation of the considered model to SU(2) gauge fields was studied in the context of holographic model of ferromagnetic superconductivity, α was incorporated in the redefined gauge fields being the mixture of *visible* and *hidden* sectors components. In our attitude we are interested in the influence of the *dark sector* on the physics and therefore we shall treat both sectors and kinetic mixing term between them.

However, as it will be revealed in section 3.1 of our work, such assumption about the homogeneity of α-coupling constant gives no response on the considered holographic model of SQUID.

In order to make the investigations more realistic, and find the influence of *dark sector* on the physics of the holographic device, we suppose that instead of the coupling in the *kinetic mixing term* we shall take into account the strength parameter function ζ, which controls the strength of *visible* and *hidden sectors* interaction. Having in mind that our line element is static, i.e., that one has time-like Killing vector field orthogonal to the three-dimensional space-like hypersurface, our strength parameter function will depend on spatial coordinates.

In our considerations we shall elaborate the problem of the response of a holographic superconducting junction/SQUID to the appearance of *dark matter particle*. Due to the geometric constraints (see for the details [49, 50]), the nontrivial response of the holographic (2+1) dimensional SQUID is expected to appear only if one of its junctions is affected by a *dark matter particle*.

As it was already mentioned, to mimic the passage of the *dark particle via* one of the junctions of the holographic SQUID we assume that the coupling ζ depends on space-like coordinates. This is taken into account in the derivation of the underlying equations of motion. Later on we specify the particular dependence $\zeta(x_a)$ used to solve the model.

The equations of motion are provided by

$$(\nabla_\mu - i\ A_\mu)(\nabla^\mu - i\ A^\mu)\psi - m^2\ \psi = 0, \tag{2.5}$$

$$\nabla_\mu F^{\mu\nu} + \frac{1}{2}\nabla_\mu(\zeta\ B^{\mu\nu}) - i\left[\psi^\dagger(\nabla^\nu - i\ A^\nu)\psi - \psi(\nabla^\nu + i\ A^\nu)\psi^\dagger\right] = 0, \tag{2.6}$$

$$\nabla_\mu B^{\mu\nu} + \frac{1}{2}\nabla_\mu(\zeta\ F^{\mu\nu}) = 0. \tag{2.7}$$

Consequently, using the last two equations one has that

$$\tilde{\zeta}\ \nabla_\mu F^{\mu\nu} + \frac{1}{2}\nabla_\mu\zeta\left(B^{\mu\nu} - \frac{1}{2}\alpha F^{\mu\nu}\right) - i\left[\psi^\dagger\ (\nabla^\nu - i\ A^\nu)\psi - \psi(\nabla^\nu + i\ A^\nu)\psi^\dagger\right] = 0, \tag{2.8}$$

where we set $\tilde{\zeta} = 1 - \zeta^2/4$.

As we have mentioned above, as a gravitational background we shall consider static four-dimensional AdS-Schwarzschild black brane line element, given by

$$ds^2 = -f(r)dt^2 + \frac{1}{f(r)}dr^2 + r^2 \, (d\xi^2 + dx^2), \tag{2.9}$$

where $f(r) = r^2 - r_0^3/r$ and r_0 is the horizon radius of the black brane, while the direction ξ is compactified with the periodicity $-\pi \, R \leq \xi \leq \pi \, R$, where R is the radius of the ξ-loop.

For further analysis it is convenient to assume that $r_0 = 1$ and $\pi \, R = 10$. According to the claim in [39], the coherence length for the considered model is estimated to be about ~ 1.20 within these units. We argue that the length of the SQUID loop should be much larger than the coherence length, in order to decrease the influence of the proximity effect and consequently the mixing of the phases. Fulfilling this condition, we obtain a homogeneous superconducting phase at the both ends of the ξ-direction. It results in a well defined phase difference for the junction under inspection. On the other hand, one wants to establish our weak link of the junction to be narrow enough, that its critical current receives a sufficiently high value. This is important from the point of view of the numerics, i.e., the precision of the solutions. Having all the above arguments in mind, we establish $R = 10/\pi$ as a reasonable choice.

In what follows one chooses the following components of the fields in the underlying theory:

$$\psi = |\psi|e^{i\phi}, \qquad A_\mu = (A_t, \, A_r, \, A_\xi, \, 0), \qquad B_\mu = (B_t, \, B_r, \, B_\xi, \, 0), \tag{2.10}$$

where we assume that all the field components and the phase are real functions dependent on $(r, \, \xi)$-coordinates. Moreover, one defines the gauge invariant quantities $M_\mu = A_\mu - \partial_\mu\phi$.

Consequently, the equations of motion yield

$$\partial_r^2|\psi| + \frac{1}{r^2 \, f}\partial_\xi^2|\psi| + \left(\frac{2}{r} + \frac{\partial_r f}{f}\right)\partial_r|\psi| + \left[\frac{1}{f^2} \, M_t^2 \; - \frac{1}{r^2 \, f} \, M_\xi\right. \tag{2.11}$$

$$\left. - M_r^2 - \frac{m^2}{f}\right] |\psi| = 0,$$

$$\partial_r M_r + \frac{1}{r^2 f}\partial_\xi M_\xi + \frac{2}{|\psi|}\left(M_r \partial_r|\psi| + \frac{M_\xi}{r^2 f} \, \partial_\xi|\psi|\right) + \left(\frac{2}{r} + \frac{\partial_r f}{f}\right) M_r = 0, \tag{2.12}$$

$$\tilde{\zeta}\left[\partial_r^2 M_t + \frac{2}{r} \, \partial_r M_t + \frac{1}{r^2 \, f} \, \partial_\xi^2 M_t\right] - \frac{2}{f} \, M_t \, |\psi|^2 \tag{2.13}$$

$$+ \frac{1}{2}\partial_r\zeta\left[(\partial_t B_r - \partial_r B_t) - \frac{\zeta}{2} \, (\partial_t M_r - \partial_r M_t)\right]$$

$$+ \frac{1}{2}\partial_\xi\zeta\left[-\frac{1}{r^2 f} \, (\partial_\xi B_t - \partial_t B_\xi) + \frac{\zeta}{2}\frac{1}{r^2 f} \, (\partial_\xi M_t - \partial_t M_\xi)\right] = 0,$$

$$\tilde{\zeta}\left[\partial_\xi^2 M_r - \partial_\xi\partial_r M_\xi\right] - 2 \, r^2 \, M_r \, |\psi|^2 + \frac{1}{2}\partial_\xi\zeta\left[(\partial_\xi B_r - \partial_r B_\xi)\right. \tag{2.14}$$

$$\left. - \frac{\zeta}{2} \, (\partial_\xi M_r - \partial_r M_\xi)\right] = 0,$$

$$\tilde{\zeta}\left[\partial_r^2 M_\xi - \partial_r\partial_\xi M_r + \frac{\partial_r f}{f} \, (\partial_r M_\xi - \partial_\xi M_r)\right] - \frac{2 \, M_\xi}{f} \, |\psi|^2 \tag{2.15}$$

$$+ \frac{1}{2}\partial_r\zeta\left[\frac{f}{r^2} \, (\partial_r B_\xi - \partial_\xi B_r) - \frac{\zeta}{2}\frac{f}{r^2} \, (\partial_r M_\xi - \partial_\xi M_r)\right] = 0.$$

The components of the relation (2.7) imply

$$\frac{2}{r}\partial_r B_t + \partial_r^2 B_t + \frac{1}{r^2 f}\partial_\xi^2 B_t + \frac{1}{2}\partial_r\zeta\ \partial_r M_t + \frac{1}{2}\partial_\xi\zeta\frac{1}{r^2 f}\partial_\xi M_t \qquad (2.16)$$

$$+\frac{\zeta}{2}\left(\frac{2}{r}\partial_r M_t + \partial_r^2 M_t + \frac{1}{r^2 f}\partial_\xi^2 M_t\right) = 0,$$

$$\partial_r^2 B_\xi - \partial_r\partial_\xi B_r + \frac{\partial_r f}{f}\left(\partial_r B_\xi - \partial_\xi B_r\right) + \frac{1}{2}\partial_r\zeta\left(\partial_r M_\xi - \partial_\xi M_r\right) \qquad (2.17)$$

$$+\frac{\zeta}{2}\left[\partial_r^2 M_\xi - \partial_r\partial_\xi M_r + \frac{\partial_r f}{f}\left(\partial_r M_\xi - \partial_\xi M_r\right)\right] = 0,$$

$$\partial_\xi\left(\partial_\xi B_r - \partial_r B_\xi\right) + \frac{1}{2}\partial_\xi\zeta\left(\partial_\xi M_r - \partial_r M_\xi\right) + \frac{\zeta}{2}\partial_\xi\left(\partial_\xi M_r - \partial_r M_\xi\right) = 0. \qquad (2.18)$$

To proceed further, we ought to choose the form of $\zeta(x_i)$. One of the possible representations of it is a Gaussian function form

$$\zeta(\xi) = \alpha_0 e^{-(\xi-\xi_0)^2/\lambda^2}, \qquad (2.19)$$

where α_0 is the peak value of the coupling and λ its decay length (half of the Gaussian width). Our choice of the strength function controlling interaction of both sectors in question $\zeta(\xi)$, was motivated by the features of static line element chosen for the description of holographic device, given by (2.9), as well as, the astrophysical observations revealing the space-like dependence of *dark matter* distribution in the observable Universe.

The half of the Gaussian width λ is an important parameter of the model as its ratio to the holographic SQUID characteristic length-scale πR and the shape of the weak link affect the holographic SQUID's response.

In principle, there are two possible attitudes for modelling the local presence of the *dark matter sector* fields in this theory. We can either pick α to be constant and impose specific boundary conditions for *dark matter* fields or as it was mentioned before, promote the strength function ζ with a spatial dependence and keep the fields in the homogeneous scenario. In this approach we selected the latter one, so we can choose the x-independent and source free solution of B_μ fields, which simply yields

$$B_\alpha\ dx^\alpha = \mu_D\left(1 - \frac{r_0}{r}\right)dt. \qquad (2.20)$$

By putting this assumption into our system of differential equations we receive a significant simplification, with only four functions to be obtained numerically. In particular the resulting equations depend on the *dark sector* only *via* the effective coupling $\tilde\zeta$ and not μ_D.

$$\partial_r^2|\psi| + \frac{1}{r^2\ f}\partial_\xi^2|\psi| + \left(\frac{2}{r} + \frac{\partial_r f}{f}\right)\partial_r|\psi| + \left[\frac{1}{f^2}\ M_t^2 - \frac{1}{r^2\ f}\ M_\xi^2 - M_r^2 - \frac{m^2}{f}\right]|\psi| = 0, \quad (2.21)$$

$$\tilde\zeta\left[\partial_r^2 M_t + \frac{2}{r}\ \partial_r M_t + \frac{1}{r^2\ f}\ \partial_\xi^2 M_t\right] - \frac{2}{f}\ M_t\ |\psi|^2 + \frac{1}{2}\partial_\xi\zeta\frac{\zeta}{2}\frac{1}{r^2 f}\partial_\xi M_t = 0, \quad (2.22)$$

$$\tilde\zeta\left[\partial_\xi^2 M_r - \partial_\xi\partial_r M_\xi\right] - 2\ r^2\ M_r\ |\psi|^2 - \frac{1}{2}\partial_\xi\zeta\frac{\zeta}{2}\left(\partial_\xi M_r - \partial_r M_\xi\right) = 0, \quad (2.23)$$

$$\tilde\zeta\left[\partial_r^2 M_\xi - \partial_r\partial_\xi M_r + \frac{\partial_r f}{f}\left(\partial_r M_\xi - \partial_\xi M_r\right)\right] - \frac{2\ M_\xi}{f}\ |\psi|^2 = 0. \quad (2.24)$$

– 9 –

The above forms of the equations envisage that comparing to the case when $\zeta = 0$, the modification is significant. Some terms are multiplied by $\tilde{\zeta}$ and moreover we have additional terms with $\zeta \partial_\xi \zeta$ factor. Numerical solutions of these equations will be presented in the subsequent part of the paper.

As we have remarked at the beginning of the section, the presented model describes SQUID with S-N-S type Josephson junctions. Nevertheless, for the completeness of the results, we shall mention the modeling of S-I-S Josephson junction. In the holographic model of the insulator the AdS soliton line element will play the crucial role. Namely, performing the double Wick rotation on the metric (2.9), we arrive at the AdS soliton line element [70]. It is provided by

$$ds^2 = -r^2 dt^2 + \frac{dr^2}{f(r)} + r^2 dx^2 + f(r)d\chi^2, \tag{2.25}$$

with the same function $f(r)$ as before. However, the coordinate χ has the period $\beta = 4\pi l/3r_0$, in order to avoid the conical singularity at $r = r_0$.

As in the previous case we assume that the following components of the gauge field are non-zero $A_\mu = (A_t, \ A_r, \ A_x, \ 0)$, and that all the field components and the phase ϕ are real functions dependent on $(r, \ x)$-coordinates. The equations of motion are very similar to the ones obtained in the previous case. In fact only the factor in front of $\partial_r M_t$ instead of $\frac{2}{r}$ reads $\frac{\partial_r f}{f}$. The results will differ only quantitatively, therefore they will be not analysed numerically.

Having discussed the model set up we shall describe appropriate boundary conditions for our model. Starting with AdS boundary where $r \to \infty$, the asymptotic of the fields in question are provided by

$$|\psi| = \frac{|\psi^{(1)}(\xi)|}{r^{\Delta_{(1)}}} + \frac{|\psi^{(2)}(\xi)|}{r^{\Delta_{(2)}}} + \mathcal{O}(r^{-3}), \tag{2.26}$$

$$M_t = \mu(\xi) - \frac{\rho(\xi)}{r} + \mathcal{O}(r^{-2}), \tag{2.27}$$

$$M_r = \mathcal{O}(r^{-3}), \tag{2.28}$$

$$M_\xi = \nu(\xi) + \frac{J(\xi)}{r} + \mathcal{O}(r^{-2}), \tag{2.29}$$

where

$$\Delta_{(1)} = \frac{1}{2}\left(3 - \sqrt{9 + 4m^2}\right), \qquad \Delta_{(2)} = \frac{1}{2}\left(3 + \sqrt{9 + 4m^2}\right). \tag{2.30}$$

In the boundary field theory the quantities $\mu(\xi)$, $\rho(\xi)$, $\nu(\xi)$, and $J(\xi)$ are connected with the chemical potential, charge density, superfluid velocity and current, respectively. On the other hand, $|\psi^{(1)}(\xi)|$ and $|\psi^{(2)}(\xi)|$ may be considered as the source and the vacuum expectation value of the dual operator of the scalar field $|\psi(\xi)^{(2)}| = \langle O \rangle$. In the numerical calculation we set $|\psi^{(1)}(\xi)| = 0$ (as turning off the source), because one has that the U(1)-gauge symmetry be broken. At the black brane event horizon we demand that $g^{tt} M_t$ ought to be regular, but because of the fact that g^{tt} is divergent on the horizon, M_t should vanish at $r = r_0$. The remaining fields should be finite at the event horizon and the simplified equations of motion place the boundary conditions therein. In our numerical calculations for simplicity we set $m^2 = -2$ which is above Breitenlohner-Freedman limit $m^2 \geq -\frac{9}{4}$, therefore $\Delta_{(1)} = 1$ and $\Delta_{(2)} = 2$.

3 Numerical results

This section will be devoted to the results of our numerical solutions of the equations of motion for the holographic Josephson junction and holographic DC SQUID device. At first we pay attention to the case of homogeneous holographic superconductor influenced by the *dark matter* sector. Then we proceed to analyse the model of SQUID with a beam of *dark matter*, i.e., we take into account the strength parameter controlling the strength of *visible* and hidden sectors interaction and allow for its ξ dependence.

3.1 Homogeneous superconductor — warm up

To commence with, let us consider the properties of homogeneous holographic superconductor, i.e., we take α as a constant value, influenced by the *dark matter* sector, and look for its critical temperature, critical chemical potential and value of the condensation. For this calculation we straight out the ξ dimension renaming it to x. Then by neglecting the spatial dependence of x-coordinate in the equations of motion, we receive the simplified system of differential equations

$$\partial_r^2 |\psi| + \left(\frac{2}{r} + \frac{\partial_r f}{f} \right) \partial_r |\psi| + \left[\frac{1}{f^2}\ M_t^2\ - \frac{1}{r^2\ f}\ M_x - \frac{m^2}{f} \right] |\psi| = 0, \tag{3.1}$$

$$\partial_r^2 M_t + \frac{2}{r}\partial_r M_t - \frac{2}{\tilde{\alpha}\ f}\ M_t\ |\psi|^2 = 0, \tag{3.2}$$

$$\partial_r^2 M_x + \frac{\partial_r f}{f}\partial_r M_x - \frac{2\ M_x}{\tilde{\alpha}\ f}\ |\psi|^2 = 0. \tag{3.3}$$

where $\tilde{\alpha} = 1 - \frac{\alpha^2}{4}$ and all the above three functions, i.e., $|\psi|$, M_t, M_x, depend only on r.

These equations establish the boundary conditions for a homogeneous region of superconductor in x-dependent approach, but for the analysis of phase transitions we set the current to zero, which implies that $M_x = 0$. Now we can move towards numerical solution of our equations. In order to proceed further, we perform coordinate transformation $z = 1 - \frac{1}{r}$ in order to work on a $(0, 1)$ grid, where $z = 0$ is the black hole horizon and $z = 1$ is the holographic boundary. We solve the boundary value problem using the standard relaxation method for different values of temperature and chemical potential, to investigate the superconductor-normal phase transition. In figures 2 and 3 we plot the condensation operator $\langle O \rangle$ as a function of temperature and the chemical potential for the different values of *dark matter* α-coupling constants.

One concludes that the bigger T/T_c is the smaller value of $\langle O \rangle/T_c$ we obtain. In the case when we fix the value of T/T_c, then the bigger α-coupling constant is taken into account the smaller $\langle O \rangle/T_c$ we get. Just, the condensation diminishes when *dark matter* coupling constant grows. On the other hand, the bigger μ one considers, the larger value of $\langle O \rangle$ we receive, for the fixed value of α-coupling constant. In the case when α grows, we deduce that, the larger α is, the smaller value of the condensation operator one perceives.

In the both types of the analysed phase transitions, the presence of *dark matter* does not shift the phase transition point (critical temperature, critical chemical potential), yet it changes the value of condensation.

Figure 4 depicts the relationship between the condensation operator and *dark matter* coupling constant, for the fixed temperature and chemical potential. The differences are not too big, but they are visible and the lines are distinguishable. However there might be a
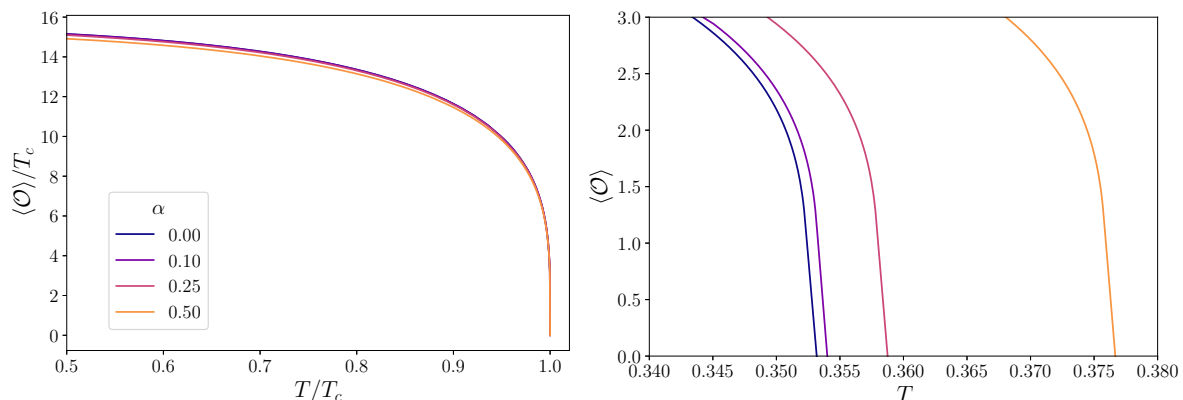
Figure 2. The superconductor-normal phase transition driven by the temperature, affected by *dark matter*. The right panel shows the zoom of the area of left plot which is close to the phase transition and without temperature normalisation. The coupling with the *dark sector* causes the increase of critical temperature.
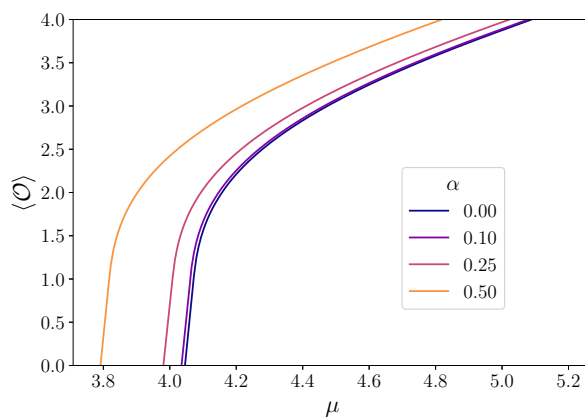

Figure 3. The normal to superconducting phase transition driven by the change of the chemical potential (which can be interpreted as doping) for different values of *dark matter* α-coupling constants. The presence of the *dark sector* coupling causes the phase transition for smaller value of the chemical potential.

problem with measuring such a deviation. Our idea to overcome this obstacle is presented in the next section — by using superconducting devices.

The calculations of this section served as a test of our numerical procedure. The procedure passed the test as the closer inspection of the equations of motion (3.1)–(3.3) shows that the parameter $\tilde{\alpha}$ can be eliminated by rescaling the ψ field, as $\tilde{\psi} = \frac{\psi}{\sqrt{\tilde{\alpha}}}$, with $\tilde{\psi}$ being independent on α. This rescaling leads to the similar rescaling of the condensation parameter $\langle O \rangle$, leading to the solution with α independent value $\langle O \rangle_0$. The expected behavior $\langle O \rangle = \sqrt{\tilde{\alpha}} \langle O \rangle_0$ is clearly visible in figure 4 as are the concomitant changes of other parameters depending on $\langle O \rangle$.

3.2 Analysis of the holographic SQUID

In this subsection we shall treat the case when one has the strength function ζ controlling the interaction between *visible* and *hidden* sectors.
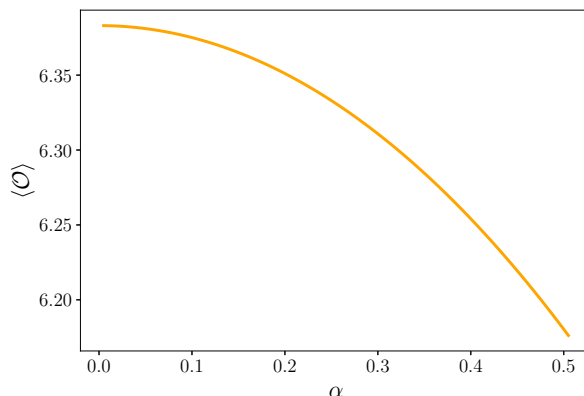
Figure 4. Value of the condensation operator for the constant value of the chemical potential $\mu = 6$ and temperature $T = 3/4\pi$ versus the *dark matter* coupling constant.
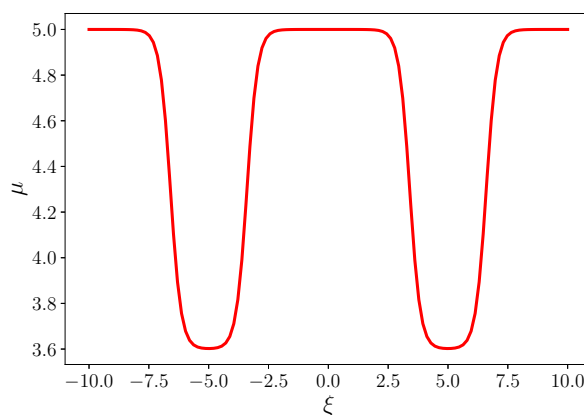

Figure 5. The schematic profile of the chemical potential in the superconducting quantum interference device consisting of two holographic Josephson junctions (lower values of μ) embedded into the superconducting loop with $\mu = 5$.

To imitate the two insulating regions embedded into the superconducting ring we take the chemical potential as given in [49]

$$\mu(\xi) = h - \sum_{i=1,\,2} d_i \left[\tanh\left(\frac{k_i\,(\xi - p_i + w_i)}{\pi} \right) - \tanh\left(\frac{k_i\,(\xi - p_i - w_i)}{\pi} \right) \right], \qquad (3.4)$$

where i = 1, 2 stand for two junctions in the SQUID ring, and h, d_i, k_i, p_i, and w_i are related to the highest value of the chemical potential (inside the superconductor), depth, slope, position, and width of the junction i, respectively. The idea behind this choice is the following: from the previous studies we know that with and/or without *dark matter* it is the value of the chemical potential which tunes the transition between insulator and metal and the temperature decrease induces metal — superconductor transition. To construct a junction it is thus enough to make the chemical potential in the normal part of the junction lower than its critical value for superconducting transition, while leaving it above this value in the superconducting parts of the junction. This is just embodied in the equation (3.4). And shown in figure 5, for the weak links located at $p_1 = 5$ and $p_2 = -5$ with $h = 5$ and identical other parameters $d_1 = d_2 = 0.7$ widths $w_1 = w_2 = 1.6$ and slopes $k_1 = k_2 = 7$.

In the discussion of the holographic SQUID we change γ_L and γ_R, defined in what follows. In our model we assume that the *dark matter* is present only in one of the junctions of SQUID. Such approach gives us a possibility to calculate the difference of the phases between junctions caused by the *dark matter* coupling. In the trivial case (without the presence of *dark matter* sector) the effective magnetic flux defined as $\Phi = \gamma_L - \gamma_R$ vanishes, therefore the critical current

$$J_c = \sqrt{J_L^2 + J_R^2 + 2J_L J_R \cos(\Phi)}, \tag{3.5}$$

becomes constant and equals to $|J_L + J_R|$ On the contrary, when *dark sector* particle is present in one of the junctions, we receive a "yes or no" type criteria for the *dark matter* occurrence.

In adverse to the previously obtained results [49], we do not impose the continuity conditions on our fields in the node points $\xi = 0$ and $\xi = \pm 10$. Moreover we argue that these points can be singular due to the presence of the additional source terms. Especially the supercurrent might not be well behaved when it inflows and outflows from our system. If we wish to model the SQUID with two currents flowing parallel, we have to take $J \sim \text{sgn}(\xi)$, because current flows into the system at $\xi = 0$, then in one branch it flows to $\xi = -10$ and in the another to $\xi = 10$, against and with the ξ axis, respectively.

As far as the boundary value problem is concerned, for the AdS/CFT boundary one has the asymptotic expansions, for the black hole horizon we require that $M_t = 0$, while the conditions for the remaining functions are given by the adequate equation of motion. On the other hand, for the ξ boundary, in both cases, we impose that the functions $|\psi|$, M_t and M_x have to be even and M_r is an odd function with respect to the central point of the junction.

In our numerical computations we implement the pseudo-spectral method with Chebyshev points, which constitutes an extremely efficient tool for smooth functions we deal with in the problem. For convenience we compactify the r-coordinate using following transformation $z = 1 - 1/r$, after which $z = 0$ corresponds to the black hole horizon and $z = 1$ to the AdS boundary. Also we squeeze ξ dimension into $(-1,\ 1)$ range which is the domain of the Chebyshev polynomials. Generally pseudo-spectral methods require only few points in the spatial discretisation to achieve satisfying results, therefore we use the grid with 37 points along ξ direction and 20 points along z axis. By expanding the functions into Chebyshev series we translate a differential problem stated by equations of motion into an algebraic one. Then we deal with a system of nonlinear algebraic equations by standard Newton-Raphson method. In the explained way we solve numerically our set of partial differential equations (2.21)–(2.24) for different values of J_0, varying from -0.06 to 0.06. In figure 6 we plot the exemplary solutions of the underlying equations of motion for $J = 0.03$ and $\alpha_0 = 0.2$. We can see the imposed shape of the chemical potential at the boundary $z = 1$ of the M_t function. The remaining functions react accordingly to the presence of the normal phase. The shapes of the solution are similar to the ones obtained in [39, 41, 49, 50]. However it contains the traces of the influence of α coupling, but they are too small to be visible on such 3D plots. Nevertheless they do have the influence on some of the properties, which will be elaborated below.

After solving our differential equations we obtain the phase differences for the left and right Josephson junctions separately, using the following formula:

$$\gamma_L = -\int_{-10}^{0} [\nu(\xi) - \nu(0)]\, d\xi, \tag{3.6}$$

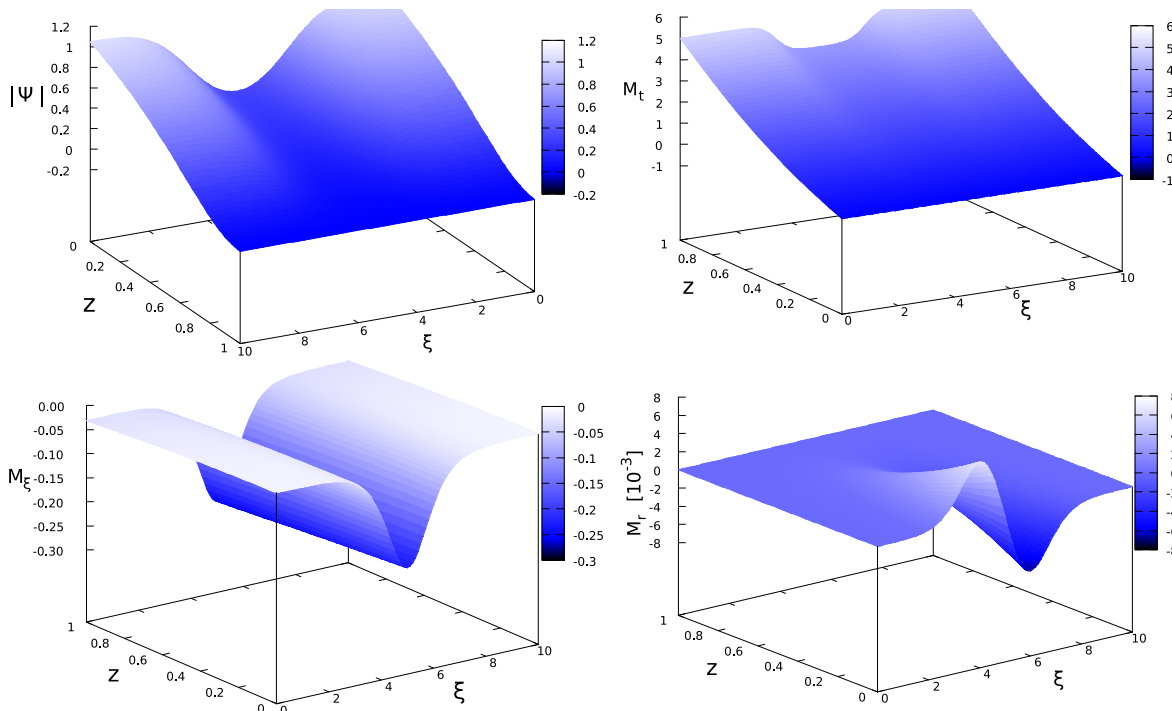$$\gamma_R = -\int_{0}^{10} [\nu(\xi) - \nu(0)]\, d\xi. \tag{3.7}$$

Figure 6. Plots of numerical solutions of equations of motion (2.21)–(2.24) for one of holographic SQUID's Josephson junction with parameters $J = 0.03$ and $\alpha_0 = 0.2$. We can see the imposed chemical potential boundary condition for M_t at the AdS boundary and the reaction of the remaining functions to it.

Next, for each of the Josephson junction we fit in a sine relation between $J_{L/R}$ and $\gamma_{L/R}$, to obtain the value of the maximum current.

Having obtained the values of the critical currents for each junction we can proceed to calculation of the *dark matter* particle induced effective magnetic flux Φ, as defined previously. We wish to see how the critical current of holographic SQUID, defined by the relation (3.5), changes with the presence of *dark matter* in the system, hence one elaborates the case when $\zeta \neq 0$. To proceed further let us define the critical current ratio, given by

$$\delta J = \frac{J_c(\Phi) - J_c(0)}{J_c(0)}. \tag{3.8}$$

In figure 7 the critical current ratio as a function of the magnetic flux, for different values of α_0, is depicted. In our model such behaviour is only possible when *dark particle* appears in one of the junctions. Otherwise, if J_c is independent of Φ the interference does not occur. This gives us the possibility to establish the criterion for detection of the discussed coupling which is correlated with the *dark sector*.

While the residuals of numerical solution of our equations (2.21)–(2.24) and the constraint relation (2.12) are relaxed to the values less than 10^{-12}, the relation from the figure 7 carries a burden of inaccuracy of the least squares method. Namely the sine function is not a perfectly fitting one and the best result we can obtain for the norm of residuals is to the order of 10^{-6}. It results that the uncertainty of the critical current is $\sim 10^{-4}$. Having this in mind, for little and yet realistic values of coupling our computed values of $J(\Phi)$ are below the level of accuracy, so we cannot state its direct value. Although when working on differences,
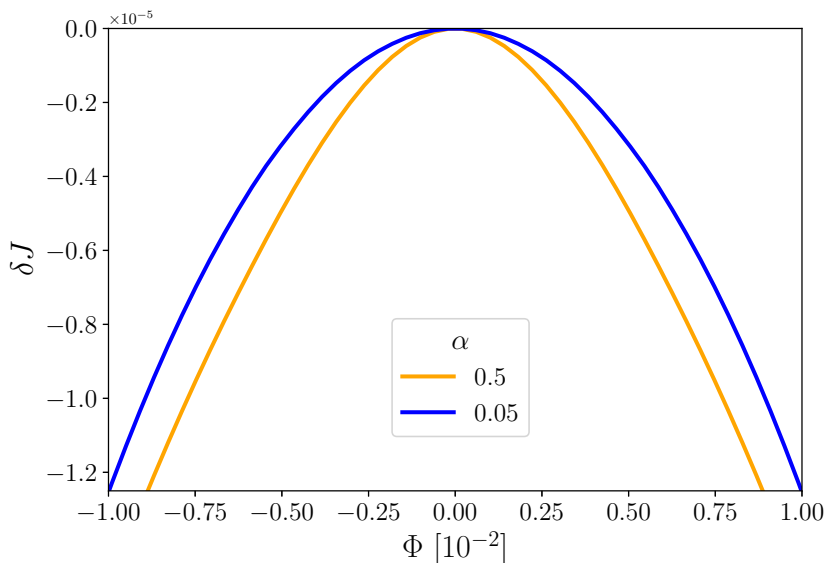
Figure 7. Relative change of critical current ratio from the relation (3.8) versus the effective magnetic flux, which appears to be non-zero in the presence of *dark matter*. The yellow curve represents solution when $\alpha_0 = 0.5$, while the blue one $\alpha_0 = 0.05$. In the case with $\alpha = 0$ such a dependence would not occur, resulting a trivial SQUID with two identical Josephson junctions and $\delta J \equiv 0$.

like in our ratio given by the relation (3.8), these uncertainties are subtracted, so using this quantity seems sensible.

We also investigated the influence of increasing the Gaussian packet decay length λ on the current-phase relation of one of the holographic SQUID's Josephson junctions. By implementing to our code various values of λ (from 1 to 5), we have found out an interesting behaviour which is depicted in figure 8. It envisages the critical Josephson current as a function of the wavelength of the decay length λ. This plot might be interpreted as the sensitivity of the holographic SQUID on detecting *dark matter* sector. On the other hand, it is a very interesting result and may constitute a guidance for future experiments. Namely, by adjusting the size of the normal/insulating part of the holographic Josephson junctions one can tune up the system to react most sensitively on possible detection of *dark particle*. The obtained value of the optimal $\lambda \approx 1.5$ is correlated, as it is expected to be, with the width w of the normal region of the junction affected by the *hidden particles*.

Having a possible range of the Gaussian packet decay length λ, one receives a possibility to prepare an adequate detector for measurements. In the present approach we are assuming that the *dark matter* particle passes the center of the junction. However, one expects that *dark particles* move slightly off the center. In such situation the sensitivity can be roughly read of from the curve shown in figure 8, as the decrease/increase of λ, mimicking the distance from the center of the holographic junction.

4 Holographic versus condensed matter SQUID

Here we compare the holographic results with the expectations based on the standard theory of laboratory SQUID as shown in figure 1. Each branch of the SQUID, in figure 1, contains
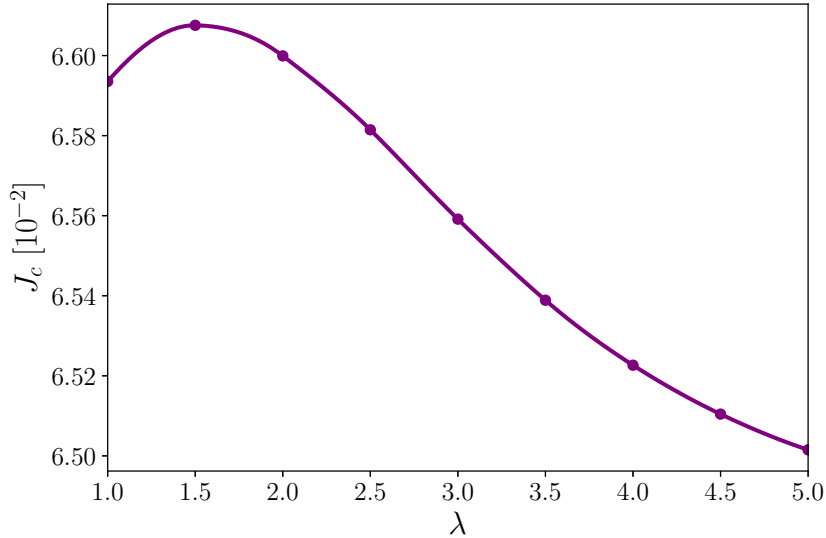
Figure 8. The critical current of *dark matter* influenced Josephson junction as a function of Gaussian broadening λ from the relation (2.19). It is clearly seen that there is a maximal sensitivity for some value of λ. In this plot we used $\alpha_0 = 0.5$, the size of the junctions is 1.6, while the separation between the junctions is 10, in the units used in the plot.

one Josephson junction. In general, if the device is biased the current phase relation reads

$$I = I_{\max} \sin\left(\Delta\phi + \frac{2\,\mathrm{eV}}{\hbar}t\right), \tag{4.1}$$

where $V = (\mu(\infty) - \mu(-\infty))/e$ is the voltage drop across the junction, $\Delta\phi$ is earlier introduced phase difference between two superconductors. Equation (4.1) shows that the current of the biased junction oscillates with frequency $\frac{2\,\mathrm{eV}}{\hbar}$. In the following, in full analogy to the holographic treatment we shall consider only direct current (dc) SQUID i.e. with $V = 0$.

The presence of the magnetic flux perpendicular to the plane of the device induces the screening currents in the superconductor and changes the phase relations in both branches. By the gauge invariance principle one finds that the flux Φ penetrating the SQUID loop modifies the relation between the phases of two junctions A and B and one gets [51]

$$\Phi = 2\pi\phi_0(\Delta\phi_A - \Delta\phi_B). \tag{4.2}$$

The total current I entering the device from the left splits into I_A and I_B. At the right hand side of the device both I_A and I_B fulfilling the relation (1.1) add to give again the current I. One thus gets (for $I_A = I_B$ and with the phase differences $\Delta\phi_A$ and $\Delta\phi_B$ in the respective branches)

$$I = I_A + I_B = 2I_{\max}\sin\left(\frac{\Delta\phi_A + \Delta\phi_B}{2}\right)\cos\left(\frac{\Delta\phi_A - \Delta\phi_B}{2}\right). \tag{4.3}$$

As was shown in [52] the phase difference is related to the total flux ϕ_{total}, which for the negligible inductance of the loop reduces to the external flux Φ as in the equation (4.2). With the symmetric distribution of the phase modifications

$$\Delta\phi_A = \Delta\phi + \frac{\pi\Phi}{\phi_0} \tag{4.4}$$

$$\Delta\phi_B = \Delta\phi - \frac{\pi\Phi}{\phi_0} \tag{4.5}$$

– 17 –

one gets

$$I = 2I_{\max} \cos\left(\frac{\pi\Phi}{\phi_0}\right) \sin\left(\Delta\phi_B + \frac{\pi\Phi}{\phi_0}\right) = 2I_{\max} \sin(\Delta\phi) \cos\left(\frac{\pi\Phi}{\phi_0}\right), \qquad (4.6)$$

where $\phi_0 \equiv hc/2e \approx 2.07 \cdot 10^{-7}\,\mathrm{Gs} \cdot \mathrm{cm}^2$ is the quantum flux. One sees that the amplitude of the current in the SQUID is modulated by the factor $\left|\cos\left(\frac{\pi\Phi}{\phi_0}\right)\right|$ and the ratio of the maximal currents flowing in the device subject to the external flux to that without it is given by this factor

$$\frac{I_m(\Phi)}{I_m(0)} = \left|\cos\left(\frac{\pi\Phi}{\phi_0}\right)\right|. \qquad (4.7)$$

For the completeness it has to be noted that if the magnetic flux Φ is piercing one of the weak links (junctions), then another "diffraction pattern" is observed [36]. It may be characterised by the ratio of the maximum current in the device with ($I_m(\Phi)$) and without ($I_m(0)$) extra flux

$$\frac{I_m(\Phi)}{I_m(0)} = \left|\frac{\sin\left(\frac{\pi\Phi}{\phi_0}\right)}{\frac{\pi\Phi}{\phi_0}}\right|. \qquad (4.8)$$

The above two possibilities to change the maximum current in the device formulated by equations (4.7) and (4.8) by applying to it the external magnetic field are plotted in the upper panel of the figure 9. The blue curve on this panel shows the current as a function of the magnetic flux ratio Φ/ϕ_0 for the flux penetrating the extended junction and the magnetic field parallel to the plane of the SQUID, while the other curve shows standard geometry with the flux penetrating the loop.

Now we discuss the possible effect of ıdark matter particle on the current through the condensed matter SQUID. For this we imagine the *dark matter particle* traversing one of its junctions. In order to find the changes of the flux Φ induced by the passage of the *dark particle*, let us consider the action (1.2), and define new gauge fields which enable us to get rid of the *kinetic mixing* term. Namely one has

$$\tilde{A}_\mu = \frac{\sqrt{2-\alpha}}{2}\left(A_\mu - B_\mu\right), \qquad (4.9)$$

$$\tilde{B}_\mu = \frac{\sqrt{2+\alpha}}{2}\left(A_\mu + B_\mu\right). \qquad (4.10)$$

It leads to

$$\frac{1}{4}F_{\mu\nu}F^{\mu\nu} + \frac{1}{4}B_{\mu\nu}B^{\mu\nu} + \frac{\alpha}{4}F_{\mu\nu}B^{\mu\nu} \Longrightarrow \frac{1}{4}\tilde{F}_{\mu\nu}\tilde{F}^{\mu\nu} + \frac{1}{4}\tilde{B}_{\mu\nu}\tilde{B}^{\mu\nu}, \qquad (4.11)$$

where $\tilde{F}_{\mu\nu} = 2\nabla_{(\mu}\tilde{A}_{\nu)}$ and respectively $\tilde{B}_{\mu\nu} = 2\nabla_{(\mu}\tilde{B}_{\nu)}$. The corresponding magnetic fluxes are provided by

$$\Phi_{\tilde{A}_\mu} = \frac{\sqrt{2-\alpha}}{2}\left[\frac{2\pi\,a}{e} - \frac{2\pi\,b}{e_d}\right], \qquad (4.12)$$

$$\Phi_{\tilde{B}_\mu} = \frac{\sqrt{2+\alpha}}{2}\left[\frac{2\pi\,a}{e} + \frac{2\pi\,b}{e_d}\right], \qquad (4.13)$$

where e stands for the charge of Maxwell field while e_d is connected with the charge of *dark matter* sector gauge field, while $a,\ b \in \mathbf{Z}$.
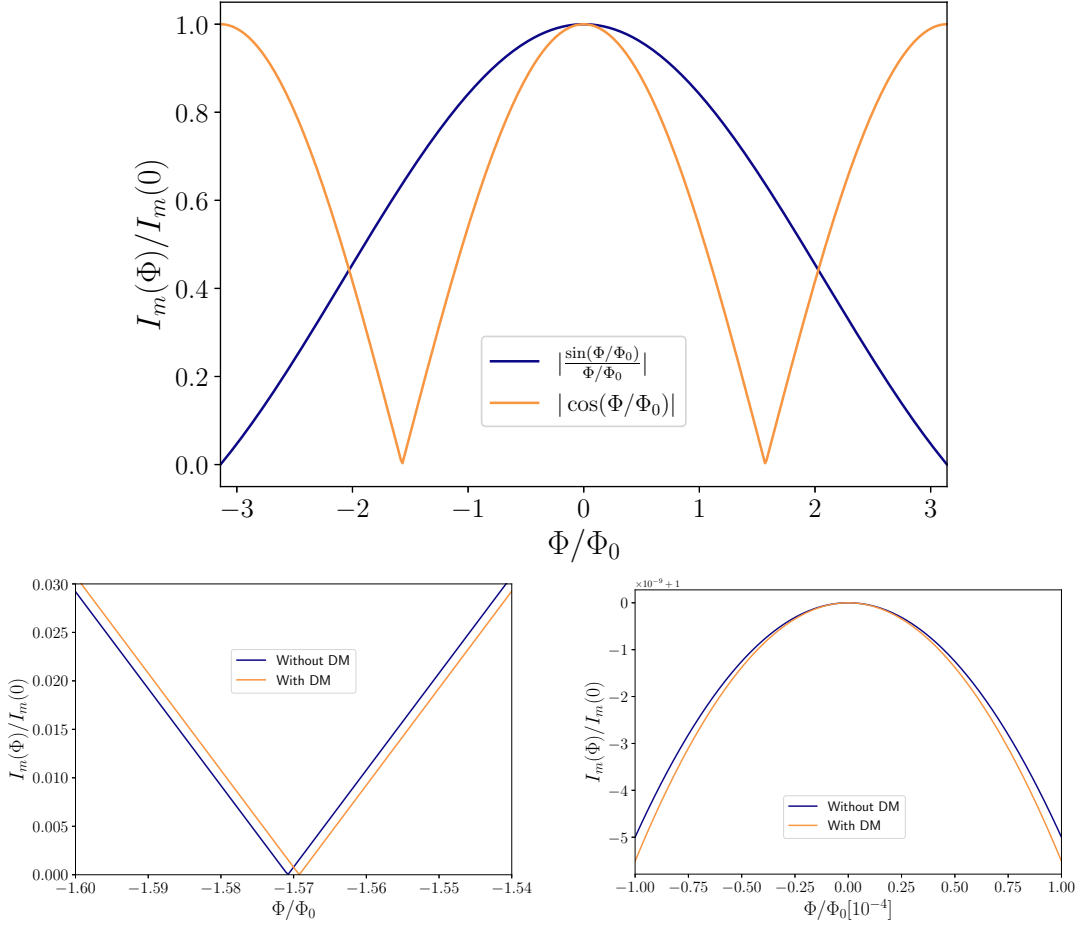
Figure 9. The interference patterns in SQUID is shown in the upper panel. Left-lower panel shows the detail SQUID responses for magnetic field tuned close to the minimum. The passage of *dark particle* shifts the minimum and the SQUID responds with a well visible signal (lower left panel $\alpha = 0.004$). The detection of the signal is much more complicated if the SQUID is tuned close to the maximum of the current (lower right panel). The differences are small even for very large values of the coupling, which in this panel is assumed to be $\alpha = 0.2$.

Thus the total magnetic flux encompassed by the SQUID is given as $\Phi_{\tilde{A}_\mu} + \Phi_{\tilde{B}_\mu}$. Having in mind that the coupling constant $\alpha \ll 1$, one can rewrite the sum as follows:

$$\Phi_{\tilde{A}_\mu} + \Phi_{\tilde{B}_\mu} \simeq \frac{2\sqrt{2}\pi}{e} \left[a + \frac{\alpha}{4} \left(\frac{e}{e_d} \right) b \right]. \tag{4.14}$$

If we assume that $a = b$ it leads to the relation

$$\Phi_{\tilde{A}_\mu} + \Phi_{\tilde{B}_\mu} \simeq \Phi_A \left[1 + \frac{\alpha}{4} \left(\frac{e}{e_d} \right) \right], \tag{4.15}$$

where Φ_A is the magnetic flux bounded with Maxwell field.

On the basis of the equation (4.15) and assuming that $\frac{e}{e_d} = 1$ we argue that due to the kinetic mixing (with the coupling α) the effective magnetic field and thus the flux through the device would change from the value Φ to the new value $(1 + \alpha/4)\Phi$ when the *dark particle* is traversing the SQUID, so obviously the current in the device would also change. This change is illustrated in the lower panels of figure 9.

The lower left panel of figure 9 compares the detected signals close to its minimum. The blue curve is the signal without *dark particle*. The zero current is expected at $\Phi/\phi_0 = \pi/2$. If the *dark particle* appears in the SQUID it changes the flux across the device. This change of the flux obtained for $\alpha = 0.004$ is visible as a nonzero current at the same external magnetic field value. In the figure both curves have been plotted as a function of the external flux Φ (no *dark particle* in the SQUID), which value is changed (locally in space and time) to $(1 + \alpha/4)\Phi$ (when *dark particle* traverses the device).

On the contrary if one looks at the SQUID signal close to the maximum current (lower right panel) the effect is hardly visible for the same value of α (not shown). In the panel we are comparing two signals using $\alpha = 0.2$. This large value of the coupling makes the signal visible. However, even the tiny change of the effective flux causes the shift of the minimum in the diffraction curves and makes the tiny effect visible. Thus the response of the SQUID which is tuned by the external **B** field to the minimum of the current seem easier to be detected. This is due to the fact that in the latter case one expects the sudden increase of the current from zero to some finite (albeit small) value. Unless the changes of the current are below the thermal or quantum fluctuations in the system the effect should be observable. This depends on the value of the kinetic mixing α and thus on the mass(es) of the *dark particle(s)*. To define real experimental conditions one should also take into account fluctuations of the external flux. The field theory analysis of the possibility of detecting *dark matter* particles is an important and complicated subject [12], which we shall not pursue here any further.

5   Discussion and conclusion

Using the holographic approach we have studied the influence of the *dark sector* particle on the holographic model of the SQUID. To this end we have assumed gravity background consisting of the four-dimensional static AdS Schwarzschild black brane. The holographic modelling of the device is achieved by use of the special form of the chemical potential mimicking the two insulating/normal regions embedded into superconducting ring. Moreover one assumes that *dark matter* sector is present only in one of the holographic Josephson junctions of the SQUID under inspection.

This supposition enables us to calculate the difference of the phases between the junctions, caused by *dark matter particle*. We solve numerically equations of motion and receive values of M_i and thus the phase, for the specific choice of the current J and ζ strength parameter function, controlling the interaction of *visible* and *hidden* sectors. This procedure leads to the critical current and the phase for each of the examined holographic junctions and allows establishing the current phase relation which has a typical sinusoidal character.

The passage of the *dark sector particle* by one of the holographic SQUID junctions modifies the phase difference in that junction and leads to the modification of the critical current. This shows up as the appearance of the *dark sector* induced effective flux Φ. The difference of the critical currents of the SQUID measured for $\zeta \neq 0$ and $\zeta = 0$, signals the *dark sector* field detection.

We have assumed that the presence in the junction of the *dark matter* sector field can be described by the Gaussian type of dependence of the coupling ζ on the ξ coordinate. It turns out that the increase of the Gaussian packet decay length λ has an effect on the current-phase relation of one of the holographic SQUID's Josephson junctions. Moreover, the critical Josephson current is a function of the decay length λ. This fact supplies us the tool

for changing the sensitivity of the holographic SQUID in the dependence on the expected properties *dark matter* sector. Interestingly the simplest possible assumption that due to the kinetic mixing between the fields the *dark particle* traversing the condensed matter SQUID increases the effective magnetic field leads to the results similar to those obtained by means of holographic analogy.

To conclude, we remark that the presented results have been obtained for the holographic s-wave Josephson junction and SQUID composed of such junctions. They envisage some features which can be utilised in future experiments aimed at detecting *dark matter* sector particles. Of course, we are aware that examination of more complicated models like p-wave or $p_x + ip_y$ might lead to even better detection methods. We shall investigate these problems elsewhere.

Acknowledgments

References

[1] G. Bertone and T.M.P. Tait, *A new era in the search for dark matter*, *Nature* **562** (2018) 51 [arXiv:1810.01668] [INSPIRE].

[2] R. Bernabei et al., *Searching for WIMPs by the annual modulation signature*, *Phys. Lett. B* **424** (1998) 195 [INSPIRE].

[3] R. Bernabei et al., *Final model independent result of DAMA/LIBRA-phase1*, *Eur. Phys. J. C* **73** (2013) 2648 [arXiv:1308.5109] [INSPIRE].

[4] COSINE-100 collaboration, *An experiment to search for dark-matter interactions using sodium iodide detectors*, *Nature* **564** (2018) 83 [*Erratum ibid.* **566** (2019) E2] [arXiv:1906.01791] [INSPIRE].

[5] XENON collaboration, *Excess electronic recoil events in XENON1T*, *Phys. Rev. D* **102** (2020) 072004 [arXiv:2006.09721] [INSPIRE].

[6] B. Fornal, P. Sandick, J. Shu, M. Su and Y. Zhao, *Boosted Dark Matter Interpretation of the XENON1T Excess*, *Phys. Rev. Lett.* **125** (2020) 161804 [arXiv:2006.11264] [INSPIRE].

[7] J. Bramante and N. Song, *Electric But Not Eclectic: Thermal Relic Dark Matter for the XENON1T Excess*, *Phys. Rev. Lett.* **125** (2020) 161805 [arXiv:2006.14089] [INSPIRE].

[8] N.F. Bell, J.B. Dent, B. Dutta, S. Ghosh, J. Kumar and J.L. Newstead, *Explaining the XENON1T excess with Luminous Dark Matter*, *Phys. Rev. Lett.* **125** (2020) 161803 [arXiv:2006.12461] [INSPIRE].

[9] A. Bally, S. Jana and A. Trautner, *Neutrino self-interactions and XENON1T electron recoil excess*, *Phys. Rev. Lett.* **125** (2020) 161802 [arXiv:2006.11919] [INSPIRE].

[10] F. Takahashi, M. Yamada and W. Yin, *XENON1T Excess from Anomaly-Free Axionlike Dark Matter and Its Implications for Stellar Cooling Anomaly*, *Phys. Rev. Lett.* **125** (2020) 161801 [arXiv:2006.10035] [INSPIRE].

[11] N. Masi, *Dark matter: TeV-ish rather than miraculous, collisionless rather than dark*, *Eur. Phys. J. Plus* **130** (2015) 69 [INSPIRE].

[12] Y. Hochberg, T. Lin and K.M. Zurek, *Detecting Ultralight Bosonic Dark Matter via Absorption in Superconductors*, *Phys. Rev. D* **94** (2016) 015019 [arXiv:1604.06800] [INSPIRE].

[13] S. Knapen, T. Lin and K.M. Zurek, *Light Dark Matter in Superfluid Helium: Detection with Multi-excitation Production*, *Phys. Rev. D* **95** (2017) 056019 [arXiv:1611.06228] [INSPIRE].

[14] S. Knapen, T. Lin, M. Pyle and K.M. Zurek, *Detection of Light Dark Matter With Optical Phonons in Polar Materials*, *Phys. Lett. B* **785** (2018) 386 [arXiv:1712.06598] [INSPIRE].

[15] R. Budnik, O. Chesnovsky, O. Slone and T. Volansky, *Direct Detection of Light Dark Matter and Solar Neutrinos via Color Center Production in Crystals*, *Phys. Lett. B* **782** (2018) 242 [arXiv:1705.03016] [INSPIRE].

[16] Y. Hochberg et al., *Detection of sub-MeV Dark Matter with Three-Dimensional Dirac Materials*, *Phys. Rev. D* **97** (2018) 015004 [arXiv:1708.08929] [INSPIRE].

[17] T. Liang, B. Zhu, R. Ding and T. Li, *Direct Detection of Axion-Like Particles in Bismuth-Based Topological Insulators*, *Int. J. Mod. Phys. A* **33** (2018) 1850135 [arXiv:1807.11757] [INSPIRE].

[18] M. Baryakhtar, J. Huang and R. Lasenby, *Axion and hidden photon dark matter detection with multilayer optical haloscopes*, *Phys. Rev. D* **98** (2018) 035006 [arXiv:1803.11455] [INSPIRE].

[19] J.M. Maldacena, *The Large N limit of superconformal field theories and supergravity*, *Int. J. Theor. Phys.* **38** (1999) 1113 [*Adv. Theor. Math. Phys.* **2** (1998) 231] [hep-th/9711200] [INSPIRE].

[20] E. Witten, *Anti-de Sitter space and holography*, *Adv. Theor. Math. Phys.* **2** (1998) 253 [hep-th/9802150] [INSPIRE].

[21] S. Sachdev, *What can gauge-gravity duality teach us about condensed matter physics?*, *Ann. Rev. Condensed Matter Phys.* **3** (2012) 9 [arXiv:1108.1197] [INSPIRE].

[22] J. Zaanen, Y.-W. Sun, Y. Liu and K. Schalm, *Holographic Duality in Condensed Matter Physics*, Cambridge University Press, Cambridge U.K. (2015) [INSPIRE].

[23] R.-G. Cai, L. Li, L.-F. Li and R.-Q. Yang, *Introduction to Holographic Superconductor Models*, *Sci. China Phys. Mech. Astron.* **58** (2015) 060401 [arXiv:1502.00437] [INSPIRE].

[24] L. Nakonieczny and M. Rogatko, *Analytic study on backreacting holographic superconductors with dark matter sector*, *Phys. Rev. D* **90** (2014) 106004 [arXiv:1411.0798] [INSPIRE].

[25] L. Nakonieczny, M. Rogatko and K.I. Wysokiński, *Magnetic field in holographic superconductor with dark matter sector*, *Phys. Rev. D* **91** (2015) 046007 [arXiv:1502.02550] [INSPIRE].

[26] L. Nakonieczny, M. Rogatko and K.I. Wysokiński, *Analytic investigation of holographic phase transitions influenced by dark matter sector*, *Phys. Rev. D* **92** (2015) 066008 [arXiv:1509.01769] [INSPIRE].

[27] M. Rogatko and K.I. Wysokiński, *P-wave holographic superconductor/insulator phase transitions affected by dark matter sector*, *JHEP* **03** (2016) 215 [arXiv:1508.02869] [INSPIRE].

[28] M. Rogatko and K.I. Wysokiński, *Holographic vortices in the presence of dark matter sector*, *JHEP* **12** (2015) 041 [arXiv:1510.06137] [INSPIRE].

[29] M. Rogatko and K.I. Wysokiński, *Viscosity of holographic fluid in the presence of dark matter sector*, *JHEP* **08** (2016) 124 [arXiv:1603.07858] [INSPIRE].

[30] M. Rogatko and K.I. Wysokiński, *Condensate flow in holographic models in the presence of dark matter*, *JHEP* **10** (2016) 152 [arXiv:1608.00343] [INSPIRE].

[31] Y. Peng, *Holographic entanglement entropy in superconductor phase transition with dark matter sector*, *Phys. Lett. B* **750** (2015) 420 [arXiv:1507.07399] [INSPIRE].

[32] Y. Peng, Q. Pan and Y. Liu, *A general holographic insulator/superconductor model with dark matter sector away from the probe limit*, *Nucl. Phys. B* **915** (2017) 69 [arXiv:1512.08950] [INSPIRE].

[33] M. Rogatko and K.I. Wysokiński, *Viscosity bound for anisotropic superfluids with dark matter sector*, *Phys. Rev. D* **96** (2017) 026015 [arXiv:1612.02593] [InSPIRE].

[34] M. Rogatko and K.I. Wysokiński, *Two interacting current model of holographic Dirac fluid in graphene*, *Phys. Rev. D* **97** (2018) 024053 [arXiv:1708.08051] [InSPIRE].

[35] B.D. Josephson, *Possible new effects in superconductive tunnelling*, *Phys. Lett.* **1** (1962) 251 [InSPIRE].

[36] M. Tinkham, *Introduction to Superconductivity*, Dover Publications, New York NY U.S.A. (2004).

[37] C. Beck, *Possible resonance effect of axionic dark matter in Josephson junctions*, *Phys. Rev. Lett.* **111** (2013) 231801 [arXiv:1309.3790] [InSPIRE].

[38] F. Wilczek, *Emergent Majorana Mass and Axion Couplings in Superfluids*, *New J. Phys.* **16** (2014) 082003 [arXiv:1401.4379] [InSPIRE].

[39] G.T. Horowitz, J.E. Santos and B. Way, *A Holographic Josephson Junction*, *Phys. Rev. Lett.* **106** (2011) 221601 [arXiv:1101.3326] [InSPIRE].

[40] E. Kiritsis and V. Niarchos, *Josephson Junctions and AdS/CFT Networks*, *JHEP* **07** (2011) 112 [*Erratum ibid.* **10** (2011) 095] [arXiv:1105.6100] [InSPIRE].

[41] Y.-Q. Wang, Y.-X. Liu, R.-G. Cai, S. Takeuchi and H.-Q. Zhang, *Holographic SIS Josephson Junction*, *JHEP* **09** (2012) 058 [arXiv:1205.4406] [InSPIRE].

[42] M. Rozali and A. Vincart-Emard, *Chiral Edge Currents in a Holographic Josephson Junction*, *JHEP* **01** (2014) 003 [arXiv:1310.4510] [InSPIRE].

[43] E. Chang-Young, H. Kim and H. Nakajima, *Noncommutative Supertori in Two Dimensions*, *JHEP* **08** (2008) 058 [arXiv:0807.0710] [InSPIRE].

[44] A. Amoretti, A. Braggio, N. Maggiore, N. Magnoli and D. Musso, *Coexistence of two vector order parameters: a holographic model for ferromagnetic superconductivity*, *JHEP* **01** (2014) 054 [arXiv:1309.5093] [InSPIRE].

[45] H.-F. Li, L. Li, Y.-Q. Wang and H.-Q. Zhang, *Non-relativistic Josephson Junction from Holography*, *JHEP* **12** (2014) 099 [arXiv:1410.5578] [InSPIRE].

[46] Y.-Q. Wang and S. Liu, *Holographic s-wave and p-wave Josephson junction with backreaction*, *JHEP* **11** (2016) 127 [arXiv:1608.06364] [InSPIRE].

[47] S. Liu and Y.-Q. Wang, *Holographic model of hybrid and coexisting s-wave and p-wave Josephson junction*, *Eur. Phys. J. C* **75** (2015) 493 [arXiv:1504.06918] [InSPIRE].

[48] Y.-P. Hu, H.-F. Li, H.-B. Zeng and H.-Q. Zhang, *Holographic Josephson Junction from Massive Gravity*, *Phys. Rev. D* **93** (2016) 104009 [arXiv:1512.07035] [InSPIRE].

[49] R.-G. Cai, Y.-Q. Wang and H.-Q. Zhang, *A holographic model of SQUID*, *JHEP* **01** (2014) 039 [arXiv:1308.5088] [InSPIRE].

[50] S. Takeuchi, *Holographic Superconducting Quantum Interference Device*, *Int. J. Mod. Phys. A* **30** (2015) 1550040 [arXiv:1309.5641] [InSPIRE].

[51] J.F. Annett, *Superconductivity, superfluids and condensates*, Oxford University Press, Oxford U.K. (2004).

[52] J.B. Ketterson and S.N. Song, *Superconductivity*, Cambridge University Press, Cambridge U.K. (1999).

[53] T. Vachaspati and A. Achúcarro, *Semilocal cosmic strings*, *Phys. Rev. D* **44** (1991) 3067 [InSPIRE].

[54] A. Achúcarro and T. Vachaspati, *Semilocal and electroweak strings*, *Phys. Rept.* **327** (2000) 347 [hep-ph/9904229] [InSPIRE].

[55] S.A. Abel and B.W. Schofield, *Brane anti-brane kinetic mixing, millicharged particles and SUSY breaking*, *Nucl. Phys. B* **685** (2004) 150 [hep-th/0311051] [INSPIRE].

[56] S.A. Abel, J. Jaeckel, V.V. Khoze and A. Ringwald, *Illuminating the Hidden Sector of String Theory by Shining Light through a Magnetic Field*, *Phys. Lett. B* **666** (2008) 66 [hep-ph/0608248] [INSPIRE].

[57] S.A. Abel, M.D. Goodsell, J. Jaeckel, V.V. Khoze and A. Ringwald, *Kinetic Mixing of the Photon with Hidden* U(1)*s in String Phenomenology*, *JHEP* **07** (2008) 124 [arXiv:0803.1449] [INSPIRE].

[58] NA64 collaboration, *Search for invisible decays of sub-GeV dark photons in missing-energy events at the CERN SPS*, *Phys. Rev. Lett.* **118** (2017) 011802 [arXiv:1610.02988] [INSPIRE].

[59] P. Jean et al., *Early SPI/INTEGRAL measurements of* 511 *keV line emission from the 4th quadrant of the Galaxy*, *Astron. Astrophys.* **407** (2003) L55 [astro-ph/0309484] [INSPIRE].

[60] J. Chang et al., *An excess of cosmic ray electrons at energies of* 300–800 *GeV*, *Nature* **456** (2008) 362 [INSPIRE].

[61] PAMELA collaboration, *An anomalous positron abundance in cosmic rays with energies* 1.5–100 *GeV*, *Nature* **458** (2009) 607 [arXiv:0810.4995] [INSPIRE].

[62] MUON G-2 collaboration, *Final Report of the Muon E821 Anomalous Magnetic Moment Measurement at BNL*, *Phys. Rev. D* **73** (2006) 072003 [hep-ex/0602035] [INSPIRE].

[63] H. Davoudiasl, H.-S. Lee and W.J. Marciano, *'Dark' Z implications for Parity Violation, Rare Meson Decays, and Higgs Physics*, *Phys. Rev. D* **85** (2012) 115019 [arXiv:1203.2947] [INSPIRE].

[64] H. Davoudiasl, H.-S. Lee, I. Lewis and W.J. Marciano, *Higgs Decays as a Window into the Dark Sector*, *Phys. Rev. D* **88** (2013) 015022 [arXiv:1304.4935] [INSPIRE].

[65] B.S. Acharya, S.A.R. Ellis, G.L. Kane, B.D. Nelson and M.J. Perry, *The lightest visible-sector supersymmetric particle is likely to be unstable*, *Phys. Rev. Lett.* **117** (2016) 181802 [arXiv:1604.05320] [INSPIRE].

[66] B. Holdom, *Two* U(1)*'s and* ϵ *charge shifts*, *Phys. Lett. B* **166** (1986) 196 [INSPIRE].

[67] D. Lüst, *Intersecting brane worlds: A Path to the standard model?*, *Class. Quant. Grav.* **21** (2004) S1399 [hep-th/0401156] [INSPIRE].

[68] S. Abel and J. Santiago, *Constraining the string scale: From Planck to weak and back again*, *J. Phys. G* **30** (2004) R83 [hep-ph/0404237] [INSPIRE].

[69] K.R. Dienes, C.F. Kolda and J. March-Russell, *Kinetic mixing and the supersymmetric gauge hierarchy*, *Nucl. Phys. B* **492** (1997) 104 [hep-ph/9610479] [INSPIRE].

[70] G.T. Horowitz and R.C. Myers, *The AdS/CFT correspondence and a new positive energy conjecture for general relativity*, *Phys. Rev. D* **59** (1998) 026005 [hep-th/9808079] [INSPIRE].

Axionlike dark matter clouds around rotating black holes

Bartlomiej Kiczek[*] and Marek Rogatko[†]

*Institute of Physics, Maria Curie-Sklodowska University, pl. Marii Curie-Sklodowskiej 1,
20-031 Lublin, Poland*

Numerical analysis of a *dark matter* axionlike cloud in the vicinity of a rotating black hole has been performed. The model where an axionlike scalar field is nontrivially coupled to the Maxwell field is studied in the spacetime of a Kerr black hole in a uniform magnetic field and in the Kerr-Newman one. The dependence of scalar mass and black hole angular momentum on accumulation of the axion dark matter cloud was given. It was revealed that condensation of the dark matter clouds is preferable for a very small mass of axion.

I. INTRODUCTION

The nature of the elusive ingredient of our Universe, *dark matter*, is one of the most intriguing mysteries of the contemporary physics and astrophysics. Ultralight bosons like axion, axionlike particles, and *dark photons* could be the answer for these tantalizing questions. From the point of view of UV theory, the QCD axions are well motivated as the solution of the *CP* problem [1–3]. Recently, axionlike particles widely emerging in the realm of string theory [4] also attract much attention.

Both axion and axionlike particles are regarded as constituting the possible *hidden sector*. This fact triggers the motivation to search for them in various kinds of experiments and theoretical researches. Namely, it turns out that axion dark matter has novel effects in polarization of the cosmic microwave background [5] and can be detected in the future terrestrial or astrophysical observations. In Ref. [6] the new mechanism where a coherently oscillating axionlike particle field can transfer its energy to a dark photon has been elucidated. Recently, it has been argued that radio telescope observations of neutron stars will enable the possible detection of axion dark matter, through the axion resonant conversion into radio-frequency photons. The conversion probabilities are proportional to the strength of the magnetic field surrounding the neutron star [7,8].

The process of lasing of an ultralight axion condensate into photons, relevant for a superradiant axion condensate around a stellar mass black hole, was elaborated in [9]. The influence of plasma properties placed around the black hole in question, on the lasing of the axion condensate, was also revealed.

It was established [10] that the superradiant instability can lead to the generation of extremely dense axion clouds in the nearby rotating black holes. Moreover, the stimulated decay may lead to extremely bright lasers. A possible connection with the observed fast radio bursts was proposed.

Neglecting the rotational effects, axion configuration around pulsars was studied in Ref. [11]. Among all it was found that the axions form a localized condensate or radiate as outgoing waves, depending on if the pulsar frequency is smaller or greater than that of the axion mass.

On the other hand, the analysis of broad-band radio telescope observations of magnetar PSR J1745-2900, enables to establish with the confidence of 95 percent limits, the resonant axion-photon conversion emission line flux density. These data were translated into limits on axion-photon coupling constant $g_{a\gamma\gamma}$ versus axion mass. If there is a dark matter cusp, then the limits reduce to $g_{a\gamma\gamma} > 6$–34×10^{-14} GeV^{-1}, overlapping the axion models with mass range over 33 eV [12,13]. It is argued [14,15] that the axion coupling to photon depends on the specific model and is related to the values $\sim 10^{-11}$–10^{-15} GeV^{-1} for intermediate, $\sim 10^{-19}$ GeV^{-1} for Grand Unification Theory, and $\sim 10^{-21}$ GeV^{-1} for Planck energy scales.

Studies of light rays passing through an axion and axionlike clouds surrounded by a stationary axisymmetric black hole, focusing on the experimental setup that is required for the detection of such an effect, and paying attention to the radio observations of linearly polarized astrophysical sources, like active galactic nuclei, have been performed in [16].

In [17] it was proposed to detect axionlike dark matter by using linearly polarized pulsar light. A pulsar linear polarization angle may vary with time, due to the birefringence effect which is caused by an oscillating galactic aforementioned hidden sector component.

*bkiczek@kft.umcs.lublin.pl
†rogat@kft.umcs.lublin.pl

The numerical solution of the laser emission problem from an axion dense cloud around a spinning black hole was presented in [18,19], where it was envisaged that the laser emission existed at classical level and the presence of electric charge or rotation leads to the appearance of the black hole with nontrivial axionic hair. Moreover, the coupling constant of the hidden sector triggers the strong instabilities affecting superradiant clouds around black holes. On the other hand, in [20] the entire spectrum of the most unstable superradiant modes of the Proca field around a Kerr black hole was obtained, as well as constraints on dark photon and axionlike particles were given.

In our paper we elaborate the subject of the possible existence of axionic dark matter clouds in the spacetime of stationary axisymmetric black holes. Numerical simulations based on the axion dark matter model, where axions are coupled to the Maxwell field invariant composed of dual and ordinary $U(1)$-gauge field strengths, enable us to reveal the basic characteristics of the system in question. We shall pay attention to two cases of black holes, i.e., a Kerr black hole in a uniform magnetic field and Kerr-Newman spacetime.

The rest of the paper is organized as follows. In Sec. II we give a short overview of the axionlike dark matter portal and provide information about studied black hole backgrounds. In the subsections we discuss underlying equations of motion and the problem of free energy for dark matter axionic clouds around rotating black holes in question. Section III is devoted to the description of the achieved results. Namely, we examine the possibilities of condensations of dark matter in the vicinity of Kerr black holes in a uniform magnetic field and around stationary axisymmetric Kerr-Newman black holes. In Sec. IV we conclude our investigations. Finally, Appendix contains the relevant technical details concerning the numerical method.

II. AXIONLIKE DARK MATTER SECTOR

In this section we shall present the basic equations standing behind the axion dark matter sector model, viewed as the axionlike scalar field coupled to the Maxwell $U(1)$-gauge field. The basic idea lies in the nontrivial axionic coupling to the Maxwell strength field invariant constructed from dual and ordinary Maxwell field strengths. In what follows one investigates the behavior of axionlike dark matter clouds surrounded spinning black hole in a uniform, say galactic magnetic field, as well as besieged the Kerr-Newman black hole. For convenience, we also refer to them as axions. To commence with, we start with the Einstein-Maxwell-axion dark matter theory described by the following action:

$$\mathcal{S} = \int d^4x \sqrt{-g} \left[R - \frac{1}{4} F_{\mu\nu} F^{\mu\nu} - \frac{1}{2} \nabla_\mu \Psi \nabla^\mu \Psi \right.$$
$$\left. - \frac{\mu^2}{2} \Psi^2 - \frac{k}{2} \Psi * F^{\mu\nu} F_{\mu\nu} \right], \tag{1}$$

where R is the Ricci scalar, $F_{\mu\nu} = 2\nabla_{[\mu} A_{\nu]}$ is the Maxwell field strength tensor, and Ψ is the scalar field (axion) with mass μ. The last term of the action describes the coupling of axion field Ψ to one of the electromagnetic field invariants, composed of Maxwell and dual Maxwell filed strengths, where by $*$ we have denoted the Hodge dual operator. Note that k constitutes the axionic coupling constant to the $U(1)$-gauge field.

Varying the action with respect to the scalar field Ψ, we obtain the equation

$$\nabla_\mu \nabla^\mu \Psi - \mu^2 \Psi - \frac{k}{2} * F^{\mu\nu} F_{\mu\nu} = 0. \tag{2}$$

On the other hand, the $U(1)$-gauge field is subject to the relation

$$\nabla_\mu F^{\nu\mu} + 2k * F^{\nu\mu} \nabla_\mu \Psi = 0. \tag{3}$$

The resulting Klein-Gordon-like equation (2) contains, despite the standard dynamical and mass terms, an additional source term, being independent of axionlike field Ψ. The presence of the nonzero source term, containing the dual invariant, explicitly defined as

$$\mathcal{I} = *F^{\mu\nu} F_{\mu\nu} = \frac{1}{2} \epsilon^{\mu\nu\rho\lambda} F_{\rho\lambda} F_{\mu\nu}, \tag{4}$$

where $\epsilon^{\alpha\beta\gamma\delta}$ stands for the totally antisymmetric Levi-Civita symbol, is crucial for the scalarization of a black hole. Namely, if it is equal to zero, the axionlike scalar field equation of motion reduces to the simple massive Klein-Gordon case, without any self-interaction potential. Then the no-hair theorem plays its role and prevents any scalar hair configuration on the black hole from emerging.

On the other hand, it is easy to check that the invariant in question, $*F_{\mu\nu} F^{\mu\nu}$, is equal to zero in the case when $F_{\mu\nu} = 0$, or for spherically symmetric spacetime. In order to be nontrivial, $*F_{\mu\nu} F^{\mu\nu} \neq 0$ has to ensure both rotational and magnetic $U(1)$-gauge field components.

In what follows the main objective of our paper will be to elaborate on the behavior of axionlike field dark matter sector in the vicinity of a black hole. As it was remarked the survivability of the $\mathcal{I}$ term in Eq. (2) would be crucial for our studies. Therefore, we implement a magnetic field in the considered stationary axisymmetric black hole spacetime in two ways: internally, as a consequence of the Kerr-Newman black hole solution and externally, as, e.g., a galactic magnetic field surrounding a Kerr black hole. The latter idea was originally proposed by Wald in [21], where the uniform magnetic field around a black hole was studied.

We shall consider both of these background line elements and investigate properties of axionic dark matter clouds around the black holes in question.

A. Kerr black hole in a uniform magnetic field

In this section we recall, for the reader's convenience, the basic idea concerning the Wald's introduction of the uniform magnetic field in the spacetime of a Kerr black hole [21]. The line element of a Kerr black hole in Boyer-Lindquist coordinates is provided by the following:

$$ds^2 = -\left(1 - \frac{2Mr}{\Sigma}\right)dt^2 - \frac{4Mra\sin^2\theta}{\Sigma}$$
$$\times\, dtd\phi + \frac{\Sigma}{\Delta}dr^2 + \Sigma d\theta^2 + \frac{\Xi\sin^2\theta}{\Sigma}d\phi^2, \quad (5)$$

with the auxiliary functions defined as

$$\Sigma(r,\theta) = r^2 + a^2\cos^2\theta,$$
$$\Delta(r) = r^2 - 2Mr + a^2,$$
$$\Xi(r,\theta) = (r^2 + a^2)^2 - a^2\Delta\sin^2\theta.$$

The solution naturally describes a rotating black hole and is parametrized by two physical quantities, black hole mass M and angular momentum parameter $a = \frac{J}{M}$. The stationary axisymmetric line element (5) possesses two Killing vector fields, the timelike $k_\mu = (\partial/\partial t)_\mu$ and axial one $m_\mu = (\partial/\partial\phi)_\mu$.

If we consider the electromagnetic field equations in the spacetime of a Kerr black hole, neglecting the metric back reaction, it is possible to derive a general analytical form of the vector potential, being a combination of Killing vectors of the underlying spacetime, such as

$$A_\mu = \frac{1}{2}B(m_\mu + 2ak_\mu). \quad (6)$$

In this way we can introduce a static magnetic field to the system, which is oriented along the black hole rotation axis. From an astrophysical perspective, such a case may seem quite idealized, however, it is an interesting starting point for including magnetic fields into field theories around black holes. One way or another, any external (galactic) magnetic field can be cast on the parallel and perpendicular (to the rotation axis) components, and the perpendicular component can be neglected. Using this set up allows us to utilize all the mathematical properties of the Kerr geometry, such as axial symmetry, in constructing the numerical solution for the scalar. One has to remember, however, that a nonzero magnetic field breaks the reflection symmetry with respect to the equatorial plane.

As it has been already mentioned, we are interested in a static magnetic field, parallel to the rotation axis, so we can drop the timelike Killing vector from the general form of the gauge potential and write it in the form as follows:

$$A_\mu dx^\mu = \frac{1}{2}Bg_{\mu\nu}m^\nu dx^\mu = \frac{B\sin^2\theta}{2\Sigma}(-2Mardt + \Xi d\phi). \quad (7)$$

In order to proceed to the analysis of the axion dark matter equation of motion, we should find the invariant $\mathcal{I}$ in the spacetime under consideration. Its explicit form is as follows:

$$\mathcal{I} = -\frac{aB^2M\sin^2\theta\cos\theta}{2\Sigma^4}[3a^6 + 2a^4Mr - 5a^4r^2 - 8a^2Mr^3 - 32a^2r^4 - 24r^6$$
$$+ 4a^2(a^4 - a^2r^2 + 2(M-r)r^3)\cos 2\theta + a^4(a^2 - 2Mr + r^2)\cos 4\theta]. \quad (8)$$

Because of the fact that the obtained formula is a bit long and complicated and it might not be easy to imagine its shape, for the convenience of the reader, we visualize it in Fig. 1.

B. Kerr-Newman black hole spacetime

As far as the Kerr-Newman spacetime is concerned, it generalizes a Kerr solution and represents a black hole that does not only rotate but also is electrically charged. The line element implies

$$ds^2 = -\left(1 - \frac{2Mr}{\Sigma} + \frac{Q^2}{\Sigma}\right)dt^2 - \frac{2a(2Mr - Q^2)\sin^2\theta}{\Sigma}dtd\phi + \frac{\Sigma}{\Delta}dr^2 + \Sigma d\theta^2 + \frac{\Xi\sin^2\theta}{\Sigma}d\phi^2. \quad (9)$$

The auxiliary functions Σ and Ξ are defined in the same way as in the previous case, however, $\Delta(r)$ has the form given by

$$\Delta(r) = r^2 - 2Mr + a^2 + Q^2, \quad (10)$$

where Q is the electric charge of the black hole. The solution naturally possesses a nonzero electromagnetic vector potential of the form
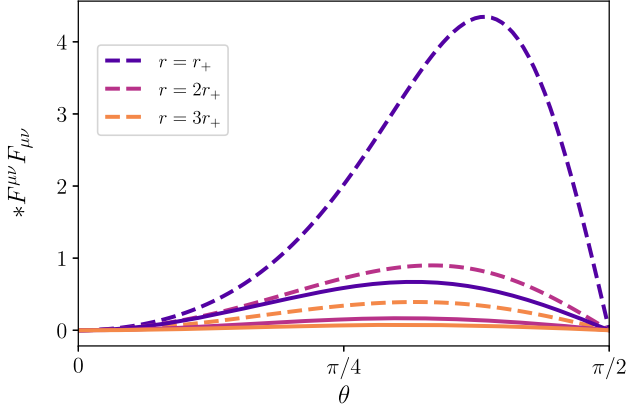
FIG. 1. Angular and radial dependence of the Maxwell field invariant in Kerr spacetime evaluated at the event horizon. Colors of the lines indicate subsequent surfaces of constant r. The solid lines correspond to $a = 0.5$, while the dashed lines to $a = 0.99$. The rise of angular momentum pumps up the value of the invariant significantly and shifts its peak towards the black hole equator.

$$A_\mu dx^\mu = \frac{rQ}{\Sigma} dt - \frac{arQ \sin^2\theta}{\Sigma} d\phi. \qquad (11)$$

On the other hand, the corresponding electromagnetic invariant, needed in the axion dark matter equations of motion, acquires a new simpler form, described by

$$\mathcal{I} = -\frac{4aQ^2 r(a^2 - 2r^2 + a^2 \cos 2\theta) \cos\theta}{\Sigma^4}. \qquad (12)$$

C. Equation of motion

Let us suppose that the axion dark matter field will be a function depending on two coordinates, radial and azimuthal ones, i.e., $\Psi = \psi(r, \theta)$. It leads to the axion equation of motion provided by the relation

$$\Delta \partial_r^2 \psi + 2(r - M)\partial_r \psi + \partial_\theta^2 \psi + \cot\theta \partial_\theta \psi - \mu^2 \Sigma \psi = \frac{k\Sigma}{2} \mathcal{I}, \qquad (13)$$

∂_m stands for the derivative with respect to the m-coordinate. The obtained equation is an elliptic partial differential equation, which is linear in ψ. The general form of this equation remains the same in both backgrounds. They differ by the shape of Δ function, which can be enriched with the electric charge, and by the source term on the right-hand side. It turns out that Eq. (13) follows a scaling transformation of the form

$$\begin{aligned} r &\to cr & a &\to ca \\ M &\to cM & k &\to kc^2 \\ Q &\to cQ & B &\to B/c \\ \mu^2 &\to \mu^2/c^2, \end{aligned}$$

which allows us to fix one quantity to unity. The scaling concerns the quantities from both backgrounds. For convenience, in our numerical simulations, we use the above scaling and fix the black hole mass to unity $M = 1$.

D. Free energy of dark matter axionic clouds in the spacetime of rotating black holes

The existence of the solution to the field equation, i.e., some state of the system, does not guarantee that it is the physically preferable configuration. To verify this, one ought to consider the thermodynamics of the system and look for the relevant quantities [22]. As we consider the gravitational system without backreaction, the thermodynamical quantities of the black hole, such as entropy and Hawking temperature, remain unaffected by the axionic dark matter condensate. Thus we wish to examine the free energy difference generated by the nontrivial profile of the scalar ψ with respect to the hairless solution. To proceed further, we consider the ψ dependent part of the underlying action,

$$\mathcal{S}_{\text{axion}} = \int d^4x \sqrt{-g} \left[-\frac{1}{2} \nabla_\mu \Psi \nabla^\mu \Psi - \frac{\mu^2}{2} \Psi^2 - \frac{k}{2} \Psi * F^{\mu\nu} F_{\mu\nu} \right]. \qquad (14)$$

In order to find the free energy contribution of the axionic cloud, we evaluate the Euclidean on-shell action related with (14).

Firstly, we use the equation of motion for the axionic field ψ (2) and substitute it into the action. This allows us to remove the term with the Maxwell field strength tensor. After few transformations we make use of the Gauss theorem and split the action into volume and surface terms. Because of the boundary conditions (see the next section for details), the surface integral vanishes. In last step we perform Wick's rotation of the time coordinate and get the explicit formula provided by

$$F = -2\pi \int_{\mathcal{M}} dr d\theta \frac{\Sigma \sin\theta}{2} [(\partial_r \psi)^2 g^{rr} + (\partial_\theta \psi)^2 g^{\theta\theta} + \mu^2 \psi^2]. \qquad (15)$$

As the integrand is positive, in the whole domain, the free energy shift is negative for every configuration of ψ field being the solution to the considered equations of motion. Although there is a caveat. It can be supposed that any nontrivial ψ will be preferred by nature. However, this is not really the case. For the given ansatz, the system has only trivial zero solution when the source term $\mathcal{I}$ is zero. This allows us to state that the considered axionic dark matter clouds are magnetically induced and are only present in the system when $\mathcal{I}$ is nontrivial.

Equation (15) will be extensively exploited, in the following section, to achieve the free energy plots. The aforementioned integral will be computed numerically.

III. NUMERICAL RESULTS

This section will be devoted to the obtained numerical solutions of both axion dark matter clouds surrounding Kerr black holes immersed in a uniform magnetic field and a Kerr-Newman one. As we have already mentioned, they differ by the shape of the source term originating from axionic coupling and the metric function Δ. We deal with the partial differential equation (13) by virtue of Chebyshev spectral methods. As the equation is fully linear in ψ, the acquired solution is unique and well defined. For technical details of the numerical method see Appendix.

In the above set up one considers the field only above the black hole event horizon (including the horizon itself). The bounds for the radial coordinate are from the event horizon to spatial infinity, precisely $r \in [r_+, \infty)$. The symmetry of the spacetime allows us to narrow the domain to one quarter of the (r, θ) plane. For convenience, we pick the first quarter, with $\theta \in [0, \pi/2]$. Values of the solution for remaining quarters can be achieved by the negative reflection with respect to the equatorial plane

$$\psi(r, \theta - \pi/2) = -\psi(r, \pi/2 - \theta), \qquad (16)$$

and the remaining part of the solution can be obtained by the rotation. Having our numerical domain defined, we can move to the necessary transformations.

To implement spectral methods based on Chebyshev polynomials, we have to map the coordinates of the manifold onto $[-1, 1]$ intervals. In order to do this we use the following transformations for r and θ:

$$z = 1 - \frac{2r_+}{r}, \qquad (17)$$

$$u = \frac{4\theta}{\pi} - 1, \qquad (18)$$

where $r_+ = M + \sqrt{M^2 - a^2 - Q^2}$, which is the standard definition of the outer event horizon of rotating black holes. After the transformation, $z = -1$ represents the inner boundary—the event horizon and $z = 1$ spatial infinity. Similarly, for $u = -1$ one thinks about a north pole of a black hole, while $u = 1$ represents the equator of the object in question.

Let us now discuss the boundary condition imposed on the solution of the axionic dark matter field equation. Namely, for the black hole event horizon $r = r_+$, we demand that the derivative with respect to the r-coordinate is given by $\partial_r \psi = 0$. This fact ensures the regularity of the solution. For $r \to \infty$, the field equation takes the simple angle independent form provided by the relation

$$\partial_r^2 \psi + \frac{2}{r} \partial_r \psi - \mu^2 \psi = 0, \qquad (19)$$

which implies that

$$\psi(r) \sim \frac{e^{-\mu r}}{r} + \frac{e^{\mu r}}{r}. \qquad (20)$$

The asymptotic flatness and regularity cause that the second term in the relation (20) vanishes, for a finite mass solution vanishes in the infinity. Thus, the requirement that $\psi(r \to \infty) = 0$ comprises the second boundary condition.

In the case of the boundaries imposed on the polar angle θ, we use the argumentation based on the symmetries of the spacetime. For the north pole $\theta = 0$, the axial symmetry of the rotating black hole obliges the solution to be invariant under the transformation $\phi \to \phi \pm \pi$. In other words the solution ought to be even along a meridian, with respect to the pole. Therefore, $\partial_\theta \psi = 0$ is the reasonable choice. However, for the equatorial plane $\theta = \pi/2$ the situation is different, as it constitutes the place where both source terms change signs, and so does the solution. For that reason we demand that $\psi = 0$, there.

A. Axionic dark matter clouds around Kerr black holes in a uniform magnetic field

Now we proceed with the conclusions achieved from the analysis of the numerical solutions of Eq. (13) in the adequate spacetimes of the rotating black holes. To commence with one considers the results obtained for a Kerr black hole in a uniform magnetic field.

In Fig. 2 we present the first series of spatial distribution plots of the axionic dark matter field. For convenience, we present the squared distribution ψ^2, where the (r, θ) plane has been cast into Cartesian coordinates (x, y). The black circle corresponds to the area hidden under the black hole's event horizon. In the first pair of plots, depicted in panels (a) and (b), one can see the distribution of the ultralight axionic dark matter field. It can be noticed that it is loosely concentrated around polar regions. The equatorial plane remains free from the scalar ψ, which results from the imposed boundary conditions and the symmetry of the problem in question. The increase of the black hole angular momentum does not drastically change the field distribution. However, it significantly influences its magnitude (see the values on colorbars). Furthermore, the field slowly decays with distance and spreads up to $r = 10r_+$ outside the event horizon. This is not the case for the massive axionic dark matter field, which is presented in panels (c) and (d) of Fig. 2. The mass μ^2 is quite large, in terms of geometrical units, however, it serves the purpose of visualizing the contrast. In the case under inspection the increase of the angular momentum causes dragging the axionic clouds towards the equatorial plane. This effect seems to be quite intuitive, by the analogy to the centrifugal

(a) $\mu^2 \to 0^+, a = 0.5$

(b) $\mu^2 \to 0^+, a = 0.996$

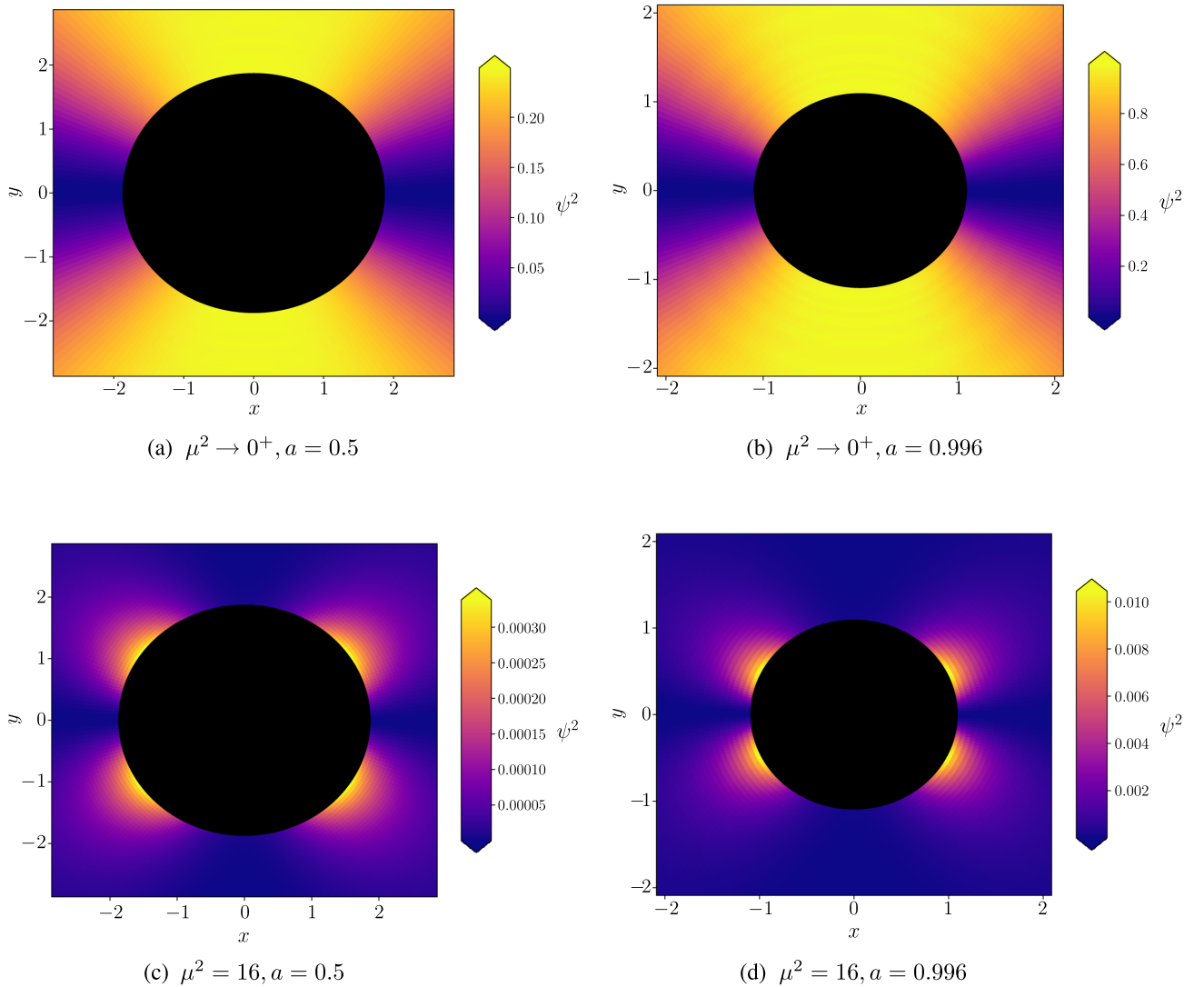(c) $\mu^2 = 16, a = 0.5$

(d) $\mu^2 = 16, a = 0.996$

FIG. 2. The distribution of the axionic dark matter clouds around a black hole with an external uniform magnetic field. Every panel corresponds to different values of field mass and black hole angular momentum. For ultralight mass the cloud concentrates in polar areas, while the large mass field is dragged towards the equator.

forces in classical mechanics. Similarly to the former case, the angular momentum increase causes a boost in the field ψ magnitude, by several orders.

It should be noted that the approximated analytical solution for this background has been derived in Ref. [19]. Our numerical solution perfectly matches the results obtained before, in the considered limit—a slow rotation of the black hole and zero mass of the axion field.

To proceed further with the studies of hairy configurations in Kerr-Wald spacetime, let us take a look at the behavior of the free energy, with respect to the change of the other parameters of the theory. In Fig. 3 the free energy shift as a function of the axion field mass can be observed. Here we present several curves for different values of the black hole angular momentum. All curves share the similar behavior, which is scaled differently. Moreover, what all

curves have in common is a significant decrease of free energy for small values of the axion mass. It means that axionic dark matter clouds are the most stable and the most strongly bound for very small, almost zero, field masses.

One might notice an interesting correlation of this result with theoretical predictions for dark matter axion mass, to be ultralight in sub eV region. Namely, the recent constraints on bosonic dark matter for ultralow field nuclear magnetic resonance were proposed in [23]. The new experimental bounds for axionlike dark matter particles are ranging from 1.8×10^{-16} to 7.8×10^{-14} eV. Recently, the direct implications on the mass of ultralight dark matter particles by studies on mass and spin of accreting and jetted astrophysical black holes have been established [24]. It was revealed that axionlike particles with the mass range $10^{-21} < \mu(\text{eV}) < 10^{-19}$ could contribute at almost
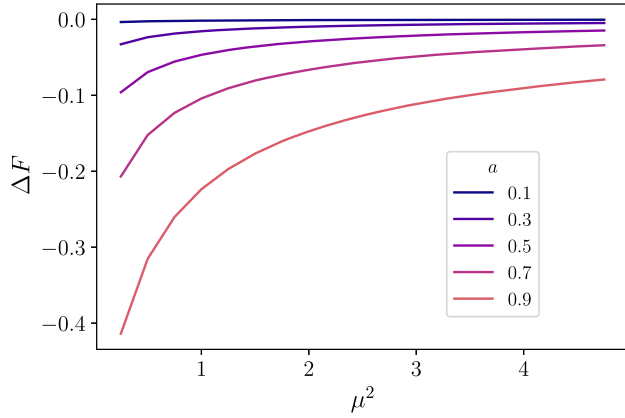
FIG. 3. Free energy shift as a function of axionlike dark matter mass. Ultralight particles are the most preferred ones as they cause the most significant free energy decrease.
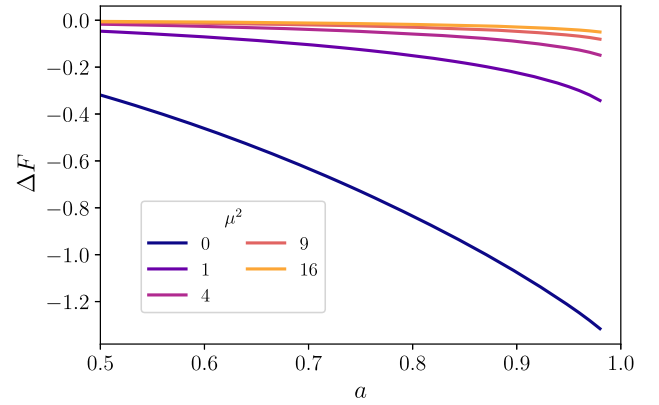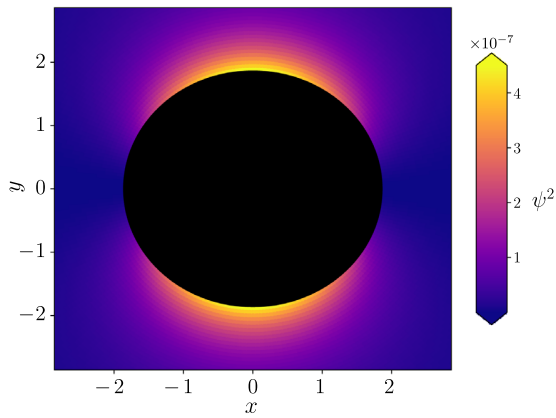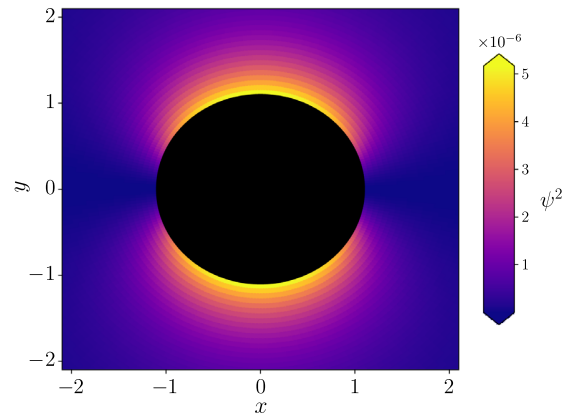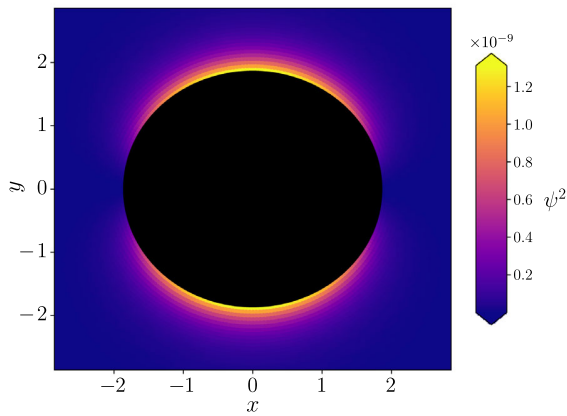
FIG. 4. Free energy shift vs the black hole angular momentum. The extremal black holes (with very high angular momentum) constitute a perfect environment for dark matter axionic hair since the free energy fall off is the biggest.
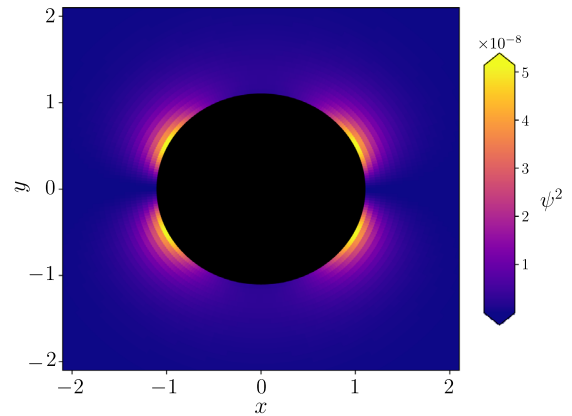

(a) $\mu^2 \to 0^+, a = 0.5$

(b) $\mu^2 \to 0^+, a = 0.99$

(c) $\mu^2 = 16, a = 0.5$

(d) $\mu^2 = 16, a = 0.99$

FIG. 5. Axionic dark matter clouds around Kerr-Newman black holes with $Q = 0.1$. High angular momentum of the black hole reveals rich geometrical structure of the clouds.

10 percent of the dark matter mass. On the contrary, for the mass range $10^{-19} > \mu(\text{eV}) > 10^{-17}$, they constitute only 0.01 to 1 percent of the *dark sector* mass.

On the other hand, Fig. 4 presents the free energy shift as a function of black hole angular momentum for different masses of the field ψ. The course of the curves is also very similar and surely they follow some kind of μ^2 dependent scaling. The shift is slight for moderate values of the angular momentum and becomes stronger for quickly rotating black holes. Extremal black holes, with a approaching to 1, bring the biggest fall off of free energy. Once again the decrease is the most drastic for the ultralight field (dark blue curve in the plot). All these observations allow us to conclude that extremal black holes constitute good environments for the emergence of the ultralight axionic dark matter clouds.

B. Axion dark matter clouds in the vicinity of Kerr-Newman black holes

Let us now discuss the characteristic features of axionic dark matter clouds nearby Kerr-Newman black holes. This background has a distinct electromagnetic vector potential, thus the behavior of axionic hair differs significantly from the former case. It can be seen in Fig. 5, where we plot analogical spatial distributions of ψ^2, just like in the case of a Kerr black hole dipped in a uniform magnetic background. However, these solutions are essentially various for two main reasons. Firstly, the shape of the $\mathcal{I}$ expression is different, hence the source term envisages the other kind of solution. Secondly, the electromagnetic component (the electrical charge Q) enters the geometric relations, such as the radius of the event horizon. Because of this interplay between a and Q, the black hole angular momentum is limited to the value below one, because of the fact that we require r_+ to be a real number. In this illustrative example one sets $Q = 0.1$. The panels (a) and (b) illustrate ultralight axionic dark matter clouds. In the case under inspection, their distribution is slightly affected by the black hole angular momentum. When its value is moderate, the cloud aggregates around polar regions of the Kerr-Newman black hole. As the angular momentum rises, axions flow towards the equator and are spread over whole hemispheres. The clouds of dark matter are distributed on the majority of the slice's area, except the equatorial region, which is naturally the result of the imposed boundary conditions. However, contrary to previous background, axionic clouds are strongly localized in the vicinity of the black hole event horizon. Their distribution quickly vanishes with the growth of the distance. The large mass case, presented on panels (c) and (d), reveals a strong concentration of the field for both values of the angular momentum. In the former case the cloud is visible over the majority of black hole hemispheres, while in the latter case it is mostly present in the equatorial area. Moreover, the axion dark matter field blurs further into the space. The rise of mass
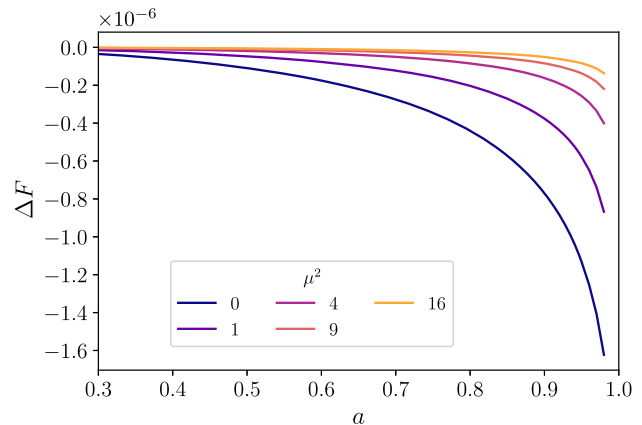

FIG. 6. Free energy shift vs black hole angular momentum in Kerr-Newman background. The presented function shows the slight drop of free energy for moderate values of angular momentum. However, the lowest free energy value is found for the extreme black hole regime.

also shrinks the spread of the clouds, as they quickly decay with distance from the horizon. Besides the rise of angular momentum, it significantly increases the magnitude of the axionic field (see colorbars).

The Kerr-Newman background can be analyzed thermodynamically in the similar manner as it has been performed in the Kerr in a uniform magnetic field system. However, for the elaborated case, the free energy dependence on the black hole angular momentum reveals a slightly different behavior. These curves are portrayed in Fig. 6. Energy characteristics are monotonic and decreasing with growth of the angular momentum. Nevertheless, in the extreme black hole regime, the dynamics of the free energy rises and the curves are steeper as $a \to 1$. Once again, the curve corresponding to the zero mass has the lowest free energy.

IV. CONCLUSION

In our paper we have elaborated on the axioniclike dark matter model, where the scalar field (axion) is nontrivially coupled to the electromagnetic $U(1)$-gauge field, via coupling to the $*F_{\alpha\beta}F^{\alpha\beta}$ invariant. We considered the possibility of accumulating axion dark matter clouds in the vicinity of a rotating black hole. Namely, we have studied the Kerr black hole immersed in a uniform magnetic field and Kerr-Newman black hole spacetime. In both cases axion dark matter clouds tend to accumulate in polar regions of the black hole in question.

As far as the Kerr black hole is concerned, it turns out that the increase of a black hole angular momentum does not change the distribution of ultralight dark matter clouds but influences its magnitude. For the increase of the axion mass, the cloud gathers in the equatorial area of the object.

For the Kerr-Newman black hole the ultralight axion dark matter cloud distribution depends on the black hole

angular momentum. The increase of its value spreads the cloud over the space surrounding the Kerr-Newman black hole. In the case of a large mass axion, the field is strongly dragged towards the equatorial area. Moreover, it was revealed that axionlike dark matter clouds are preferable for very small, almost zero mass, axion fields.

Considering that axionic dark matter clouds do not emerge spontaneously, but are rather magnetically induced, this mechanism naturally requires a magnetic component, such as a galactic magnetic field or a charged rotating black hole. Nevertheless, if such dark matter clouds constitute reality, it will be a complicated observational challenge to reveal their existence. This task will require advanced numerical relativity simulations, which should take into account additional astrophysical and particle-related scenarios, such as, e.g., plasma-axion dark matter interactions. We hope to return to these problems elsewhere.

APPENDIX: TECHNICAL DETAILS ON THE NUMERICAL METHOD

The implemented numerical method relies on the Chebyshev differentiation matrices, which are used to discretize the partial differential equation, on a Chebyshev grid. Similarly to finite difference methods (FDMs), the usage of differentiation matrix allows one to translate a differential equation into a system of linear equations $L\psi = B$. Unlike the FDM, spectral differentiation requires only a few grid points in order to achieve high accuracy. Having our discrete differential operator constructed, we impose the boundary conditions by substituting particular rows in the matrix and solve the system with standard linear algebra tools. In result we obtain the vector of ψ values on the grid points. We have implemented the numerical scheme in PYTHON, based on the MATLAB counterpart [25], using open source libraries.
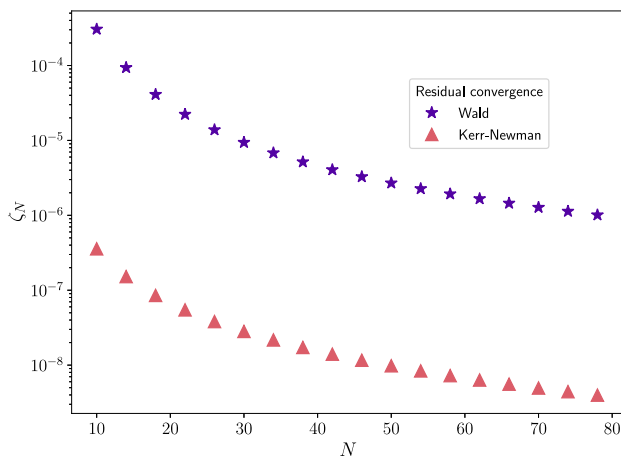
FIG. 7. Convergence of the mean value of residuals calculated at the set of random points. The error smoothly decays with the growth of the grid.
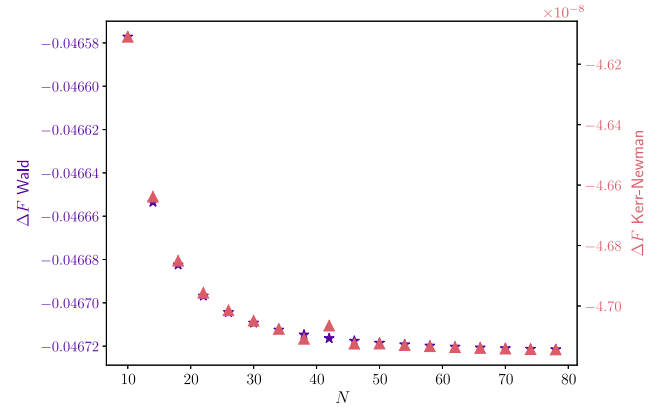
FIG. 8. Convergence of the free energy of the system. Left y-scale corresponds to the Wald background (purple stars), while the right y-scale to the Kerr-Newman solution (red triangles). The value of the free energy quickly converges to the limit.

The numerical code has undergone two convergence trials on the $N \times N$ grid. The first relies on evaluating the mean of the residuals

$$\zeta = \langle |L\psi - B| \rangle, \tag{A1}$$

on a set of random points, which do not belong to the spectral grid. However, we calculate this metric using another differentiation scheme, in this case, standard central finite difference derivative. This allows us to verify if the spectral solutions are relevant [26]. The result of this test is presented in Fig. 7. The increase of the number of grid points lowers the error of the solution in both gravitational backgrounds.

The second numerical test uses the free energy from Eq. (15). For the same set of physical parameters we evaluate the free energy, increasing the number of grid points in each step. This test is visualized in Fig. 8. One can see that the free energy quickly converges to its limit. For
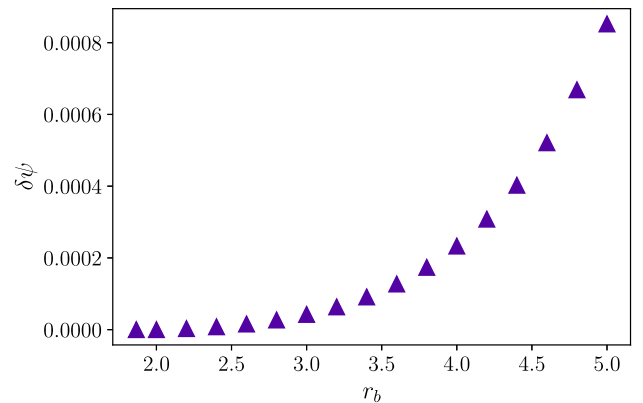
FIG. 9. Dependence of the value of the solution at a distant point in the numerical domain on the location of the inner boundary. The event horizon radius is $r_+ \approx 1.86$ for this case.

convenience, we refer to the Kerr black hole in a uniform magnetic field as the Wald solution.

By the analysis of the convergence of the algorithm we picked $N = 50$ in each direction, as it constitutes a reasonable compromise between the accuracy and the length of computation. Both presented tests were executed for $\mu = 1$, $a = 0.5$, and $Q = 0.1$ in case of the Kerr-Newman background. This is one of the considered cases in Figs. 4 and 6. For different physical parameters the numerical scheme revealed similar behaviors. All solutions shown in the plots in this work meet the requirement $\zeta < 10^{-5}$.

Finally, we check if the numerical solution is invariant for any change of the location of the inner boundary. In the whole work we always use the black hole event horizon as the inner boundary $r_b = r_+$ of our numerical domain.

However, to make sure that our results are reliable, one can shift the inner boundary arbitrarily and check the behavior of the solution in the deep interior of the numerical domain. This is being tested by calculating the value of ψ at the point $\eta(r = 10, \theta = \pi/4)$, systematically for subsequent inner boundary locations. We define a ratio

$$\delta\psi = \frac{\psi(\eta)_{r_b} - \psi(\eta)_{r_b = r_+}}{\psi(\eta)_{r_b = r_+}}, \tag{A2}$$

and compute it for several values of the position of inner boundary r_b. The result of this test is presented in Fig. 9. The value of the function very weakly depends on the position of the inner boundary. Relative error is to the order of 10^{-4} within huge changes of r_b—up to $3r_+$.

[1] R. D. Peccei and H. R. Quinn, *CP* Conservation in the Presence of Pseudoparticles, Phys. Rev. Lett. **38**, 1440 (1977).

[2] S. Weinberg, A New Light Boson?, Phys. Rev. Lett. **40**, 223 (1978).

[3] F. Wilczek, Problem of Strong *P* and *T* Invariance in the Presence of Instantons, Phys. Rev. Lett. **40**, 279 (1978).

[4] P. Svrcek and E. Witten, Axions in string theory, J. High Energy Phys. 06 (2006) 051.

[5] M. A. Fedderke, P. W. Graham, and S. Rajendram, Axion dark matter detection with CMB polarization, Phys. Rev. D **100**, 015040 (2019).

[6] R. T. Co, A. Pierce, Z. Zhang, and Y. Zhao, Dark photon dark matter produced by axion oscillations, Phys. Rev. D **99**, 075002 (2019).

[7] F. P. Huang, K. Kadota, T. Sekiguchi, and H. Tashiro, Radio telescope search for the resonant conversion of cold dark matter axions from magnetized astrophysical sources, Phys. Rev. D **97**, 123001 (2018).

[8] J. W. Foster, Y. Kahn, O. Macias, Z. Sun, R. P. Eatough, V. I. Kondratiev, W. M. Peters, C. Weniger, and B. R. Safdi, Green Bank and Effelsberg Radio Telescope Searches for Axion Dark Matter Conversion in Neutron Star Magnetospheres, Phys. Rev. Lett. **125**, 171301 (2020).

[9] S. Sen, Plasma effects on lasing of a uniform ultralight axion condensate, Phys. Rev. D **98**, 103012 (2018).

[10] J. G. Rosa and T. W. Kephart, Stimulated Axion Decay in Superradiant Clouds Around Primordial Black Holes, Phys. Rev. Lett. **120**, 231102 (2018).

[11] B. Garbrecht and J. I. Mc Donald, Axion configurations around pulsars, J. Cosmol. Astropart. Phys. 07 (2018) 044.

[12] J. Darling, New limits on axionic dark matter using the magnetar PSR J1745-2900, Astrophys. J. Lett. **900**, L28 (2020).

[13] J. Darling, Search for Axion Dark Matter Using the Magnetar PSR J1745-2900, Phys. Rev. Lett. **125**, 121103 (2020).

[14] P. Arias, D. Cadamuro, M. Goodsell, J. Jaeckel, J. Redondo, and A. Ringwald, WISPy cold dark matter, J. Cosmol. Astropart. Phys. 06 (2012) 013.

[15] P. W. Graham, I. G. Irastorza, S. K. Lamoreaux, A. Lindner, and K. A. van Bibber, Experimental searches for axion and axion-like particles, Annu. Rev. Nucl. Part. Sci. **65**, 485 (2015).

[16] A. D. Plascencia and A. Urbano, Black hole supperadiance and polarization-dependent bending of light, J. Cosmol. Astropart. Phys. 04 (2018) 059.

[17] X. Bi, Y. Gao, J. Guo, N. Houston, T. Li, F. Xu, and X. Zhang, Axion and dark photon limits from Crab Nebula high energy gamma-rays, arXiv:2002.01796.

[18] T. Ikeda, R. Brito, and V. Cardoso, Blasts of Light From Axions, Phys. Rev. Lett. **122**, 081101 (2019).

[19] M. Boskovic, R. Brito, V. Cardoso, T. Ikeda, and H. Witek, Axionic instabilities and new black hole solutions, Phys. Rev. D **99**, 035006 (2019).

[20] V. Cardoso, O. J. C. Dias, G. S. Harnett, M. Middleton, P. Pani, and J. E. Santos, Constraining the mass of dark photons and axion-like particles through black-hole superradiance, J. Cosmol. Astropart. Phys. 03 (2018) 043.

[21] R. M. Wald, Black hole in a uniform magnetic field, Phys. Rev. D **10**, 1680 (1974).

[22] B. Kiczek and M. Rogatko, Influence of dark matter on black hole scalar hair, Phys. Rev. D **101**, 084035 (2020).

[23] A. Gracon *et al.*, Constraints on bosonic dark matter for ultralow-field nuclear magnetic resonance, Sci. Adv. **5**, eaax4539 (2019).

[24] C. Ünal, F. Pacucci, and A. Loeb, Properties of ultralight bosons from heavy quasar spins via superradiance, arXiv:2012.12790.

[25] L. N. Trefethen, *Spectral Methods in MATLAB* (SIAM, Philadelphia, 2000).

[26] J. P. Boyd, *Chebyshev and Fourier Spectral Methods* (DOVER Publications Inc, Mineola, New York, 2000).

Check for updates

Static axionlike dark matter clouds around magnetized rotating wormholes–probe limit case

Bartlomiej Kiczek[a] , **Marek Rogatko**[b]

Institute of Physics, Maria Curie-Sklodowska University, pl. Marii Curie-Sklodowskiej 1, 20-031 Lublin, Poland

Abstract The problem of the distribution of axionlike particle, being the model of *dark matter*, in the nearby of rotating wormholes has been investigated numerically. In the model in question the axion scalar is non-trivially coupled to the Maxwell gauge field. We consider two toy models of rotating wormholes embedded in magnetic field, Kerr-like and Teo rotating wormholes. Moreover one assumes that the matter fields will not backreact on the wormhole spacetimes, i.e., we shall study the problem in the probe limit case. We point out the differences in the distribution of *dark matter* comparing to the location of it in the vicinity of rotating magnetized black holes.

1 Introduction

Recently there has been observed a big resurgence of interests in a special class of Einstein field equation solutions representing tunnel-like structures connecting spatially separated regions or even more different Universes, nowadays called wormholes. These fascinating objects are not only important for popular culture, but also gain a lot of scientific attention as their properties allow them to be black hole mimickers.

From historical point of view, the first description of such kind of objects begins with the issue of [1], devoted to spatial part of Schwarzschild solution studies. The prototype of wormhole emerged from the studies devoted to particle model, where the mathematical construction which tried to eliminate coordinate or curvature singularities, dubbed as Einstein–Rosen bridge, was proposed in [2]. Later on, the Kruskal-Szekeres coordinates were implemented for the description of Schwarzschild wormhole [3], while the Euclidean form of wormhole solution was obtained in [4]. One should remark that all these concepts were postulated at quantum scale.

a e-mail: bkiczek@kft.umcs.lublin.pl (corresponding author)

b e-mail: rogat@kft.umcs.lublin.pl

The current understanding of wormholes was revealed in [5], where the conditions for traversability for Lorentzian wormholes were defined by the survivability of human travellers. This redefinition was not only of great importance to physics, but also to futurology and is still seen as a main way to travel at large distances in space by humans. On the other hand, models of a wormhole, possessing no event horizon and physical singularities, were elaborated in [6–8].

In order to obtain such kind of wormhole solutions one should invoke phantom field (exotic matter), whose energy momentum tensor violates the null, weak and strong energy conditions, as well as, its kinetic energy term is of the reversed sign.

However, traversability requires also stability of the wormhole solution, except small acceleration and tidal forces. To achieve this goal we may consider a generalized Einstein gravity theories, like Gauss-Bonnet-dilaton theory. Moreover in this theory wormholes can be built with no use of such exotic kind of matter [9,10]. On the other hand, the method of constructing traversable wormholes by applying duality rotation and complex transformations was proposed [11,12]. By assuming that the dilaton field constitutes a phantom one, an electrically charged traversable wormhole solution in Einstein–Maxwell-phantom dilaton gravity, has been revealed [13].

Soon after the rotating wormhole solutions were paid attention to [14–16]. There were also conceived perturbative and numerical attempts to construct spinning generalization of static wormhole solutions [17–19]. It was claimed that the rotating wormholes would be with a higher possibility stable [21] and therefore traversable.

The other interesting problem in wormhole physics is their classification. Having in mind classification delivered by the black hole uniqueness theorem, the first work in this direction was provided in [22], delivering the uniqueness theorem for wormhole spaces with vanishing Ricci scalar. Further, the uniqueness of Ellis–Bronikov wormhole with phantom field

was found in [23], while the uniqueness for four-dimensional case of the Einstein–Maxwell-dilaton wormholes with the dilaton coupling constant equal to one, was presented in [24]. The case of higher-dimensional generalization of wormhole solution, valid from the point of view of the unification theories like string/M-theory attracts also attention. The uniqueness theorem for higher-dimensional case of the static spherically symmetric phantom wormholes was treated in [25], while the case of of static spherically symmetric traversable wormholes with two asymptotically flat ends, subject to the higher-dimensional solutions of Einstein–Maxwell-phantom dilaton field equations with an arbitrary dilaton coupling constant, was elaborated in [26].

Various other aspects of physics of these objects were under intensive studies (for a detailed review of the blossoming subject the reader may consult [27]).

Wormholes being a fascinating subject of their possible impact on space and time travels, may also be regarded as potential astrophysical objects, that can be observationally search for. From the astrophysical point of view, it is persuasive to consider rotating wormholes. The problem that arises is how to observationally distinguish rotating wormholes from stationary axisymmetric black holes of Kerr-type. Remarkable attention to the aforementioned problem was paid to after the Even Horizon Telescope observed the black hole shadow in the center of the galaxy M87.
The first studies to what extent wormholes can imitate the observational characteristics of black holes were conducted in [28], where the simple generalization of Schwarzschild-like line element was revealed. The considered metric differs from the static general relativity one by introducing the dimensionless parameter λ. The value of the parameter equal to zero is responsible for the ordinary Schwarzschild black hole solution.

Of course one should be aware that for non-zero values of the parameter the presented line element is no longer the static solution of Einstein equations and changes the structure of the manifold. Therefore the matter with almost vanishing energy density ought to be required to maintain the aforementioned gravitational configuration (for the discussion of the influence of the parameter λ on the static manifold structure see, e.g., [29]).

Further generalization of the idea given in [28] to describe Kerr-like wormhole spacetime as a toy model, was achieved by applying a modification on the Kerr metric similar to the procedure performed in [28]. The embedding diagrams, geodesic structure, as well as, shadow characteristics of the obtained Kerr-like wormhole were given in [30]. On the other hand, the throat-like effects on the shadow of Kerr-like wormholes were elaborated in [31].

However, the problem of the structure at the horizon scale of black hole which gives rise to echoes of the gravitational wave signal bounded with the postmeger ring-down phase

in binary coalescences, in the case of static and rotating toy models of traversable wormholes, has been elucidated in [29].

The other subject acquiring much attention in contemporary astrophysics and physics is the unrelenting search for finding *dark matter* sector particles. The nature of this elusive ingredient of our Universe is a mystery and several models try to explain it and constitute the possible guidance for the future experiments. The main aim of our work will be to investigate the behavior of axion-like particle *dark matter* model clouds, around the mimickers of rotating black holes, stationary axially symmetric wormholes. The work will provide some continuity with our previous studies [32], where we have paid attention to the main features of axionic clouds *dark matter* in the vicinity of magnetized rotating black holes.

The principal goal of the investigations will be to find the possible differences in characteristic features of the axion-like condensate, between those two classes of compact objects, i.e., rotating black holes and black hole mimickers. Our studies will constitute the first glimpse at the problem in question. Namely, we restrict our consideration to the probe limit case, when one has the complete separation of the degrees of freedom, i.e., matter fields do not backreact on wormhole spacetime.

The organization of the paper is as follows. In Sect. 2 we deliver the basic facts about the axion-like *dark matter* model. Section 3 will be devoted to the description of the rotating wormholes models surrounded by *dark matter* clouds, in the considered model of axion-like *dark matter*. In Sect. 4 we describe the numerical results of the studies, while in Sect. 5 we conclude our investigations and aim the possible problems for the future investigations.

2 Model of axion-like *dark matter* sector

The explanation of astronomical and cosmological observations require *dark matter* existence, whose nature is one of the most tantalizing questions confronting contemporary physics and cosmology. A large number of ongoing or planned experimental searches for its detection and understanding of the *dark sector* role in a fundamental description of the Universe. Axions are among the strongest candidates for the possible explanation of the existence of *hidden sector* [33–35]. Their existence has been postulated to explain the apparent lack of violation of charge conjugate parity [36–38] and in the strong interaction motivated the absence of observable electric dipole moment of the neutron [39]. Axionlike particles are also widely spotted in the realm of string theories [40].

In what follows, we shall study axionlike scalar particles coupled to the Maxwell $U(1)$-gauge field. The non-trivial coupling of axion field to the Maxwell field strength invariant plays the crucial role in the model in question. The field

equations of motion are provided by the variation procedure with respect to the action given by

$$S = \int d^4x \sqrt{-g} \left[R - \frac{1}{4} F_{\mu\nu} F^{\mu\nu} - \frac{1}{2} \nabla_\mu \Psi \nabla^\mu \Psi \right.$$
$$\left. - \frac{\mu^2}{2} \Psi^2 - \frac{k}{2} \Psi * F^{\mu\nu} F_{\mu\nu} \right], \tag{1}$$

where we set R for the Ricci scalar, $F_{\mu\nu} = 2\nabla_{[\mu} A_{\nu]}$, while Ψ stands for the scalar field (axion) with mass μ. $*F^{\mu\nu} = 1/2\epsilon_{\mu\nu\alpha\beta} F^{\alpha\beta}$ is the dual to Maxwell field strength.

The equation of motion for the scalar field Ψ, which constitutes a covariant Klein–Gordon equation with a source term of the dual Maxwell field invariant, implies

$$\nabla_\mu \nabla^\mu \Psi - \mu^2 \Psi - \frac{k}{2} * F^{\mu\nu} F_{\mu\nu} = 0, \tag{2}$$

while the $U(1)$-gauge field is subject to the relation as follows:

$$\nabla_\mu F^{\nu\mu} + 2k * F^{\nu\mu} \nabla_\mu \Psi = 0. \tag{3}$$

We refer to the Ψ field as axionlike, because the axions (originating from QCD) have adequate constrains on both mass and coupling parameter. Here however we consider particles with physics given by an analogical Lagrangian yet with arbitrary values of physical parameters. However for simplicity we might refer to the studied axionlike particles as simply axions.

The *dark matter* model in question was widely elaborated in studies of black hole superradiance and light polarization effects, possible experimental signals of *dark sector* around these objects [32,41–45], and neutron stars [46–49], as well as, the influence of axionic *dark matter* on the physics on early Universe and primordial black holes [50–53].

The form of the relation (2) envisages the fact that the presence of the non-zero source term, containing the dual invariant, given by

$$\mathcal{I} = * F^{\mu\nu} F_{\mu\nu} \neq 0, \tag{4}$$

is crucial. In the opposite case, when the invariant is equal to zero, the axion-like scalar field equation of motion reduces to the simple massive Klein–Gordon case, without any self-interaction potential. It means that no scalar hair configuration on the studied line element can emerge. Although it has been shown that in Kerr spacetime scalar hair may emerge in certain situations [54], here we pick a different ansatz (see below) as we focus on stationary configurations, which appear to be magnetically induced in this approach. On the other hand, it can be noticed that the discussed invariant, $*F_{\mu\nu} F^{\mu\nu}$, is equal to zero in the case when $F_{\mu\nu} = 0$, or for spherically symmetric spacetime. However, it has a nontrivial form, $*F_{\mu\nu} F^{\mu\nu} \neq 0$, when both rotation and magnetic $U(1)$-gauge field components are present in the spacetime under consideration.

To introduce the magnetic field we use the method proposed by Wald [55], where the vector potential is sourced by Killing vectors of the rotating spacetime. In general it has a form

$$A_\mu = \frac{1}{2} B(m_\mu + 2ak_\mu), \tag{5}$$

where k_μ and m_μ are the Killing vectors connected with temporal invariance and ϕ rotation respectively.

As in [32], where we have studied rotating magnetized black holes submerged into axionic *dark matter* cloud, one can introduce a static magnetic field to the system, which will be oriented along the rotation axis. It seems to be plausible from the point of astrophysical perspective and can be regarded as a starting point for studies of the magnetic field influence of the system in question. Because of the fact that our investigations focus on static magnetic field, parallel to the wormhole rotation axis, the gauge potential may be rewritten in the form as $A_\mu dx^\mu = B/2 \, g_{\mu\nu} m^\nu dx^\mu$.

For our considerations we choose a static, time independent ansatz. The symmetry of the problem enables us to elaborate the axion field in the form provided by

$$\Psi = \psi(r, \theta), \tag{6}$$

which will be plugged into the Eq. (2), for the considered line element.

3 Rotating wormhole metrics

The simplicity of the static line element describing a wormhole may suggest that the spinning generalization can be achieved analytically and ought to be globally regular. But in vain, it happens that finding the stationary solution with an extended source is far more complicated (see for the recent aspects of this problem [20]). However, the rotating wormhole solutions are widely discussed in literature [14,19], but one should be aware that they do not constitute the exact solutions of the equations of motion but rather comprise some model of geometries.

In this section, we shall study two kinds of rotating wormhole model metrics. First one accounts for the extension of the regular black hole Kerr metric [29,30]. The other is the Teo class wormhole [14], a rotating generalization of Morris-Thorne wormhole, which serves us as comparison to a bit more realistic Kerr-like wormhole.

3.1 Kerr-like wormhole

To begin with, we consider the metric of Kerr-like rotating wormhole. It is constructed by a slight modification of stationary axisymmetric line element with a parameter λ. For the first time, such construction was proposed in [28], where

the static Schwarzschild black hole was considered. Then, it was generalized to the case of stationary axisymmetric line element [29,30]. The Kerr-like wormhole line element yields

$$
ds^2 = -\left(1 - \frac{2Mr}{\Sigma}\right)dt^2 - \frac{4Mar\sin^2\theta}{\Sigma}dt d\phi
$$
$$
+\frac{\Sigma}{\tilde{\Delta}}dr^2 + \Sigma d\theta^2
$$
$$
+\left(r^2 + a^2 + \frac{2Ma^2r\sin^2\theta}{\Sigma}\right)\sin^2\theta d\phi^2, \tag{7}
$$

where we set

$$
\Sigma(r,\theta) = r^2 + a^2\cos^2\theta, \tag{8}
$$
$$
\tilde{\Delta}(r) = r^2 + a^2 - 2M(1 + \lambda^2)r. \tag{9}
$$

The parameters M and aM correspond to mass and angular momentum of a wormhole. For a small deviation parameter λ, one achieves almost indistinguishable from of Kerr black hole line element. These three parameters describe the system as seen from the outside. Moreover its Arnowitt-Deser-Misner (ADM) mass, as seen by the observer at asymptotic spatial infinity, is given by $M_{ADM} = M(1 + \lambda^2)$.

The largest root of $\tilde{\Delta}(r) = 0$, establishes the surface provided by

$$
r_+ = M(1 + \lambda^2) + \sqrt{M^2(1 + \lambda^2)^2 - a^2}. \tag{10}
$$

For the model in question it does not constitute a radius of the event horizon, but describes the radius of the throat of the rotating wormhole, which connects two asymptotically flat regions of the spacetime. It can be explicitly seen by the adequate changes of variables [29,30]. The points with the condition $r < r_+$ do not exist.

Consequently the axion field equation written in the Kerr-like wormhole spacetime implies the following:

$$
\tilde{\Delta}\partial_r^2\psi + \frac{2(r - M)\tilde{\Delta} - M\lambda^2(r^2 + a^2)}{\Delta}\partial_r\psi + \partial_\theta^2\psi
$$
$$
+ \cot\theta\partial_\theta\psi - \mu^2\Sigma\psi = \frac{k\Sigma}{2}\mathcal{I}_{KWH}, \tag{11}
$$

where the electromagnetic field invariant is provided by

$$
\mathcal{I}_{KWH} = -\frac{aB^2M\tilde{\Delta}\sin^2\theta\cos\theta}{2\Delta\Sigma^4}
$$
$$
\times \left[3a^6 + 2a^4Mr - 5a^4r^2 - 8a^2Mr^3\right.
$$
$$
- 32a^2r^4 - 24r^6 + 4a^2(a^4 - a^2r^2
$$
$$
+ 2(M - r)r^3)\cos 2\theta + a^4(a^2 - 2Mr + r^2)\cos 4\theta\Big]. \tag{12}
$$

The Eq. (11) undergoes a following scaling transformation

$$
r \to \eta r, \quad a \to \eta a, \quad M \to \eta M, \quad B \to B/\eta,
$$

$$
\mu^2 \to \mu^2/\eta^2, \quad r_+ \to \eta r_+, \tag{13}
$$

which allows us to fix one of model parameters to unity. For this we pick $M = 1$.

3.2 Teo rotating wormhole

The well-known Morris–Thorne metric, introduced in Ref. [5], describes a traversable wormhole spacetime, which is stabilised by exotic matter in the area of its throat. That solution was achieved by using reverse engineering of general relativity, namely the metric was postulated first and with a help of Einstein equations the suitable matter components were found. Generalization of the aforementioned solution, by including the rotation into the consideration, was performed in [14]. The resulting metric of the rotating wormhole has a following form:

$$
ds^2 = -N^2dt^2 + \frac{dr^2}{1 - \frac{b}{r}}
$$
$$
+K^2r^2\left[d\theta^2 + \sin^2\theta(d\phi - \omega dt)^2\right], \tag{14}
$$

where, as in the Morris-Thorne case, one has a lot of freedom in choosing the shape of N, b, K and ω functions, as long as they meet specific requirements. Firstly, all the functions can be functions of r and θ and should be regular on the symmetry axis $\theta = 0, \pi$. Secondly, N, the gravitational redshift function, ought to be finite and nonzero, b as the shape function determining the shape of the wormhole throat, should satisfy $b \leqslant r$. K accounts for the radial distance with respect to the coordinate origin and ω stands for the angular velocity of the wormhole.

The embedding of constant t and θ-cross sections in the three-dimensional Euclidean space reveals the well-recognizable form of the wormhole spacetime. The constructed geometry describes two regions, where the radial coordinates are given by $r \in [r_+, \infty)$, which are joined together at the wormhole throat $r = r_+$. At spatial infinity, the requirement of asymptotic flatness regions provides that the metric coefficients ought to satisfy the following expansions:

$$
N = 1 - \frac{M}{r} + \mathcal{O}\left(\frac{1}{r^2}\right), \quad K = 1 + \mathcal{O}\left(\frac{1}{r}\right), \quad \frac{b}{r} = \mathcal{O}\left(\frac{1}{r}\right),
$$
$$
\omega = \frac{2J}{r^3} + \mathcal{O}\left(\frac{1}{r^4}\right), \tag{15}
$$

where we have denoted by M the mass of the wormhole and by J its angular momentum. In general, one encounters the whole range of functions, which fulfil the aforementioned conditions and constitute a regular rotating wormhole solution.

For the numerical calculations, we pick a set of functions which appear to be quite popular in the literature of the subject, and were previously used by different authors [56–60]

$$N = \exp\left[-\frac{r_+}{r}\right], \qquad b(r) = r_+\left(\frac{r_+}{r}\right)^\gamma, \qquad \omega = \frac{2ar_+}{r^3}$$
$$K = 1, \tag{16}$$

where we use the r_+ symbol, for denoting the wormhole throat radius. The angular momentum parameter is defined in the standard way $a = J/M$. Using the asymptotic relations (15) we find that for the picked set of functions (16) $M = r_+$. Thus, the family of the above solutions is described by three parameters, i.e., the throat radius r_+, angular momentum parameter a and the shape parameter γ.

After putting the ansatz (6) and the metric into the field equation (20) we arrive at the equation of motion

$$\left[r^2 - r_+ r\left(\frac{r_+}{r}\right)^\gamma\right]\partial_r^2\psi + \left[2r + r_+ \right.$$
$$\left. + \left(\frac{r_+}{r}\right)^\gamma\left(\frac{1}{2}r_+\gamma - \frac{r_+^2}{r} - \frac{3}{2}r_+\right)\right]\partial_r\psi$$
$$+ \partial_\theta^2\psi + \cot\theta\partial_\theta\psi - \mu^2 r^2\psi = \frac{1}{2}kr^2\mathcal{I}_{TWH}, \tag{17}$$

which radial part is strongly dependent on γ. The Maxwell field invariant related to uniform magnetic field in this spacetime implies

$$\mathcal{I}_{TWH} = \frac{12aB^2 r_+ \cos\theta \sin^2\theta}{r^{5/2}}\sqrt{\frac{r - r_+\left(\frac{r_+}{r}\right)^\gamma}{\exp\left[-\frac{2r_+}{r}\right]}}. \tag{18}$$

The Eq. (17) follows a scaling transformation

$$r \to \eta r, \quad r_+ \to \eta r_+, \quad a \to \eta a,$$
$$B \to B/\eta, \quad \mu^2 \to \mu^2/\eta^2. \tag{19}$$

Using this transformation we fix $r_+ = 1$.

3.3 Free energy

As a benchmark for the thermodynamical preference of the obtained states we use free energy by evaluating the on-shell action of the axion dependent part of the theory

$$\mathcal{S}_{axion} = \int d^4x\sqrt{-g}\left[-\frac{1}{2}\nabla_\mu\Psi\nabla^\mu\Psi - \frac{\mu^2}{2}\Psi^2\right.$$
$$\left. - \frac{k}{2}\Psi * F^{\mu\nu}F_{\mu\nu}\right]. \tag{20}$$

By substituting the equations of motion into the action and imposing the ansatz of the field we arrive to the formula for the free energy

$$F = -2\pi\int_{\mathcal{M}} dr d\theta \sqrt{-g}\left[(\partial_r\psi)^2 g^{rr} + (\partial_\theta\psi)^2 g^{\theta\theta} + \mu^2\psi^2\right]. \tag{21}$$

The straightforward integration of the Eq. (21) appears to be problematic. It is because both considered backgrounds have singular metric determinant at the throat, which makes simple integration from throat to infinity impossible in these coordinates. It should be noted that this singularity is merely a coordinate singularity, as the curvature of both wormholes is regular and finite at the throat.

In the case of Kerr-like wormhole metric, we have

$$\sqrt{-g} = \sqrt{\frac{\Delta}{\tilde{\Delta}}}\Sigma \sin^2\theta, \tag{22}$$

where for the case of λ equal to zero we obtain that $\Delta = \tilde{\Delta}$. This fact naturally eradicates the singularity problem in the black hole scenario. Here, however, as we radially fall toward the wormhole, the root of $\tilde{\Delta}$ comes first and creates the singularity. On the other hand, for the Teo rotating line element we get

$$\sqrt{-g} = \frac{\exp\left(-\frac{r_+}{r}\right) r^2 \sin\theta}{\sqrt{1 - \left(\frac{r_+}{r}\right)^{\gamma+1}}}, \tag{23}$$

with the denominator naturally generating the infinity.

To deal with the integration in such spacetimes we use energy differences instead. Also we introduce a cutoff to the lower integration bound, so we start from $r_+ + \epsilon$ rather than simply r_+. In this way we ensure the finiteness of energy differences and give them straightforward physical interpretation. With the change of the background parameter the solution becomes more or less thermodynamically stable with respect to some *ground* solution.

4 Results

In this section we pay attention to the solutions of the equations of motion for the previously described two toy models of rotating wormholes. Due to the complications of the relations (11) and (17), we solve them numerically by virtue of spectral methods. Firstly the adequate equation is discretized on Gauss-Lobato grid [61] and next translated into a system of algebraic equations with spectral differentiation matrices. The method in question has already been implemented in Python and tested for the numerical stability. The technical details, especially convergence tests of the numerical method are described in the Appendix of [32], where we studied the problem of axionlike particle clouds in the spacetimes of rotating magnetized black holes.

The spectral nature of the numerical scheme requires remapping the coordinates onto the $[-1, 1]$ intervals. It can be achieved by the coordinate transformation provided by

$$z = 1 - \frac{2r_+}{r}, \tag{24}$$

$$u = \frac{4\theta}{\pi} - 1, \tag{25}$$

where r_+ is the wormhole throat radius. After such operation, our numerical domain may be written in the form $[-1, 1] \times [-1, 1]$. For z-coordinate, the boundaries are the wormhole throat ($z = -1$) and spatial infinity ($z = 1$), while for $u = -1$, one talks about *north pole* of a wormhole and the *equator* with $u = 1$.

Consequently after the coordinate transformation in the underlying equations, one shall impose the adequate boundary conditions. Namely, on the throat surface we demand that the axion field should be regular, therefore $\partial_r \psi = 0$ provides a desirable conduct of the field. Alternatively, setting the field to a constant value, such as zero in a wormhole scenario, is also a possible choice. However we wish to explore the Kerr-like solution for different values of λ parameter, including its zeroing when it simplifies to the Kerr black hole. Given that for the consistency between these two kinds of solutions we use the Neumann boundary condition. At the spatial infinity, we take a look on the asymptotic behaviour of the equation itself and the source term $\mathcal{I}$. It appears that the Maxwell field invariants in both backgrounds are vanishing functions. As $r \to \infty$, we have

$$I_{KWH} = \mathcal{O}\left(\frac{1}{r^4}\right), \tag{26}$$

$$I_{TWH} = \mathcal{O}\left(\frac{1}{r^2}\right). \tag{27}$$

Which means that both Eqs. (11) and (17) reach a simple, asymptotic form, to the leading order

$$\partial_r^2 \psi + \frac{2}{r}\partial_r \psi - \mu^2 \psi = 0. \tag{28}$$

This simple equation has a solution

$$\psi = A\frac{\exp(\mu r)}{r} + B\frac{\exp(-\mu r)}{r}, \tag{29}$$

where A and B are constants. Naturally the field ought to decay for the sake of asymptotic flatness of the spacetime. Given that we are allowed to choose $A = 0$, with arbitrary B. This means that a boundary condition $\psi(r \to \infty) = 0$ is an adequate and mathematically motivated choice.

On the other hand, the boundary conditions for the angular dependency are built on the basis of the spacetime symmetry. Both considered spacetimes are rotating, therefore we demand $\partial_\theta \psi = 0$ on the *north pole*. On the *equator*, the presence of magnetic field combined with the spacetime symmetry implies that $\psi = 0$.

4.1 Kerr-like wormhole

To commence with, we solve the Eq. (11) for the Kerr-like background metric. A portion of obtained distributions is depicted in Fig. 1. In the following panels we see the increasing mass of the axionic field. In the panel (a) the field is ultralight, subsequently in (b) $\mu^2 = 0.01$, (c) $\mu^2 = 0.1$ and finally in (d) $\mu^2 = 1$. In every panel we have $a = 0.99$ and $\lambda = 0.5$. We can clearly see how the mass of the axionlike field changes the angular distribution of it around the wormhole. For little masses the clouds are concentrated around the poles of the wormhole and spread in the space for several throat radii. As we increase the axion mass we see that the polar regions of the wormhole become depleted and the field drifts towards the equator. The largest concentration is visible on the latitude $\theta \simeq \pi/4$.

Second important effect is the influence of the field mass on the magnitude of the field. Inspection of the colorbars reveals that the larger the mass the smaller the field. The spatial tail of the field is also much shorter, when the mass of the field is larger. Intuitively, in the asymptotic solution (29) μ enters the suppressing exponential term. The field decays faster for larger masses, which means the massive fields are localized in the vicinity of the throat surface.

Another important thing that stands out in relation to the black hole solutions is the repulsion of the axion cloud from the wormhole throat surface. While in the case of the black hole, the field had non-zero values on the surface of the event horizon, and its radial character was monotonically decreasing, here we have a completely different situation. For the wormhole, the field vanishes or at least has a significantly smaller value on the throat. Then it grows with the radius as it reaches the maximum and finally decreases. This effect is particularly visible for the high values of the angular momentum.

The radial behaviour of the axionic field can be seen more precisely in Fig. 2. We present there a slice of ψ as a function of r in throat radius units, for constant $\theta = \pi/4$ and few different values of the λ parameter. In contrast, we also plot the behaviour of axions in Kerr black hole metric (that is $\lambda = 0$).

What we can see is the increasing λ consequently extinguishes the axionic hair. In the foreground a structural change in the field profile is visible as we compare it to the black hole scenario. An axionic field over a black hole has a maximum value on the event horizon. The opposite is true for a wormhole, on the throat the field vanishes, then grows to its maximum and fades away with the radius. Then, the bigger is λ the smaller are the maxima and overall magnitude of the axionic hair.

In the next step we investigate the free energy of the obtained axion cloud configurations. It is interesting to see how the parameters describing the spacetime geometry around the wormhole influence the thermodynamics of the axion clouds. Due to the previously mentioned difficulties in computing the free energy in these metrics, we rather talk about energy differences, than the exact values. In Fig. 3
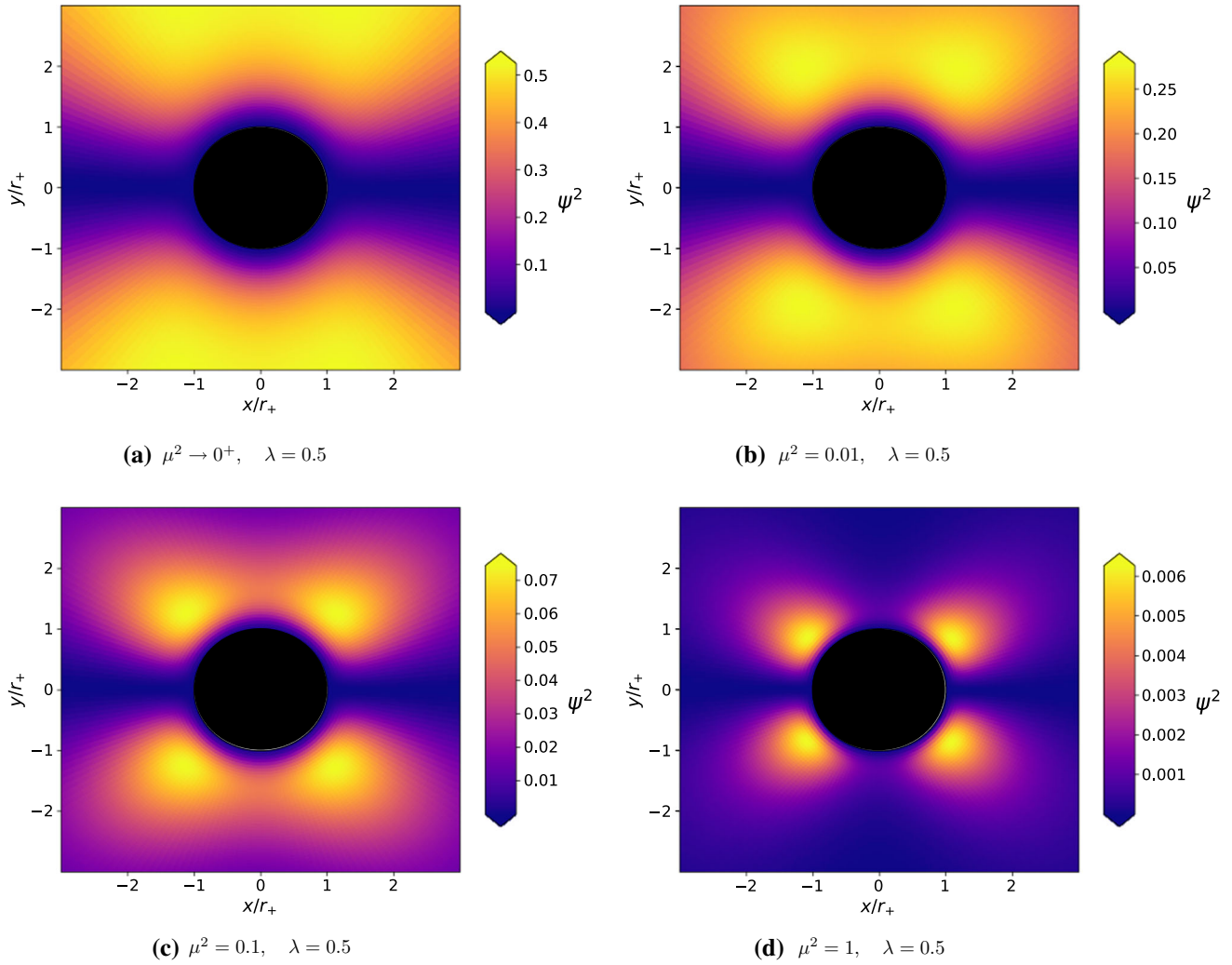
(a) $\mu^2 \to 0^+$, $\lambda = 0.5$

(b) $\mu^2 = 0.01$, $\lambda = 0.5$

(c) $\mu^2 = 0.1$, $\lambda = 0.5$

(d) $\mu^2 = 1$, $\lambda = 0.5$

Fig. 1 Axion field distribution around Kerr-like wormholes for given sets of parameters. The blank space in the vicinity of wormhole throat distinguishes the solution from the black hole counterpart, where the field appears to be non-zero on the event horizon. Subsequent panels for each mass parameter show how the angular distribution of the field is affected
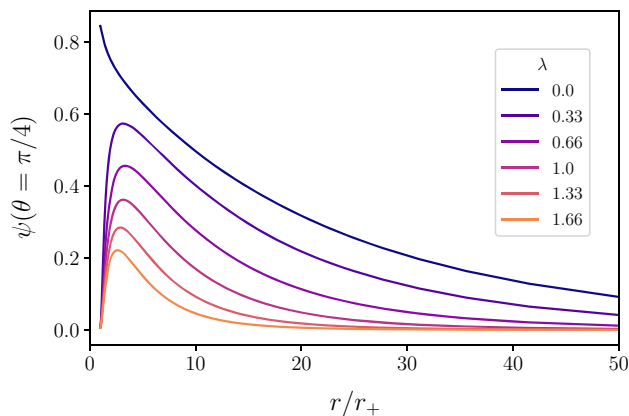

Fig. 2 A closer look on the axion cloud gap near the wormhole throat. Here we show slices of ψ for constant $\theta = \pi/4$, with parameters $a = 0.99, \mu^2 = 0^+$. Increasing of λ decreases the magnitude of the axions and cuts off its tail

we present the differences of the free energy versus angular momentum a, with respect to the $\lambda = 0$ level, which constitutes a plain Kerr black hole. It is clearly visible that the larger value of the distortion parameter λ one takes into account, the higher value of the free energy of the cloud we achieve. It turns out, that the more the gravitational background deviates from from the black hole metric, the less thermodynamically desirable axion clouds are. This effect works together with the diminishing magnitude of the field on the previously discussed Fig. 2. Additionally the increasing angular momentum of the wormhole also increases the free energy difference. This means that for *extreme* Kerr-like wormhole axion hair is the least favourable.
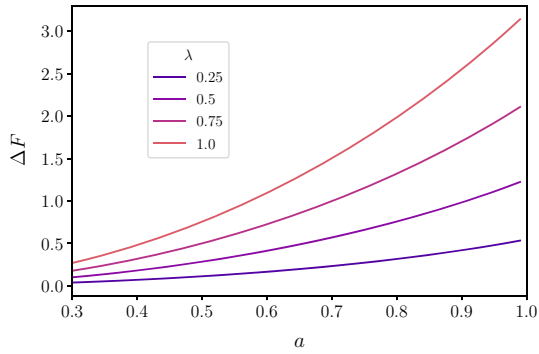
Fig. 3 Free energy differences as a function of angular momentum (with $\lambda = 0$ as the ground curve) for different values of λ. With axion mass $\mu^2 = 0^+$ we see that the cloud thermodynamical favourability decreases with growth of both angular momentum and λ parameter

4.2 Teo rotating wormhole

Teo class wormhole has a different set of parameters and it does not simply transform into a black hole solution, just like a Kerr-like wormhole does. Here the throat radius is independent of the other parameters and is imposed manually in g_{tt} and g_{rr}. With the particular choice of functions (16), we can only steer with the shape of metric components via γ parameter. Therefore, let us consider values of γ in the interval $(-1, 1]$, where for $\gamma = -1$ the function g_{rr} is singular, so we can only approach this value.

As it was mentioned, the Kerr-like wormhole can be reduced to a black hole solution by setting $\lambda = 0$. Teo solution does not share this feature, but is a well-known wormhole metric, just like its non-rotating counterpart the archetypi-
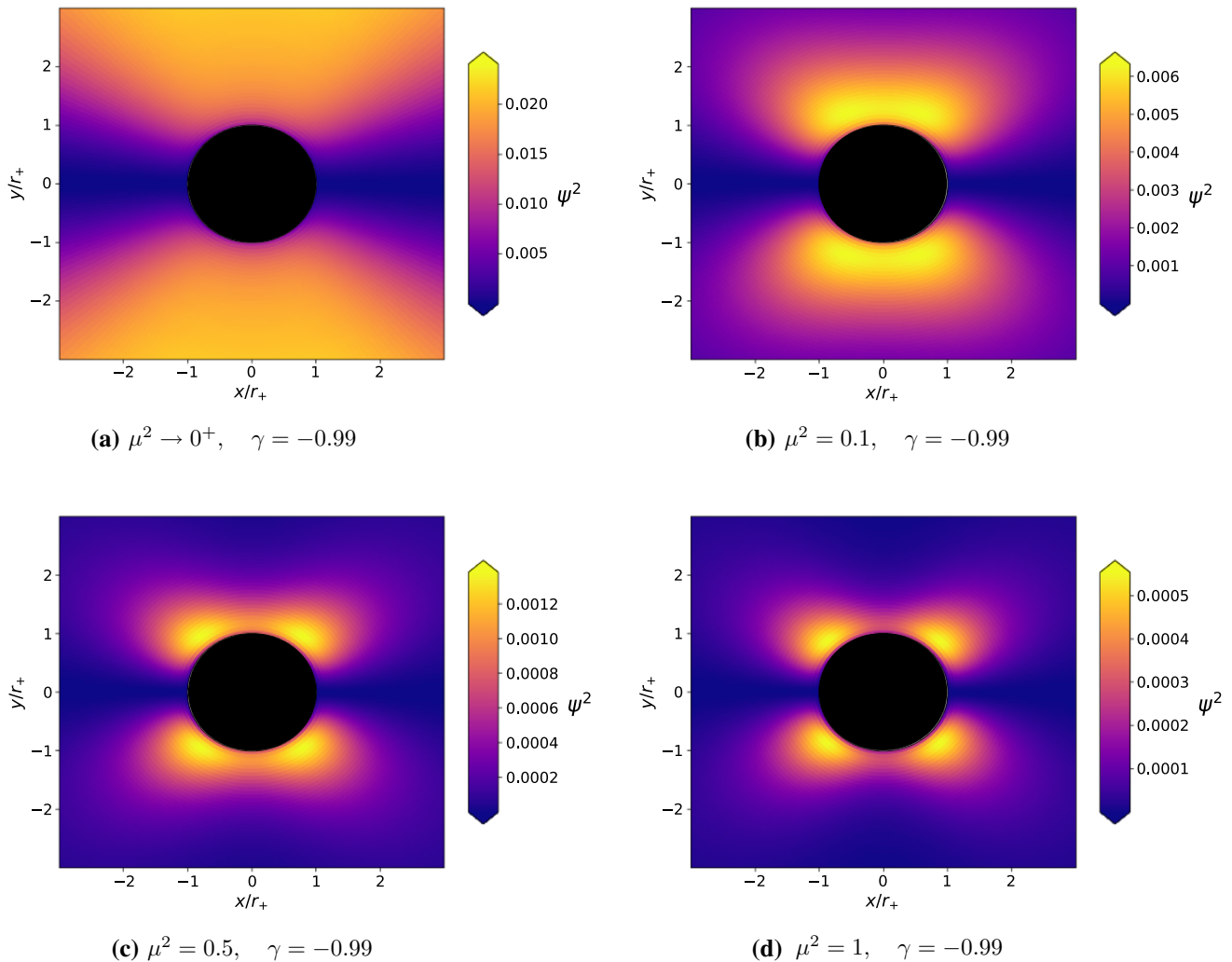

(a) $\mu^2 \to 0^+$, $\gamma = -0.99$

(b) $\mu^2 = 0.1$, $\gamma = -0.99$

(c) $\mu^2 = 0.5$, $\gamma = -0.99$

(d) $\mu^2 = 1$, $\gamma = -0.99$

Fig. 4 Axion cloud distribution around the magnetized Teo type wormhole. The negative value of γ resembles the results for Kerr-like wormhole, with large λ value, i.e., the decreasing of the field magnitude. Each panel depicts the field distribution for different axionlike masses. Once

again a big mass results with a localized field, concentrated closely to the throat with depleted polar region. For bigger values of γ we observe similar influence of μ on the spatial distribution

cal Morris-Thorne wormhole. While it can not serve as a testing field for differences between axion clouds around wormholes and black holes, one can treat it as a benchmark for behaviours of the axion hair in another wormhole environment. Using this background might help us to see if the obtained axion solutions share similar features.

In Fig. 4 one can see the distribution of the axionic cloud around a Teo wormhole for different axionlike field masses. In the panel (a) we have an ultralight field, then it takes values 0.1, 0.5 and 1.0 for (b), (c) and (d) respectively. In all panels we use $\gamma = -0.99$, which gives us tiny value of the axionic field (see the colorbars).

The angular distribution has similar features to the Kerr-like metric. For ultralight axions the field is localized in the majority of the wormhole surroundings. As the mass increases the hair tightens spatially and disappears from the polar regions. For the large mass case the axionic clouds are drifting toward the equator with the polar caps left almost empty. Moreover the radial reach is very short - around one throat radius.

One can clearly notice that for the negative gamma value the analogous effect to the Kerr-like scenario is observed. The axionic cloud is also pushed away from the throat surface - in its vicinity the field acquires small values, reaches the maximum and the descends monotonically to zero. However in this gravitational background this effect is not as dramatic as in case of Kerr-like wormhole. The weakening of the axionic field in the vicinity of the throat is easily visible in the distributions, although it is not that large. Increasing γ up to zero and beyond causes the rise of ψ field. It grants bigger values, but the spatial qualitative characteristic remains intact.

The next figure brings a closer look on the field drop near the throat. In Fig. 5 we present radial slices of the field distribution with $\theta = \pi/4$. In this particular figure we depict the behaviour for ultralight field, however a similar tendencies are shown by more massive fields. First of all, we observe a significant amplification of the field with the growth of γ. The field does not acquire new features however, but it seems that the curves follow some kind of scaling related to gamma. Additionally the profiles resemble the results obtained for Kerr-like wormholes. As we have previously mentioned, Teo class wormhole cannot be simply transformed into a black hole by a simple choice of parameter value. However the features like a drop near the throat surface, then maximum and monotonic fall show that these might be more general wormhole related behaviours of axionic hair.

If we consider the free energy, it appears that the axion clouds for the background with negative γ, are definitely less thermodynamically favourable. In Fig. 6 we plot the free energy difference as a function of angular momentum for several values of the gamma parameter. We use the curve with $\gamma = 0$ as a baseline for calculating energy differences.
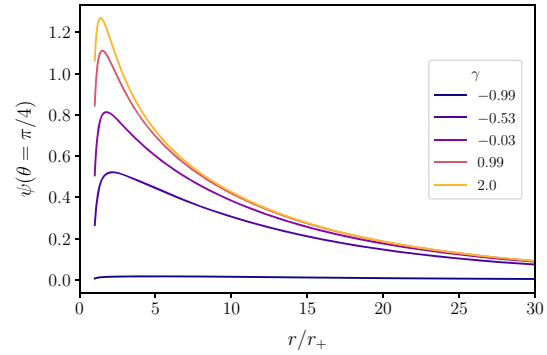

Fig. 5 Radial slices of the axion field for constant angle $\theta = \pi/4$. The growth of γ increases the maximum value of the field. However in this metric the significant growth of the blank space near the throat is not present. Also the growth of γ does not seem to greatly affect the tail of the field, away from the throat, which is different from the Kerr-like wormhole results
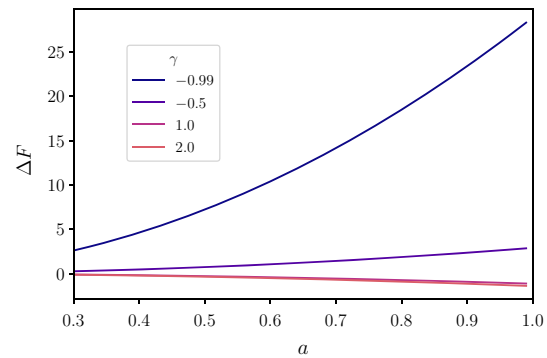

Fig. 6 Free energy differences vs. angular momentum for different values of γ. The curve of $\gamma = 0$ is the reference level. We see that free energy increases for negative values of gamma and slightly drops for positive ones, as angular momentum grows

Free energy difference curves for $\gamma < 0$ are positive, especially the $\gamma = -0.99$ curve reaches relatively big values. Therefore thermodynamically speaking wormholes with γ close to -1 have least chances to hold axionic hair. With the growth of the parameter, the free energy of the cloud decreases, which makes the axions more thermodynamically favourable. However this fall is rather moderate comparing to the rise of the top curve.

In both cases the increase of angular momentum amplifies the tendencies of the curves. Curves for negative gamma grow, while the positive fall. A consequent growth of γ parameter leads the hair to some limit characteristics which can be seen in Figs. 5 and 6.

Finally let us conduct qualitative comparison of the axionic clouds in considered metrics. The solutions have undoubtedly similar features, especially when one takes a look on the ψ slices. We also observe the separation of the cloud from the surface of the throat in both cases. This allows us to notice some general wormhole related phenomena,

which are not present around the black holes [32]. Naturally we cannot speak in a fully general manner, as we only considered here merely two distinct gravitational backgrounds, which on the other hand should be treated as toy models.

5 Conclusion

In our paper, we have considered the problem of the distribution of axionlike particles, being regarded as *dark matter* sector model, around the toy models of rotating wormholes. We have investigated the Kerr-like wormhole line element with the distortion parameter λ and Teo model of a rotating axisymmetric wormhole. The models under inspection were characterized by the mass, angular momentum, distortion parameter (for Kerr-like wormhole) and the shape parameter γ (for the Teo model). We numerically solve the equations of motion for the underlying cases, using spectral methods.

Among all we have found that the axion clouds are pushed forward from the wormhole throat, especially for the case of large value of the rotation parameter a. The voids in the vicinity of the wormhole throat appear for the larger value of the distortion parameter λ. This phenomenon distinguishes the studied system from the previously elaborated black holes [32]. On the other hand, for the larger λ, one achieves higher value of the free energy, and therefore this solution is less thermodynamically favoured.

As far as the Teo class of rotating wormholes is concerned, we have for the negative value of γ the analogous effect as in the latter case is obtained. However for the positive value, the behavior of axionic clouds resembles features of the *dark matter* clouds around Kerr black hole in a uniform magnetic field. The solution with negative γ is not thermodynamically favourable, as it has been revealed in free energy studies. However when γ increases, the free energy of the axionic cloud decreases.

We have found that the behavior of the axionic clouds significantly differs from the black hole scenario, which we discussed in our previous work [32]. This fact will account for the possible guidance, enabling one to distinguish between these two classes of compact objects. Nevertheless, the search for astronomically observable criteria require far more complex approach. A more realistic dynamical gravitational model is needed, when the time dependence of the studied fields is taken into account, as well as, the direct mathematical proofs of the stabilities of rotating wormhole spacetimes ought to be found. These subjects impose a real mathematical challenge and require also solid numerical relativity machinery. These problems shall be investigated elsewhere.

Data Availability Statement This manuscript has no associated data or the data will not be deposited. [Authors' comment: The numerical code is not ready yet to be published. However, it is available upon Reader's request.]

References

1. L. Flamm, Beiträge zur Einsteinischen Gravitationstheorie. Phys. Z. **17**, 448 (1916)
2. A. Einstein, N. Rosen, The particle problem in the general theory of relativity. Phys. Rev. **48**, 73 (1935)
3. J.A. Wheeler, Geons. Phys. Rev. **97**, 511 (1955)
4. S.W. Hawking, Wormholes in space-time. Phys. Rev. D **37**, 904 (1988)
5. M.S. Morris, K. Thorne, Wormholes in space-time and their use for interstellar travel: A tool for teaching general relativity. Am. J. Phys. **56**, 395 (1988)
6. H.G. Ellis, Ether ow through a drainhole: A particle model in general relativity. J. Math. Phys. **14**, 104 (1973)
7. K. Bronikov, Scalar-Tensor Theory and Scalar Charge. Acta Phys. Polonica B **4**, 251 (1973)
8. H.G. Ellis, The evolving, owless drainhole: A nongravitating-particle model in general relativity theory. Gen. Rel. Grav. **10**, 105 (1979)
9. P. Kanti, B. Kleinhaus, J. Kunz, Wormholes in dilatonic Einstein–Gauss–Bonnet Theory. Phys. Rev. Lett. **107**, 271101 (2011)
10. T. Harko, F.S.N. Lobo, M.K. Mak, S.V. Sushkov, Modifíed-gravity wormholes without exotic matter. Phys. Rev. D **87**, 067504 (2013)
11. G.W. Gibbons, M.S. Volkov, Ring wormholes via duality rotations. Phys. Lett. B **760**, 324 (2016)
12. G. W. Gibbons and M. S. Volkov, Weyl metrics and wormholes, JCAP 05 (039) 2017
13. P. Goulart, Phantom wormholes in Einstein-Maxwell-dilaton theory. Class. Quant. Grav. **35**, 025012 (2018)
14. E. Teo, Rotating tranversable wormholes. Phys. Rev. D **58**, 024014 (1998)
15. G. Clement, A class of wormhole solutions to higher-dimensional general relativity. Gen. Rel. Grav. **16**, 131 (1984)
16. K.A. Bronikov, V.G. Krechet, J.P.S. Lemos, Rotating cylindrical wormholes. Phys. Rev. D **87**, 084060 (2013)
17. P.E. Kashargin, S.V. Sushkov, Slowly rotating scalar fíeld wormholes: The second order approximation. Phys. Rev. D **78**, 064071 (2008)
18. B. Kleinhaus, J. Kunz, Rotating Ellis wormholes in four dimensions. Phys. Rev. D **90**, 121503 (2014)
19. X.Y. Chew, B. Kleinhaus, J. Kunz, Geometry of spinning Ellis wormholes. Phys. Rev. D **94**, 104031 (2016)
20. M.S. Volkov, Stationary generalization for Bronnikov-Ellis wormhole and for the vacuum ring wormhole. Phys. Rev. D **104**, 124064 (2021)
21. T. Matos, D. Nunez, Rotating scalar fíeld wormhole. Class. Quant. Grav. **23**, 4485 (2006)

22. P. J. Ruback, A uniqueness theorem for wormholes in quantum gravity. Class. Quant. Grav. **6**, L21 (1989)
23. S. Yazadjiev, Uniqueness theorem for static wormholes in Einstein phantom scalar fíeld theory. Phys. Rev. D **96**, 044045 (2017)
24. B. Lazov, P. Nedkova, S. Yazadjiev, Uniqueness theorem for static phantom wormholes in Einstein-Maxwell-dilaton theory. Phys. Lett. B **778**, 408 (2018)
25. M. Rogatko, Uniqueness of higher-dimensional phantom fíeld wormholes. Phys. Rev. D **97**, 024001 (2018)
26. M. Rogatko, Uniqueness of higher-dimensional Einstein–Maxwell–phantom dilaton fíeld wormholes. Phys. Rev. D **97**, 064023 (2018)
27. M. Visser, Lorentzian Wormholes, New York, American Institute of Physics 1995, F. S. N. Lobo ed., Wormholes, warp drives and energy conditions, New York, Springer Fundamentals in Theor. Phys., 2017
28. T. Damour, S.N. Solodukhin, Wormholes as black holes foils. Phys. Rev. D **76**, 024016 (2007)
29. P. Bueno, P.A. Cano, F. Goelen, T. Hertog, B. Vercnocke, Echoes of Kerr-like wormholes. Phys. Rev. D **97**, 024040 (2018)
30. M. Amir, K. Jusufí, A. Banerjee, S. Hansraj, Shadow images of Kerr-like wormholes. Class. Quant. Grav. **36**, 215007 (2019)
31. S. Kasuya, M. Kobayashi, Throat efíects on shadows of Kerr-like wormholes. Phys. Rev. D **103**, 104050 (2021)
32. B. Kiczek, M. Rogatko, Axionlike dark matter clouds around rotating black holes. Phys. Rev. D **103**, 124021 (2021)
33. J. Preskill, M.B. Wise, F. Wilczek, Cosmology of the invisible axion. Phys. Lett. B **120**, 127 (1983)
34. L.F. Abbott, P. Sikivie, Cosmological bound on the invisible axion. Phys. Lett. B **120**, 133 (1983)
35. M. Dine, W. Fischler, The not so harmless axion. Phys. Lett. B **120**, 137 (1983)
36. R. D. Peccei, H. R. Quinn, CP conservation in the presence of pseudoparticles. Phys. Rev. Lett. **38**, 1440 (1977)
37. S. Weinberg, A new light boson? Phys. Rev. Lett. **40**, 223 (1978)
38. F. Wilczek, Problem of strong P and T invariance in the presence of instantons. Phys. Rev. Lett. **40**, 279 (1978)
39. J. M. Pendlebury et al., Revised experimental upper limit on the electric dipole moment of the neutron. Phys. Rev. D **92**, 092003 (2015)
40. P. Svrcek, E. Witten, Axions in string theory. JHEP **06**, 051 (2006)
41. A. D. Plascencia, A. Urbano, Black hole supperadiance and polarization-dependent bending of light. JCAP **04**, 059 (2018)
42. X. Bi, Y. Gao, J. Guo, N. Houston, T. Li, F. Xu, and X. Zhang, Axion and dark photon limits from Crab Nebula high energy gamma-rays. arXiv:2002.01796 (2020)
43. T. Ikeda, R. Brito, V. Cardoso, Blasts of light from axions. Phys. Rev. Lett. **122**, 081101 (2019)
44. M. Boskovic, R. Brito, V. Cardoso, T. Ikeda, H. Witek, Axionic instabilities and new black hole solutions. Phys. Rev. D **99**, 035006 (2019)
45. V. Cardoso, O.J.C. Dias, G.S. Harnett, M. Middleton, P. Pani, J.E. Santos, Constraining the mass of dark photons and axion-like particles through black-hole superradiance. JCAP **03**, 043 (2018)
46. B. Garbrecht and J. I. Mc Donald, Axion confígurations around pulsars. JCAP **07**, 044 (2018)
47. J. Darling, New limits on axionic dark matter using the magnetar PSR J1745–2900. Astrophys. J. Lett. **900**, L28 (2020)
48. J. Darling, Search for axion dark matter using the magnetar PSR J1745–2900. Phys. Rev. Lett. **125**, 121103 (2020)
49. P. W. Graham, I. G. Irastorza, S. K. Lamoreaux, A. Lindner, K. A. van Bibber, Experimental searches for axion and axion-like particles. Annu. Rev. Nucl. Part. Sci. **65**, 485 (2015)
50. M. A. Fedderke, P. W. Graham, S. Rajendram, Axion dark matter detection with CMB polarization. Phys. Rev. D **100**, 015040 (2019)
51. R. T. Co, A. Pierce, Z. Zhang, Y. Zhao, Dark photon dark matter produced by axion oscillations. Phys. Rev. D **99**, 075002 (2019)
52. S. Sen, Plasma efíects on lasing of a uniform ultralight axion condensate. Phys. Rev. D **98**, 103012 (2018)
53. J. G. Rosa, T. W. Kephart, Stimulated axion decay in superradiant clouds around primordial black holes. Phys. Rev. Lett. **120**, 231102 (2018)
54. C. A. R. Herdeiro, E. Radu, Kerr Black Holes with Scalar Hair. Phys. Rev. Lett. **112**, 221101 (2014)
55. R. M. Wald, Black hole in a uniform magnetic fíeld. Phys. Rev. D **10**, 1680 (1974)
56. R. Shaikh, Shadows of rotating wormholes. Phys. Rev. D **98**, 024044 (2018)
57. P. G. Nedkova, V. Tinchev, S. S. Yazadjiev, Shadow of a rotating traversable wormhole. Phys. Rev. D **88**, 124019 (2013)
58. A. Abdujabbarov, B. Juraev, B. Ahmedov, Z. Stuchlik, Shadow of rotating wormhole in plasma environment. Astrophys. Space Sci. **361**, 226 (2016)
59. T. Harko, Z. Kovacs, F. Lobo, Thin accretion disks in stationary axisymmetric wormhole spacetimes. Phys. Rev. D **79**, 064001 (2009)
60. C. Bambi, Broad Kfí iron line from accretion disks around traversable wormholes. Phys. Rev. D **87**, 084039 (2013)
61. N. Lloyd, *Trefethen* (Spectral methods in MATLAB, SIAM, Philadelphia, 2000)

4.3 Other activities

During my doctoral studies I also participated in different research, engineering and R&D projects, which might not be fully connected with the main topic of this thesis. However, for completeness I shall list them here.

4.3.1 Conference presentations

1. The 6th Conference of the Polish Society on Relativity (POTOR-6), Szczecin, Poland, 23-26.09.2019 (talk).

2. New Trends in Physics, Paris, France, 28-29.11.2019 (poster).

3. Virtual Conference of the Polish Society on Relativity 2020 (Virtual POTOR), online, 24-26.09.2020 (talk).

4. Alternative Gravities and Fundamental Cosmology AlteCosmoFun '21, online, 6-10.09.2021 (talk).

5. The 28th Annual International Conference On Mobile Computing And Networking (MobiCom 2022), Sydney, Australia, 17–21 Oct 2022 (poster).

4.3.2 Other papers in physics

1. **B. Kiczek**, M. Rogatko and K. I. Wysokinski, *Anomalous Hall conductivity of the holographic $\mathbb{Z}_2$ Dirac semimetals*, Phys. Rev. D 104, 086022 (2021).

4.3.3 Papers in computer science

1. D. Wójcik, B. Stefaniak, M. Woś, **B. Kiczek**, T. Rymarczyk, *Image reconstruction for lung monitoring in wearable electrical impedance tomography*, Przegląd elektrotechniczny, ISSN 0033-2097, r. 98 nr 3/2022.

2. **B. Kiczek**, M. Gołąbek, D. Wójcik, K. Kania, E. Kozłowski, T. Rymarczyk, and J. Sikora, *A wearable ultrasonic bladder monitoring device*, In Proceedings of the 28th Annual International Conference on Mobile Computing And Networking (MobiCom '22). Association for Computing Machinery, New York, NY, USA, 886–888.

3. **B. Kiczek**, D. Wójcik, M. Oleszek, T. Rymarczyk, J. Sikora, B. Baran, B. Przysucha, *LETS - a wearable heart and lung monitoring device for the diagnosis of cardiac and respiratory diseases*, To be published in proceedings of Ubicomp 2022.

4. **B. Kiczek**, D. Wójcik, M. Oleszek, T. Rymarczyk, K. Król, E. Kozłowski, *Electrical impedance tomography bladder monitoring wearable device*, To be published in proceedings of ISWC 2022.

5. T. Rymarczyk, G. Kłosowski, P. Adamkiewicz, M. Styła, **B. Kiczek**, *Use of a Long Short-Term Memory Network in Radio Tomography to Track People Indoors*, To be published in proceedings of Sensys 2022.

6. M. Styła, **B. Kiczek**, et al., *Machine Learning-Enhanced Radio Tomographic Device for Energy Optimization in Smart Buildings*, Energies **2023**, 16(1), 275

4.4 Future investigations

The results obtained within this thesis can be treated as a starting point for some future investigations. There are multiple directions that can be taken, let me list few examples.

Study of the backreaction Most of the dark matter structures in this thesis were obtained in the probe limit. It means only equations of matter were solved with the gravitational background being fixed. However, this should be extended on the analysis of the impact of dark sector clouds on the metric. It could be a quite challenging task, especially if one considers a rotating spacetime. Having this, one can obtain several quantities which can be observed with telescopes.

For instance, one can study light rays bending by a compact object hosting an axion cloud. Similarly, the geodesics of charged particles forming the accretion disk can be examined. Finally, a timely topic, one can verify how a dark matter structure impacts the shape of the black hole shadow. These quantities can be compared to dark matter free scenarios, where the key differences can be pointed.

Time dependent simulations In works [73, 74] we have shown the existence of stationary axion cloud solutions around magnetised black holes and wormholes. Nevertheless, this is merely a beginning, as there are lots of things that should be tested concerning that setup.

The time dependence ought to be included at first. Then one can look for physical processes that would lead to formation of such axion clouds. On the other hand, the stationary clouds can be tested under various perturbations, such as changes of magnetic field.

Stellar evolution It is particularly interesting to see if an addition of some dark matter candidates into the stellar plasma can impact the evolution of a star. By using the equation of state and TOV equations one could model these phenomena. Following questions may arise: How would it affect the ageing process? How the addition of DM would distort star's path on Hertzsprung–Russell diagram?

There are, naturally, more examples that could be brought here. However this thesis shall end somewhere, and this is a good place.

4.5 Co-author statements

Oświadczenie współautorów publikacji

Niniejszym podaję procentowy wkład autorski w publikację pt.

Bartłomiej Kiczek & Marek Rogatko, *Ultra-compact spherically symmetric dark matter charged star objects*, JCAP 09 (2019) 049.

Imię i nazwisko współautora	Procentowy wkład autorski	Data i podpis współautora
Bartłomiej Kiczek	50%	*BKiczek* 19.08.22
Marek Rogatko	50%	*MRogtk* 19/08/22

Oświadczenie współautorów publikacji

Niniejszym podaję procentowy wkład autorski w publikację pt.

Bartłomiej Kiczek & Marek Rogatko, *Influence of dark matter on black hole scalar hair*, Phys. Rev. D **101**, 084035 (2020).

Imię i nazwisko współautora	Procentowy wkład autorski	Data i podpis współautora
Bartłomiej Kiczek	50%	*[podpis]* 19.08.22
Marek Rogatko	50%	*[podpis]* 19/08/22

Oświadczenie współautorów publikacji

Niniejszym podaję procentowy wkład autorski w publikację pt.

Bartłomiej Kiczek, Marek Rogatko & K. I. Wysokiński, *Holographic DC SQUID in the presence of dark matter*, JCAP 01 (2021) 063.

Imię i nazwisko współautora	Procentowy wkład autorski	Data i podpis współautora
Bartłomiej Kiczek	52%	10.01. 2023
Marek Rogatko	33%	10/01/23
Karol I. Wysokiński	15%	

Oświadczenie współautorów publikacji

Niniejszym podaję procentowy wkład autorski w publikację pt.

Bartłomiej Kiczek & Marek Rogatko, *Axionlike dark matter clouds around rotating black holes*, Phys. Rev. D **103**, 124021 (2021).

Imię i nazwisko współautora	Procentowy wkład autorski	Data i podpis współautora
Bartłomiej Kiczek	70%	*[podpis]* 19.08.22
Marek Rogatko	30%	*[podpis]* 19/8/22

Oświadczenie współautorów publikacji

Niniejszym podaję procentowy wkład autorski w publikację pt.

Bartłomiej Kiczek & Marek Rogatko, *Static axionlike dark matter clouds around magnetized rotating wormholes–probe limit case*, Eur. Phys. J. C **82** (2022) 586.

Imię i nazwisko współautora	Procentowy wkład autorski	Data i podpis współautora
Bartłomiej Kiczek	70%	*Kiczek* 19.08.22
Marek Rogatko	30%	*M Rogatko* 19/08/22

Bibliography

[1] F. Zwicky, *The Redshift of Extragalactic Nebulae*, Helvetica Physica Acta, Vol. **6**, p. 110-127, 1933.

[2] V. C. Rubin and W. K. Ford, *Radial Velocities and Line Strengths of Emission Line Across the Nuclear Disk of M31*, Astrophys. J. **170**, 25-52 (1971).

[3] Planck Collaboration (2016), *Planck 2015 results. XIII. Cosmological parameters*, Astron. Astrophys. **594**, 13:A13 (2016).

[4] G. Bertone and T. M. P. Tait, *A New Era in the Quest for Dark Matter*, Nature **562**, 51 (2018).

[5] R. D. Peccei and H. R. Quinn, *CP Conservation in the Presence of Pseudoparticles*, Phys. Rev. Lett. **38**, 1440 (1977).

[6] J. Preskill, M. B. Wise, F. Wilczek, *Cosmology of the Invisible Axion*, Phys. Lett. B **120**, 127 (1983).

[7] L. F. Abbott, P. Sikivie, *A Cosmological Bound on the Invisible Axion*, Phys. Lett. B **120**, 133 (1983).

[8] M. Dine, W. Fischler, *The Not So Harmless Axion*, Phys. Lett. B **120**, 137 (1983).

[9] F. Chadha-Day, J. Ellis, D. J. E. Marsh, *Axion dark matter: What is it and why now?*, Sci. Adv. **8**, eabj3618 (2022).

[10] S. Weinberg, *A New Light Boson?*, Phys. Rev. Lett. **40**, 223 (1978).

[11] F. Wilczek, *Problem of Strong P and T Invariance in the Presence of Instantons*, Phys. Rev. Lett. **40**, 279 (1978).

[12] E. Witten, *Some Properties of O(32) Superstrings*, Phys. Lett. B **149**, 351 (1984).

[13] J. Jaeckel and A. Ringwald, *The Low-Energy Frontier of Particle Physics*, Annu. Rev. Nucl. Part. Sci. 2010. 60:405-37.

[14] K. Ehret et al., *New ALPS results on hidden-sector lightweights*, Phys. Lett. B **689**, 149-155 (2010).

[15] T. Braine et al. (ADMX Collaboration), *Extended Search for the Invisible Axion with the Axion Dark Matter Experiment*, Phys. Rev. Lett. **124**, 101303 (2020).

[16] E. Armengaud et al, *Conceptual design of the International Axion Observatory (IAXO)*, JINST 9 (2014) T05002.

[17] CAST Collaboration, *New CAST limit on the axion–photon interaction*, Nature Phys. **13**, 584–590 (2017).

[18] A. Abeln et al, *Conceptual Design of BabyIAXO, the intermediate stage towards the International Axion Observatory*, arXiv: physics.ins-det **2010.12076** (2020).

[19] J. Galan, *Axion search with BabyIAXO in view of IAXO*, arXiv: physics.ins-det **2012.06634** (2020).

[20] K. Schutz and K. M. Zurek, *Detectability of Light Dark Matter with Superfluid Helium*, Phys. Rev. Lett. **117**, 121302 (2016).

[21] Y. Hochberg et al., *Detecting ultralight bosonic dark matter via absorption in superconductors*, Phys. Rev. D **94**, 015019 (2016).

[22] S. Griffin et al., *Directional detection of light dark matter with polar materials*, Phys. Rev. D **98**, 115034 (2018).

[23] J. Gooth et al., *Axionic charge-density wave in the Weyl semimetal $(TaSe_4)2I$*, Nature **575**, 315 (2019).

[24] T. Ikeda et al., *Blasts of Light from Axions*, Phys. Rev. Lett. **122**, 081101 (2019).

[25] M. Boskovic et al., *Axionic instabilities and new black hole solutions*, Phys. Rev. D **99**, 035006 (2019).

[26] T. Fujita et al., *Hunting Axion Dark Matter with Protoplanetary Disk Polarimetry*, Phys. Rev. Lett. **122**, 191101 (2019).

[27] M. A. Fedderke, P. W. Graham, and S. Rajendram, *Axion dark matter detection with CMB polarization*, Phys. Rev. D **100**, 015040 (2019).

[28] B. Garbrecht and J. I. Mc Donald, *Axion configurations around pulsars*, J. Cosmol. Astropart. Phys. 07 (2018) 044.

[29] J. Darling, *New limits on axionic dark matter using the magnetar PSR J1745-2900*, Astrophys. J. Lett. **900** (2020) L28.

[30] J. Darling, *Search for axion dark matter using the magnetar PSR J1745-2900*, Phys. Rev. Lett. **125**, 121103 (2020).

[31] B. Holdom, *Two $U(1)$'s and ϵ charge shifts*, Phys. Lett. B **166**, 196-198 (1986).

[32] M. Fabbrichesi, E. Gabrielli, G. Lanfranchi, *The Physics of the Dark Photon: A Primer*, SpringerBriefs in Physics, Springer 2021.

[33] W. DeRocco, P. W. Graham, D. Kasen, G. Marques-Tavares and S. Rajendran, *Observable signatures of dark photons from supernovae*, J. High Energy Phys. 02 (2019) 171.

[34] G. G. Raffelt, *Stars as laboratories for fundamental physics*, Chicago Univ. Pr., Chicago, IL, USA (1996).

[35] M. D. Diamond and G. Marques-Tavares, *γ-Ray Flashes from Dark Photons in Neutron Star Mergers*, Phys. Rev. Lett. **128**, 211101 (2022).

[36] B. S. Acharya, S. A. R. Ellis, G. L. Kane, B. D. Nelson, and M. J. Perry, *Lightest Visible-Sector Supersymmetric Particle is Likely to be Unstable*, Phys. Rev. Lett. **117**, 181802 (2016).

[37] R. Bernabei et al., *Searching for WIMPs by the annual modulation signature*, Phys. Lett. B **424**, 195 (1998).

[38] R. Bernabei et al., *Final model independent result of DAMA/LIBRA-phase 1*, Eur. Phys. J. C **73**, 2648 (2013).

[39] COSINE-100 collaboration, *An experiment to search for dark-matter interactions using sodium iodide detectors*, Nature **564**, 83 (2018).

[40] A. Geringer-Sameth et al., *Indication of Gamma-Ray Emission from the Newly Discovered Dwarf Galaxy Reticulum II*, Phys. Rev. Lett. **115**, 081101 (2015).

[41] P. Jean et al., *Early SPI/INTEGRAL measurements of 511 keV line emission from the 4th quadrant of the Galaxy*, Astron. Astrophys. **407**, L55 (2003).

[42] J. Chang et al., *An excess of cosmic ray electrons at energies of 300-800 GeV*, Nature **456**, 362 (2008).

[43] O. Adriani et al. (PAMELA Collaboration), *An anomalous positron abundance in cosmic rays with energies 1.5-100 GeV*, Nature **458**, 607 (2009).

[44] K. K. Boddy and J. Kumar, *Indirect detection of dark matter using MeV-range gamma-ray telescopes*, Phys. Rev. D **92**, 023533 (2015).

[45] K. Van Tilburg et al., *Search for Ultralight Scalar Dark Matter with Atomic Spectroscopy*, Phys. Rev. Lett. **115**, 011802 (2015).

[46] J. H. Chang, R. Essig, and S. D. McDermott, *Revisiting Supernova 1987A constraints on dark photons*, J. High Energy Phys. 01 (107) 2017.

[47] J. P. Lees et al., *Search for a Dark Photon in e^+e^- Collisions at BaBar*, Phys. Rev. Lett. **113**, 201801 (2014).

[48] L. Barak et al. (SENSEI Collaboration), *SENSEI: Direct-Detection Results on sub-GeV Dark Matter from a New Skipper CCD*, Phys. Rev. Lett. **125**, 171802 (2020).

[49] E. Aprile et al. (XENON Collaboration), *Excess electronic recoil events in XENON1T*, Phys. Rev. D **102**, 072004 (2020).

[50] W. Israel, *Event Horizons in Static Vacuum Space-Times*, Phys. Rev. **164**, 1776 (1967).

[51] B. Carter, *Axisymmetric Black Hole Has Only Two Degrees of Freedom*, Phys. Rev. Lett. **26**, 331 (1971).

[52] S. W. Hawking and G. F. R. Ellis, *The Large Scale Structure of Space-Time*, Cambridge University Press, Cambridge, England, 1973.

[53] C. A. R. Herdeiro and E. Radu, *Asymptotically flat black holes with scalar hair: A review*, Int. J. Mod. Phys. D **24**, 1542014 (2015).

[54] J. E. Chase, *Event horizons in static scalar-vacuum space-times*, Commun. Math. Phys. **19**, 276-288 (1970).

[55] J. D. Bekenstein, *Transcendence of the Law of Baryon-Number Conservation in Black-Hole Physics*, Phys. Rev. Lett. **28**, 452 (1972).

[56] M. Heusler and N. Strauman, *Scaling arguments for the existence of static, spherically symmetric solutions of self-gravitating systems*, Class. Quantum Grav. **9**, 2177 (1992).

[57] J. D. Bekenstein, *Novel "no-scalar-hair" theorem for black holes*, Phys. Rev. D **51**, R6608(R) (1995).

[58] I. Peña and D. Sudarsky, *Do collapsed boson stars result in new types of black holes?*, Class. Quantum Grav. **14**, 3131 (1997).

[59] M. Heusler, S. Droz, N. Straumann, *Stability analysis of self-gravitating skyrmions*, Phys. Lett. B **271**, 61-67 (1991).

[60] E. Berti et al., *Spin-Induced Black Hole Scalarization in Einstein-Scalar-Gauss-Bonnet Theory*, Phys. Rev. Lett. **126**, 011104 (2021).

[61] C. A. R. Herdeiro et al., *Spin-Induced Scalarized Black Holes*, Phys. Rev. Lett. **126**, 011103 (2021).

[62] J. M. Maldacena, *The Large N Limit of Superconformal Field Theories and Supergravity*, Adv. Theor. Math. Phys. **2**, 231-252 (1998).

[63] J. D. Brown and J. W. York, *Quasilocal energy and conserved charges derived from the gravitational action*, Phys. Rev. D **47**, 1407-1419 (1993).

[64] S. A. Hartnoll et al., *Building a Holographic Superconductor*, Phys. Rev. Lett. **101**, 031601 (2008).

[65] R. M. Wald, *General Relativity*, The University of Chicago Press, Chicago and London, 1984.

[66] John P. Boyd, *Chebyshev & Fourier Spectral Methods*, DOVER Publications, Inc., New York, 2000.

[67] Lloyd N. Trefethen, *Spectral Methods in MATLAB*, SIAM, Philadelphia, 2000.

[68] A. Einstein and N. Rosen, *The particle problem in the general theory of relativity*, Phys. Rev. **48**, 73 (1935).

[69] M. S. Morris and K. Thorne, *Wormholes in space-time and their use for interstellar travel: A tool for teaching general relativity, Am. J. Phys.* **56** (1988) 395.

[70] **B. Kiczek** and M. Rogatko, *Ultra-compact spherically symmetric dark matter charged star objects*, J. Cosmol. Astropart. Phys. 09 (2019) 049.

[71] **B. Kiczek** and M. Rogatko, *Influence of dark matter on black hole scalar hair*, Phys. Rev. D **101**, 084035 (2020).

[72] **B. Kiczek**, M. Rogatko and K. I. Wysokiński, *Holographic DC SQUID in the presence of dark matter*, J. Cosmol. Astropart. Phys. 01 (2021) 063.

[73] **B. Kiczek** and M. Rogatko, *Axionlike dark matter clouds around rotating black holes*, Phys. Rev. D **103**, 124021 (2021).

[74] **B. Kiczek** and M. Rogatko, *Static axionlike dark matter clouds around magnetized rotating wormholes - probe limit case.* Eur. Phys. J. C **82**, 586 (2022).

[75] **B. Kiczek**, M. Rogatko and K. I. Wysokiński, *Anomalous Hall conductivity of the holographic $\mathcal{Z}_2$ Dirac semimetals*, Phys. Rev. D **104**, 086022 (2021).